博士論文

A Study on Numerical Analysis Method for Flow of Fresh Concrete in Pipes
（フレッシュコンクリートの管内流動に関する数値解析方法の研究）

西暦　2021 年 3 月

Xu　Zhisong

山口大学大学院創成科学研究科

Acknowledgements

Time flies, I have been at Yamaguchi University for nearly four years, and my Ph.D. research work is coming to an end. I am deeply grateful to the China Scholarship Council (CSC) for its financial support of living expenses. I also thank the Architectural Institute of Japan for funding one of my research projects.

Looking back on the research work in the past few years, it is full of difficulties and challenges. Fortunately, many people gave me support and help during this period and left a deep impression on me. Here, I would like to express my sincere thanks to those people.

First of all, I sincerely thank my supervisor Professor Zhuguo Li for his constant encouragement and guidance over the past several years. Professor Li's international vsion, cutting-edge and profound research ideas, and meticulous research spirit have a subtle influence on me and will benefit to my future research work.

I am also greatly indebted to Dr. Fei Jiang, who gave me helpful advice and suggestions in the process of establishing the numerical model in my research.

I am very glad to have Guodong Cao, Sha Li, Kun Guo, Xuezhong Li, Rei Yoshioka, Hiromit Tabai, Ryusei Kondo, Shuto Minami, et al. as my colleagues and friends. I would like to thank them for not only their assistance during my experiments, but also their company to enrich my daily life.

Last but not the least, I am very grateful that my family has been giving me support in various forms. Thanks to my parents for their understanding and encouragement of my decision to study abroad. Thanks to my wife for her company and taking care of my daily life. Our lovely daughter is the spiritual motivation for my continuous efforts. I especially want to thank my father-in-law and mother-in-law for taking care of my daughter, so that I can have more time and energy for my research work.

Abstract

Pumping has become the most widely used methods to transport concrete for placement. The requirement for concrete pumping technology has been increasing due to the increase of large-scale construction projects such as high-rise buildings, long-span bridges, and others. Correspondingly, pumping construction has gradually become a difficult and challenging work. With the development and use of various chemical and mineral admixtures, the rheological performance of fresh concrete exhibits complexity and diversity. The experience and the guidelines of concrete pumping based on conventional concrete may be no longer applicable to new types of concrete. Thus, the development of prediction method of concrete pumping has been becoming a crucial issue for the concrete industry.

Although a few experimental devices such as sliding pipe rheometer have been proposed to predict pumping pressure required for concrete flow, besides the pumping pressure, other concern about pumped fresh concrete is the segregation, i.e. the separation of aggregate from cement paste or matrix mortar. When pumping, it is considered that large particles, such as coarse aggregate and larger sand particles, undergo the shear-induced migration towards the inner, forming a slip layer (also referred to as lubrication layer) near the pipe wall. Also, in front of the concrete, the concentration of coarse aggregate is high, which may form a plug of coarse aggregates to lead to the pipe blockage. Thus, the segregation prediction of pumped concrete is also an important issue.

Dynamic segregation and slip layer play a dominant role during pumping. However, the test methods commonly used to measure the consistency of fresh concrete, such as slump test, cannot encapsulate the effects of segregation and slip layer, and has been proved to not be relevant to the pumpability of concrete. Therefore, it is urgent to develop a new method for evaluating and predicting the pumpability of fresh concrete.

Pumping experiment is possible to confirm the pumpability of fresh concrete. However, numerical flow simulation is thought to be a rapid, inexpensive, and time & labor saving method. Among the existing numerical methods, meshless particle methods, such as SPH and MPS, are suitable to pipe flow of fresh concrete. Since the interaction between particles can be well considered in particle methods, they have the potential to simulate heterogeneous properties of concrete and provide information about the dynamic segregation of concrete in pipe.

As a fundamental study of numerical analysis method of concrete pumping, this research aims to develop a numerical pipe flow approach based on the particle method to predict the flow & segregation behaviors of fresh concrete in pipe.

In Chapter 1, background, objectives, highlights and frame of the present research were explained.

In Chapter 2, the previous researches on numerical methods, rheological properties, segregation, and pipe flow of fresh concrete were reviewed, and the problems waiting to be resolved were summarized.

In Chapter 3, the original MPS method was improved to have complete implicit algorithms to simulate the flow of fresh concrete with high efficiency. The calculation efficiency and the applicability of weakly compressible SPH (WCSPH) and complete implicit MPS (I-MPS) approaches to the flow simulation of freshly mixed cementitious materials (FCM) were discussed. By comparing the numerical and experimental results of L-flow of fresh mortars, it is found that the WCSPH method would be suitable for flow simulation of fresh cementitious materials have low fluidity or they are subjected to low pressure, whereas the I-MPS method is of a wide application, especially for the fresh cementitious materials with high fluidity or subjected to a high pressure.

In Chapter 4, the I-MPS method was further improved to have the ability to calculate two-phases flow problems, considering the differences in particle size, density, and interaction of different sorts of particle. A new constituent model, called Double-phase & multi-particle (DPMP) model, was proposed and incorporated into the I-MPS to establish a numerical flow & segregation model for fresh concrete. It was verified that the flow & segregation model can simulate the segregation behavior of coarse aggregate in fresh concrete together with fresh concrete's flow behavior. Both the static and dynamic segregation behaviors of fresh concrete were investigated numerically, and the author found that the smaller the yield stress of the matrix mortar, the easier it is for the coarse aggregate to segregate. Low plastic viscosity of matrix mortar, large size of coarse aggregate, and large difference of flow speed between coarse aggregate and matrix mortar will result in an increase in the segregation velocity of coarse aggregate.

In Chapter 5, a numerical pipe flow method was proposed based on the flow & segregation model described in Chapter 4 to simulate the flow &segregation behaviors of fresh concrete in pipe. First, a macroscopic approach was used to describe the slip layer in pipe flow. This macroscopic approach can not only avoid the assumption of the composition and thickness of slip layer, but also simplify the numerical model and thus raise the calculation efficiency of numerical simulation. Then, based on this macroscopic approach of slip layer, the pressure-pipe flow rate relationship was clarified by theoretical investigation. Finally, a new numerical method of concrete's pipe flow was developed based on the flow & segregation model, the slip layer model, and the I-MPS method described in Chapter 3, and was used to predict the pumping pressure of concrete, and to simulate the flow & segregation behaviors of fresh concrete in the pipeline, including particle velocity distribution, pressure distribution, deformation distribution, and coarse aggregate distribution, etc. By comparing the numerical and theoretical results, the numerical pipe flow method developed in this study was verified.

Contents

Abstract ..... **i**

List of Figures ..... **vii**

List of Tables ..... **xi**

Chapter 1 Introduction **1**

1.1 Background of Research 1

1.2 Objectives of Research 5

1.3 Highlights of Research 6

1.4 Frame of Research 7

Reference 9

Chapter 2 Review of Previous Researches **11**

2.1 Introduction 11

2.2 Rheological Properties of Fresh Concrete 12

2.2.1 Direct Measurement of rheological properties *12*

2.2.2 Prediction of rheological properties *13*

2.3 Segregation of Fresh Concrete 16

2.3.1 Segregation Measurement Methods *16*

2.3.2 Influencing Factors of Segregation *17*

2.3.3 Segregation in Pipe Flow *18*

2.4 Concrete Flow in Pipeline 20

2.4.1 Pipe Flow of Fresh Concrete *20*

2.4.2 Formation of Slip Layer *21*

2.4.3 Properties of Slip Layer *21*

2.4.3 Prediction of Pumping Pressure *24*

2.5 Numerical Methods for Fresh Concrete 26

2.5.1 Computational Fluid Dynamics (CFD) Methods *26*

2.5.2 Discrete Particle Flow Methods *29*

2.5.3 Suspension Flow Methods *33*

2.6 Summary 35

Reference 36
Chapter 3 Comparison and Selection of Numerical Analysis Methods 41
3.1 Introduction 41
3.2 WCSPH and I-MPS Methods 44
3.2.1 Governing Equations 44
3.2.2 Kernel Function 44
3.2.3 Particle Density 45
3.2.4 Viscous Term Calculation 45
3.2.5 Pressure Solution 45
3.2.6 Pressure Term Calculation 46
3.3 Constitutive Models 48
3.3.1 Bingham Model 48
3.3.2 VGM Model 48
3.4 Boundary Conditions 50
3.5 Experiment 51
3.5.1 Mortar Mixtures and Rheological Parameters Type 51
3.5.2 L-Flow Test 53
3.6 Numerical Simulation of the L-flow Tests of Fresh Mortar 55
3.6.1 Numerical Analysis Conditions 55
3.6.2 Time Consumption of Numerical Simulation 56
3.6.3 Discussion of Calculation Accuracy 57
3.6.4 Applicable Condition of WCSPH 64
3.7 Conclusions 66
Reference 67
Chapter 4 Numerical Method for Predicting Flow and Segregation Behaviors of Fresh Concrete 69
4.1 Introduction 69
4.2 Numerical Simulation Method 71
4.2.1 Governing Equations 71
4.2.2 Algorithm of I-MPS Method 71
4.2.3 Rheological Model Used of Fresh Concrete 71
4.2.4 Boundary conditions 72

4.2.5 Validation of I-MPS method ... 72
4.3 Numerical Analysis Model of Fresh Concrete ... 74
4.3.1 Constituent model of fresh concrete ... 74
4.3.2 Interaction models between various particles in fresh concrete ... 75
4.3.3 Rheological Parameters for Expressing Inter-Particle Resistance ... 77
4.3.4 Movement calculation of coarse aggregate particle ... 80
4.4 Experimental Program and Numerical Simulations ... 82
4.4.1 Concrete Mixtures and Rheological Properties ... 82
4.4.2 L-box flow test and segregation measurement ... 83
4.4.3 Configuration of Numerical Simulations ... 84
4.5 Results and Discussion ... 85
4.5.1 L-box Flow Behaviors ... 85
4.5.2 Segregation Simulation of Fresh Concrete ... 86
4.5.3 Dynamic viscosity distribution ... 91
4.6 Conclusions ... 93
Reference ... 94
Chapter 5 Numerical Approach to Pipe Flow of Fresh Concrete ... 97
5.1 Introduction ... 97
5.2 Numerical Model of Pipe Flow ... 100
5.2.1 Numerical Analysis Method ... 100
5.2.2 Rheological Model of Bulk Concrete ... 100
5.2.3 Slip Layer Treatment ... 100
5.2.4 Constituent Models of Fresh Concrete ... 104
5.3 Numerical Simulation ... 105
5.3.1 Concrete Mixtures ... 105
5.3.2 Rheological Properties ... 105
5.3.3 Configuration of Numerical Simulations ... 106
5.4 Numerical Results and Discussion ... 110
5.4.1 Pumping Pressure-Flow Rate Relationship ... 111
5.4.2 Velocity Profile ... 112
5.4.3 Uneven Migration of Coarse Aggregates ... 113
5.5 Summary ... 115
Reference ... 116

Chapter 6 Conclusions and Future Works.....119

6.1 Conclusions..... 119

6.2 Future Works..... 121

6.2.1 Influencing Factors of Segregation During Pipe Flow 121

6.2.2 Flow Behaviors in Bend and Taper Pipes 121

6.2.3 Formation Mechanism of Concrete Blockage in Pipeline..... 121

List of Figures

Fig. 1.1 Pumping construction of concrete 1
Fig. 1.2 Concrete blockage in pipeline 2
Fig. 1.3 Frame of research 7
Fig. 2.1 Rheometers used to measure the rheological properties (yield stress and plastic viscosity) of fresh cementitious materials 12
Fig. 2.2 Segregation measurement methods 16
Fig. 2.3 3D segregation-rheology relationship 18
Fig. 2.4 Dynamic segregation in pumping pipe 19
Fig. 2.5 Pipe flow of fresh concrete (no slippage) 20
Fig. 2.6 Kaplan's model along with a representation of the flow in the pipe for both portion of the model 21
Fig. 2.7 Schematic representation of lubricating layer formation in a pipeline due to flow-induced particle migration in a pumped concrete 21
Fig. 2.8 Apparent slip velocity and slip layer: velocity in the fluid at the fluid –solid interface. Macroscopic scale (left) microscopic scale (right) 22
Fig. 2.9 Tribometers used to measure the properties of slip layer in literatures 23
Fig. 2.10 Slip resistance measurement device for fresh concrete 24
Fig. 2.11 Slid pipe rheometer 24
Fig. 2.12 Experimental results (left) and numerical simulations (right) at the same flow distance but different times 27
Fig. 2.13 Experimental results and numerical simulation of min-slump flow test 27
Fig. 2.14 Pressure distribution and velocity profile in pumping simulated by ANSYS 28
Fig. 2.15 Examples of obtained shapes of numerical results of ASTM slump test 29
Fig. 2.16 Pipe flow in the half open channel simulated by VOF 29
Fig. 2.17 Standard contact model between particles in DEM 30
Fig. 2.18 SPH simulation of fiber orientation in UHPC beams 32
Fig. 2.19 Simulation of self-compacting concrete flow in the J-ring test using SPH 32
Fig. 2.20 Different ways to discretize a system with particles and/or grid 33
Fig. 2.21 Numerical simulation of the slump flow test using a homogeneous approach (top) and using a heterogeneous approach (bottom) 34
Fig. 3.1 Original and regularized Bingham models 49
Fig. 3.2 VGM model and simplified VGM model 49

Fig. 3.3 Influence area of boundary particle 50
Fig. 3.4 The RSNS rheometer 51
Fig. 3.5 Shear stress-shear rate relationship of Series No.3 measured by B-type viscometer 52
Fig. 3.6 Position of mean stress τ_m on the rotor 53
Fig. 3.7 Relationship between slippage stress τ_m and slippage velocity V_S (series No.3) 53
Fig. 3.8 Geometry of L-box 54
Fig. 3.9 Experimental results of L-flow distance-flow time relationship 54
Fig. 3.10 Final flow shape and total flow time of mortars with different initial heights 54
Fig. 3.11 Flow distance - elapse time relationship for different particle resolutions (Series No.2) ... 55
Fig. 3.12 Simulation runtime of different numerical methods 56
Fig. 3.13 Particle distributions and pressure fields 57
Fig. 3.14 Influence of BSR on the numerical flow distance 58
Fig. 3.15 Numerical results and calculation errors for different mortars, considering boundary slippage resistance 59
Fig. 3.16 Effect of fluidity on calculation error of flow distance 60
Fig. 3.17 Effect of boundary repulsive force 60
Fig. 3.18 Effect of constitutive model on the error of numerical analysis 61
Fig. 3.19 Numerical results and calculation errors, using different constitutive models 61
Fig. 3.20 Numerical results and their errors for different initial heights of mortar in the vertical room 62
Fig. 3.21 Compression situations of fluid particles in the two simulations (initial height of mortar is 50cm) 63
Fig. 3.22 Statistical errors of numerical results for different initial heights of mortar in the vertical room 63
Fig. 3.23 The pressure acting on the center of the vertical room's bottom 63
Fig. 3.24 Permitted maximum flow velocity range (blue, orange, green solid line) for reliable WCSPH simulation 65
Fig. 4.1 Imaged fluid composition in MPS 71
Fig. 4.2 Influence domain of analyzed particle 71
Fig. 4.3 Interaction between particle *i* and neighbor particles 71
Fig. 4.4 Flow chart of I-MPS algorithm 72
Fig. 4.5 Taylor-Couette flow model 72
Fig. 4.6 Rotation velocity profiles in Taylor-Couette flow 73
Fig. 4.7 Constituent model of fresh concrete 74
Fig. 4.8 Constituent model of fresh concrete 75
Fig. 4.9 Formation of aggregate particle 75
Fig. 4.10 Random sizes and shapes of coarse aggregate particles (2D) 75

Fig. 4.12 Change of mean dynamic viscosity with aggregate volume fraction 77
Fig. 4.11 Three types of particle interaction models in fresh concrete 77
Fig. 4.13 Schematic diagram of normal fresh concrete and CA particle system 78
Fig. 4.14 Coarse aggregates with different sizes and shapes 78
Fig. 4.15 Increasement of CA particle size due to adhesive mortar 79
Fig. 4.16 Determination of rheological parameters used in numerical simulation 80
Fig. 4.17 Position calculation and modification of CA particle 81
Fig. 4.18 The slump test of two concretes 82
Fig. 4.19 RSNS rheometer 83
Fig. 4.20 Geometry of L-box 83
Fig. 4.21 Final flow shape of the fresh concrete in the L-box flow test 85
Fig. 4.22 Velocity profile of fresh concrete simulated by using DPMP model 86
Fig. 4.23 The static *SD* of coarse aggregate in each portion (left: No.1, right: No.2) 87
Fig. 4.24 Schematic diagram of forces acting on coarse aggregate particle 87
Fig. 4.25 Change of *SD* before and after static segregation 87
Fig. 4.26 Segregation velocities of CA particles with different size ranges (static segregation, No.2).. 88
Fig. 4.27 Vertical segregation velocities of aggregates in different concretes (dynamic segregation)... 89
Fig. 4.28 Vertical segregation velocities of aggregates with different sizes (dynamic segregation).. 89
Fig. 4.29 Horizontal segregation velocities of aggregates in different concrete (dynamic segregation)90
Fig. 4.30 Horizontal segregation velocities of aggregates with different sizes (dynamic segregation).. 90
Fig. 4.31 Segregation degree of coarse aggregate in different horizontal zones 91
Fig. 4.32 Position change of three parts of fresh concrete in the vertical room during the L-flow (No.1).... 91
Fig. 4.33 Viscosity distribution of fresh concrete in the vertical room after static segregation (upper: No.1, lower: No.2) 92
Fig. 4.34 Viscosity distribution of fresh concrete after dynamic segregation (Left: No.1, Right: No.2).. 92
Fig. 5.1 Concrete flow in pipe 100
Fig. 5.2 Apparent slip velocity and slip layer: velocity in the fluid at the fluid –solid interface. Macroscopic scale (left) microscopic scale (right) 101
Fig. 5.3 Velocity profile of pipe flow considering slip layer 103
Fig. 5.4 Constituent models of fresh concrete 104
Fig. 5.5 Schematic diagram of slip resistance measurement device 106
Fig. 5.6 Pressure analysis in 3D and 2D models 107
Fig. 5.7 Pumping pressure under 1500 cm^3/s of flow rate, calculated by using different diameters of fluid particle 108
Fig. 5.8 Pumping pressure under 1500 cm^3/s of flow rate, considering different thicknesses of slip layer 108

Fig. 5.9 Pressure distribution in Concrete No.1 at a flow rate Q=1500cm^3/s (t=5s) 110
Fig. 5.10 Velocity profile in Concrete No.1 at a flow rate Q=1500cm^3/s (t=5s)..... 110
Fig. 5.11 Numerical and theoretical pressures under different flow rates for Concretes No.1~No.3 111
Fig. 5.12 Comparison of numerical and theoretical pressures 111
Fig. 5.13 Velocity profile in the pipe at different height h (Concrete No.1) 112
Fig. 5.14 Migration of coarse aggregates 113
Fig. 5.15 Zoning of concrete for segregation analysis..... 114
Fig. 5.16 Variations of volume fraction φ of coarse aggregate with pipe flow time 114

List of Tables

Table 2.1 Summarization of the thickness of slip layer given in literatures 22
Table 3.1 Comparison of WCSPH and I-MPS 47
Table 3.2 Mix proportions of fresh mortar 51
Table 3.3 Mix proportions of fresh mortars and rheological parameters 53
Table 3.4 Outline of analytical models 56
Table 3.5 Numerical results and calculation errors of final flow distance with and without BSR 59
Table 4.1 Parameters for Taylor-Couette flow 73
Table 4.2 Mix proportions of concrete mixture 82
Table 4.3 Rheological parameters of materials 83
Table 4.4 Configuration information of particles 84
Table 5.1 Mix proportions of concrete mixture 105
Table 5.2 Bingham constants of fresh concretes 105
Table 5.3 Rheological constants of slip resistance equation 106
Table 5.4 Configuration information of particles 109

Chapter 1 Introduction

1.1 Background of Research

1.2 Objectives of Research

1.3 Highlights of Research

1.4 Frame of Research

Chapter 1
Introduction

1.1 Background of Research

Pumping technology of fresh concrete dates back to the 20th century and has become one of the most widely used approaches to place concrete. Concrete pumping plays a critical role in the modern construction industry. Pumping construction not only can shorten the construction time and reduce the labor intensity by offering a speedy, continuous casting, it also allows concrete casting in the locations where are difficulty to access. The simplified diagram of pumping construction is shown in **Fig. 1.1**. The usage of pumping construction continues to grow due to an increase in demand for large-scale construction projects such as high-rise buildings, long-span bridges, and others. Correspondingly, the requirements for concrete pumping technology are increasing, and pumping construction has gradually become a difficult and challenging matter. Some problems may occur during pumping, such as insufficient pumping pressure, pipe blockage, segregation, slump loss and air loss [1,2], etc. For these pumping problems, the workability of concrete has a crucial impact. Fresh concrete with low fluidity is not easy to be pumped, and will greatly reduce the pumping efficiency. Although high fluidity can improve pumping efficiency, concrete is easy to segregate, thereby reducing construction quality. Therefore, it is particularly important to prepare fresh concrete with appropriate workability according to pumping demands.

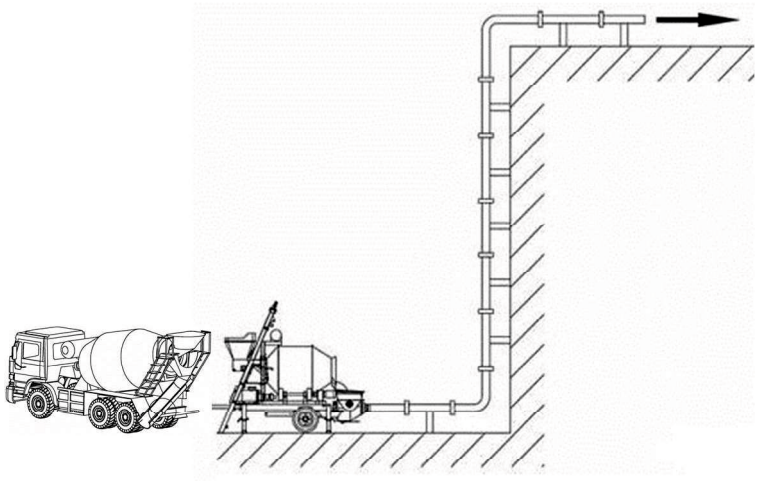

Fig. 1.1 Pumping construction of concrete

With the development of concrete's admixtures, various chemical and mineral admixtures, especially high-range water reducing agent provide great opportunity for the property improvement of concrete. As a result, the performances of fresh concrete present complexity and diversity. The properties of fresh concrete, such as self-compacting concrete (SCC) and high-performance concrete (HPC), are very different from conventional concrete [20], so that the knowledge and the guidelines of concrete pumping based on conventional concrete may be no longer applicable to new types of concrete [21]. Consequently, the optimization and development of prediction methods for concrete pumping have been becoming a crucial issue for the concrete industry.

In many construction sites and guidelines, the use of pumping is determined according to qualitative assessment of concrete pumpability based on the slump test or the slump flow test. However, for concrete pumping, the shear rate is typically around 10 s^{-1} to 100 s^{-1}, whereas, for the slump test, it is only 1 s^{-1} or less [22]. At such low shear rate, the results of slump test do not encapsulate the effects such as dynamic segregation and slip layer (also referred to as a boundary layer or lubrication layer), which may play a dominant role during pumping. Hence, the slump test may not be relevant for predicting the ability of concrete to flow in a pipe. Some fresh concrete, which are evaluated with proper pumpability according to current methods, may still have problems during pumping process (seen in **Fig. 1.2**) [23]. In other words, the test methods commonly used to measure the workability of fresh concrete cannot accurately evaluate and predict the pumpability of fresh concrete. Therefore, it is urgent to develop a new method for evaluating and predicting the pumpability of fresh concrete.

If one can accurately predict required pressure for pumping of a concrete mixture based on its properties, and accurately evaluate other aspects of pumpability such as static and dynamic stability, concrete mixtures can be adjusted in the laboratory for optimizing the pumpability. Although a few experimental devices such as sliding pipe rheometer have been invented to predict pumping pressure, besides the pumping pressure required for concrete flow, other concern about fresh concrete under pumping flow is the possibility of segregation, i.e. the separation of the paste from the aggregate phase, which usually leads to hose blockage. As mentioned above, the slip layer plays a dominant role during pumping. The slip layer is formed by that large aggregate particles tend to migrate towards the low shear zone. It is considered that coarse aggregates undergo the shear-induced migration towards the inner, while cement paste and a fraction of finer material move towards the pipe wall [24–26]. Thus,

Fig. 1.2 Concrete blockage in pipeline

the slip layer is composed of cement paste and a limited fraction of fine aggregate, aggregates are not evenly distributed in diameter direction. Also, in front of the concrete, the concentration of coarse aggregate is high, even a plug of coarse aggregates is formed [1,27]. Thus, the segregation prediction of pumped concrete is also an important issue.

Although the concrete pumping experiment is able to evaluate the pump pressure, limited by experimental conditions and insufficient measurement methods, the observable results in the experiment are limited. It is almost impossible to clear segregation behaviors of solid particles during the pumping process due to the invisibility of internal flow. Numerical analysis is thought to be a rapid, inexpensive, and time & labor saving method for pipe flow prediction. Among the existing numerical simulation methods, meshless particle methods, such as SPH and MPS, are suitable for simulating pipe flow of fresh concrete. In addition to the advantage that large deformation can be calculated because of unnecessity of computational grid generation, the particle methods have the possibility of analyzing the segregation behavior of fresh concrete [28], since the interaction between particles can be well considered in particle methods. Hence, the development of flow simulation methodology of fresh concrete based on the particle methods is an issue.

In numerical simulation, the meshless particle method is suitable for large deformation problem with fresh surface [4], i.e., the flow of fresh concrete. Now there are mainly three particle methods, so-called meshless method, which are Discrete Element Method (DEM), Smoothed Particle Hydrodynamics (SPH), and Moving Particle Semi-Implicit (MPS), respectively. Many DEM-based flow simulations of fresh concrete have been reported so far [5–7], but the input parameters, e.g. viscosity coefficient of dash-pot, stiffness of spring, representing interactions of imaginary rigid particles need to be calibrated, thus for different concrete mixtures, the setup of the input parameters is not easy. The SPH was originally developed in 1977 by Lucy [8] and, Monaghan and Gingold [9] for astrophysical applications (here called standard SPH). Later, Monaghan [10] further developed the new SPH algorithm for simulating the slightly compressible flows, which is usually called weakly compressible SPH. In weakly compressible SPH, incompressible fluids are treated as slightly compressible fluids for using WCSPH method. To completely solve this particle compression problem, the MPS algorithm was developed in 1996 in Japan [11], which solves a pressure Poisson equation at every time step to ensure the incompressibility of particle. However, for a fluid with high viscosity, such as fresh concrete, since an explicit algorithm is used for the viscous item, the calculation time step needs to be set very small to stabilize the calculation results [12], accordingly the calculation efficiency is reduced. Therefore, the MPS algorithm needs to be improved for the flow simulation of fresh concrete. So far, many flow simulation studies of fresh concrete have been found, using SPH method [13–16] and MPS method [17–19]. At this time, there is still a lack of detailed discussion on respective applicability and practicality of SPH and MPS in the concrete field.

Moreover, almost all current particle method based numerical analyses of fresh cementitious materials are for slump flow, L-flow or flow behaviors in rheometer. There is no meshless particle method that can predict pressure loss together with segregation behavior of pumped concrete now. It is urgent to establish a proper numerical model for concrete pumping based on the flow characteristics of fresh concrete in pipe. It is urgent to establish a proper numerical model to predict the pumping flow of fresh concrete in pipe based on particle method.

1.2 Objectives of Research

The main objectives of the present research are as following:

1. Optimize the MPS method by a completely implicit algorithm to make it more appropriate to fluids with high viscosity, such as fresh concrete. Clarify the applicability of weakly compressible SPH and complete implicit MPS methods for the flow simulation of fresh cementitious materials. Various factors on the applicability of these two numerical methods should be discussed quantitatively, including fluidity, adopted constitutive model, flow pressure, etc. Discuss which one is more suitable for pipe flow simulation.

2. Regarding the fresh concrete as a mixture of matrix mortar and coarse aggregate. Based on the meshless particle method, establish a two-phase flow & segregation model to calculate the interaction between different constituents in concrete. The numerical flow & segregation model should be able to predict the segregation behaviors of coarse aggregate in the flow process.

3. Develop a numerical approach to the pipe flow of fresh concrete based on the flow & segregation model. This approach should take into account the influence of the slip layer on the pumping flow, and use an appropriate method to calculate the influence. Using this numerical approach, it should be possible to predict not only the pipe flow of fresh concrete but also the segregation behaviors during pumping.

1.3 Highlights of Research

1. The original MPS method is improved to have complete implicit algorithms to simulate the flow of fresh concrete with high efficiency. Moreover, the optimized MPS method can be used to calculated two-phase flow problems of different sizes, different densities, and different rheological parameters. Therefore, the optimized MPS method has an ability to simulate the segregation behaviors of coarse aggregate in fresh concrete.

2. A macroscopic approach is proposed to describe the slip layer in pipe flow. This approach can not only avoid the assumption of the microstructure and properties of the slip layer, but also simplify the numerical pipe flow model and raise the calculation efficiency of the numerical simulation. Moreover, based on the treatment method of slip layer, the pressure - pipe flow rate relationship is clarified by a series of theoretical investigations.

3. Fresh concrete mixture is considered as a discontinuous system built up by matrix mortar and coarse aggregate. The coarse aggregates are supposed to be wrapped by excess mortar, and the excess mortar plays a lubricating role in the flow process. The rheological properties of specific concrete with the maximum compact volume fraction are used as those of coarse aggregate wrapped by excess mortar. An interaction model between discrete particles in fresh concrete is proposed, using multi-viscosity model and multi-density model to calculate the viscosity interaction and pressure acting between different constituents in concrete, respectively.

4. As a new constituent model, Double-phase & multi-particle (DPMP) model is proposed and incorporated into the MPS to simulate the pipe flow of fresh concrete. The DPMP model regards fresh concrete as a mixture of matrix mortar and coarse aggregate, instead of treating concrete as a homogeneous material as in the general fluid model. The DPMP model can be used to predict the pumping pressure of concrete and simulate the flow behaviors of concrete in the pipeline (such as velocity distribution, pressure distribution, and deformation distribution). More importantly, the model can predict the segregation behaviors of fresh concrete.

1.4 Frame of Research

The thesis contains six chapters, and the frame of the research is shown in **Fig. 1.3**.

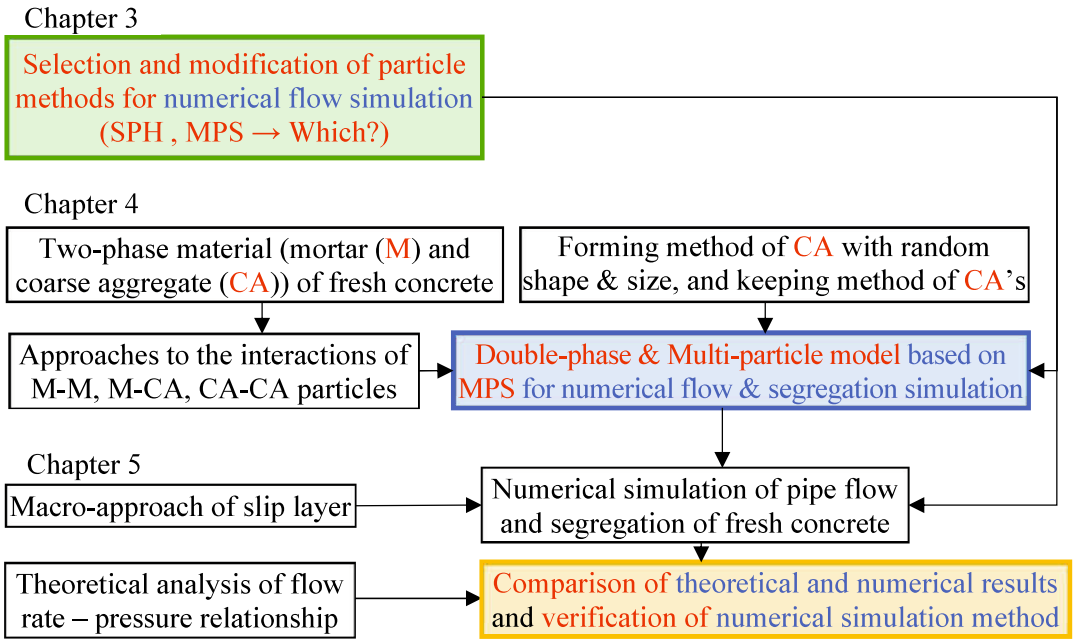

Fig. 1.3 Frame of research

Chapter 1 represents the background together with the motivation of the research, and gives the outline of the whole thesis.

Chapter 2 concludes the previous research achievements containing the development of particle method (SPH and MPS) and its application in flow simulation of fresh concrete, the discussion of two-phase flow particle method, the prediction of concrete rheological parameters, and the research of concrete pumping.

Chapter 3 clarifies the respective applicability of weakly compressible SPH (WCSPH) and complete implicit MPS (I-MPS) methods for the flow simulations of fresh cementitious materials. In this chapter flow behaviors of fresh mortars in the L-box are observed experimentally and simulated by WCSPH and I-MPS, respectively. Then the effects of various factors on the applicability of two numerical methods are discussed quantitatively, including mortar's fluidity, constitutive law used, boundary slippage resistance, and initial gravity-induced pressure. Through the discussion above, this chapter is trying to find an appropriate particle method for simulating flow and segregation under high pressure.

Chapter 4 proposes a MPS (Moving Particle Semi-explicit) based numerical flow segregation approach for fresh concrete, named Double-Phase & Multi-Particle (DPMP) model. In DPMP model, the fresh concrete is regarded as mixture of coarse aggregates and matrix mortar. The coarse aggregates are represented by rigid bodies, the interaction between different constituent materials is considered separately. And the density difference between mortar and coarse aggregate is also

considered. The DPMP model is used to simulate the L-box flow of high fluidity concrete. Both the static segregation and dynamic segregation behaviors are discussed.

Chapter 5 develops a numerical method to simulate pipe flow and dynamic segregation of fresh concrete. The MPS method is chosen and improved for the pipe flow simulation of fresh concrete. The effect of slip layer in the pipe flow is considered by a macroscopic approach. The apparent slip velocity is used to calculate the slip resistance and the slip flow rate of slip layer. Two constituent models are used to describe fresh concrete, called single-phase & mono-particle (SPMP) model and double-phase & multi-particle (DPMP) model, respectively. By comparing the numerical and theoretical pumping pressures of three concretes, it is validated that both of the constituent models can predict the pumping pressure and velocity profile of concrete in pipe flow. Moreover, the DPMP model can also simulate the segregation behaviors of coarse aggregate particles during the pipe flow.

Chapter 6 summarizes the thesis by presenting the most significant findings and briefly discusses the future work.

Reference

[1] M. Jolin, D. Burns, B. Bissonnette, F. Gagnon, L.-S. Bolduc, B. Bissonnette, Understanding the pumpability of concrete, in: Shotcrete Undergr. Support XI, 2009.

[2] H. Kwon, C.K. Park, J.H. Jeong, S.D. Jo, S.H. Lee, Prediction of concrete pumping : part II — analytical prediction and experimental verification, ACI Mater. J. 110 (2013) 657–668.

[3] Z. Li, State of workability design technology for fresh concrete in Japan, Cem. Concr. Res. 37 (2007) 1308–1320.

[4] G.R. Liu, M.B. Liu, Smoothed Particle Hydrodynamics, World Scientfic, 2003.

[5] X. Zhang, Z. Zhang, Z. Li, Y. Li, T. Sun, Filling capacity analysis of self-compacting concrete in rock-filled concrete based on DEM, Constr. Build. Mater. 233 (2020).

[6] V. Mechtcherine, S. Shyshko, Simulating the behaviour of fresh concrete with the Distinct Element Method - Deriving model parameters related to the yield stress, Cem. Concr. Compos. (2015).

[7] Y. Zhan, J. Gong, Y. Huang, C. Shi, Z. Zuo, Y. Chen, Y. Zhan, J. Gong, Y. Huang, C. Shi, Z. Zuo, Y. Chen, Numerical study on concrete pumping behavior via local flow simulation with Discrete Element Method, Materials (Basel). 12 (2019) 1415.

[8] L.B. Lucy, A numerical approach to the testing of the fission hypothesis, Astron. J. 82 (1977) 1013–1024.

[9] R.A. Gingold, J.J. Monaghan, Smoothed particle hydrodynamics: Theory and application to non-spherical stars, Mon. Not. R. Astron. Soc. 181 (1977) 375–389.

[10] J.J. Monaghan, Simulating free surface flows with SPH, J. Comput. Phys. 110 (1994) 399–406.

[11] S. Koshizuka, Y. Oka, Moving-Particle Semi-implicit method for fragmentation of incompressible fluid, Nucl. Sci. Eng. 123 (1996) 421–434.

[12] J.J. Monaghan, J. J., On the problem of penetration in particle methods, J. Comput. Phys. 82 (1989) 1–15.

[13] R. Deeb, S. Kulasegaram, B.L. Karihaloo, 3D modelling of the flow of self-compacting concrete with or without steel fibres. Part I: slump flow test, Comput. Part. Mech. 1 (2014) 373–389.

[14] R. Deeb, S. Kulasegaram, B.L. Karihaloo, 3D modelling of the flow of self-compacting concrete with or without steel fibres. Part II: L-box test and the assessment of fibre reorientation during the flow, Comput. Part. Mech. 1 (2014) 391–408.

[15] H. Lashkarbolouk, M.R. Chamani, A.M. Halabian, A.R. Pishehvar, Viscosity evaluation of SCC based on flow simulation in the L-box test, Mag. Concr. Res. 65 (2013) 365–376.

[16] G. Cao, Z. Li, Numerical flow simulation of fresh concrete with viscous granular material model and smoothed particle hydrodynamics, Cem. Concr. Res. 100 (2017) 263–274.

[17] Y. Uehara, K. Sakihara, Y. Yamada, S. Urano, A basic study on slump analysis of high accuracy MPS for fresh concrete, Cem. Sci. Concr. Technol. 67 (2013) 626–633.

[18] S. Urano, H. Nemoto, K. Sakihara, Application of flow simulation for evaluation of filling-ability of self-compacting concrete, J. Japan Soc. Civ. Eng. Ser. E2 (Materials Concr. Struct. 68 (2012) 38–48.

[19] I. Tsunakiyo, I. Shigeo, Y. Yoshitomo, T. Jun, Three-dimensional flow analysis of fresh concrete considering coarse aggregate by MPS method, Proc. Japan Concr. Inst. 26 (2004) 1161–1166.

[20] D. Feys, G. De Schutter, R. Verhoeven, K.H. Khayat, Similarities and differences of pumping conventional and self-compacting concrete, RILEM Bookseries. (2010).

[21] D. Feys, G. De Schutter, R. Verhoeven, Parameters influencing pressure during pumping of self-compacting concrete, Mater. Struct. Constr. 46 (2013) 533–555.
[22] M. Choi, C.F. Ferraris, N.S. Martys, D. Lootens, V.K. Bui, H.R.T. Hamilton, Metrology deeds for predicting concrete pumpability, Adv. Mater. Sci. Eng. 2015 (2015) 1–10.
[23] E. Secrieru, W. Mohamed, S. Fataei, V. Mechtcherine, Assessment and prediction of concrete flow and pumping pressure in pipeline, Cem. Concr. Compos. 107 (2020).
[24] M. Choi, N. Roussel, Y. Kim, J. Kim, Lubrication layer properties during concrete pumping, Cem. Concr. Res. 45 (2013) 69–78.
[25] G. De Schutter, D. Feys, Pumping of fresh concrete: insights and challenges, RILEM Tech. Lett. 1 (2016) 76.
[26] E. Secrieru, J. Khodor, C. Schröfl, V. Mechtcherine, Formation of lubricating layer and flow type during pumping of cement-based materials, Constr. Build. Mater. 178 (2018) 507–517.
[27] M. Choi, C.F. Ferraris, N.S. Martys, V.K. Bui, H.R.T. Hamilton, D. Lootens, Research needs to advance concrete pumping technology, Gaithersburg, MD, 2015.
[28] Z. Li, Z. Xu, R. Yoshioka, Flow simulation of fresh concrete using SPH method with consideration of geometry of particles, in: Sixth Int. Conf. Constr. Mater., Fukuoka, Japan, 2020: p. (in CD).

Chapter 2 Review of Previous Researches

2.1 Introduction

2.2 Rheological Properties of Fresh Concrete

2.3 Segregation of Fresh Concrete

2.4 Concrete Flow in Pipeline

2.2 Numerical Methods for Fresh Concrete

2.6 Summary

Chapter 2
Review of Previous Researches

2.1 Introduction

In this chapter, the previous researches relating to the present research are summarized and commented.

Section 2.2 investigated the prediction methods of rheological properties of fresh concrete materials are investigated. Section 2.3 summarized the segregation of fresh concrete and its influencing factors. The important results of concrete pumping research and future research needs have been concluded in Section 2.4. Section 2.5 discussed the development and application of numerical methods for flow simulation of fresh concrete.

2.2 Rheological Properties of Fresh Concrete

The workability of fresh concrete plays an important role in concrete construction. The workability of fresh concrete is mainly determined by the rheological properties of fresh concrete. Thus, the rheological properties of fresh concrete have a significant effect on evaluating the mix proportion of the concrete mixture as well as flowing behaviors and pumpability. The rheological properties of fresh concrete are usually described by a constitutive model (rheological model). Nowadays, in most of the flow simulations, the Bingham model is adopted as a constitutive model of fresh concrete. The Bingham model has a linear relationship between shear stress (τ) and shear strain rate ($\dot{\gamma}$). This defines yield stress (τ_b) and plastic viscosity (μ_b). Their relationship is expressed as follow:

$$\tau = \tau_b + \mu_b \dot{\gamma} \tag{2.1}$$

The measurement and prediction methods of rheological parameters (yield stress and plastic viscosity) are summarized below.

2.2.1 Direct Measurement of rheological properties

Many kinds of rheometer are developed for measuring the rheological properties of fresh cementitious materials. The widely used rheometers for measuring the yield stress and plastic viscosity are BML, BTRHEOM, and Two-Point, as shown in **Fig. 2.1**. Each instrument employs a different rotational geometer: BML uses coaxial cylinders, BTRHEOMB uses parallel plates (blades), Two-Point uses rotating vanes.

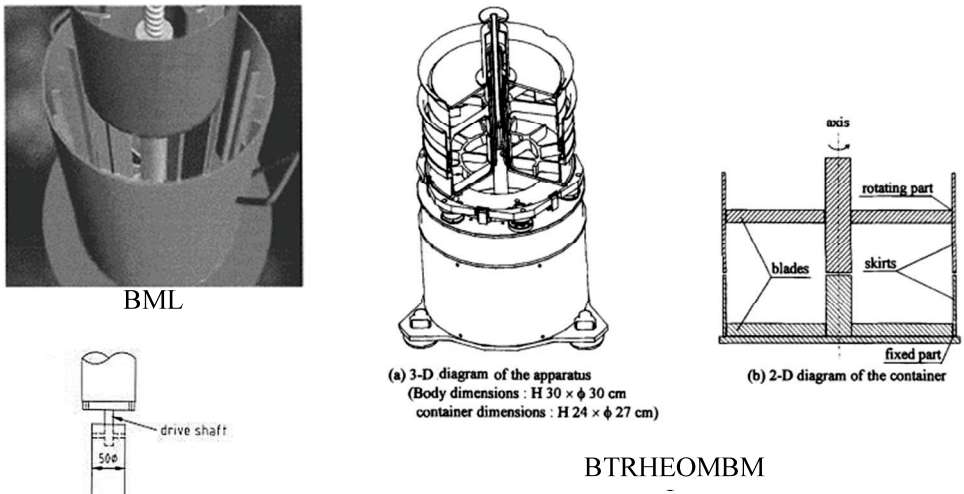

Fig. 2.1 Rheometers used to measure the rheological properties (yield stress and plastic viscosity) of fresh cementitious materials

■ **The BML Rheometer**

The BML rheometer [1,2] is coaxial cylinders rheometer. The outer cylinder of the BML viscometer rotates while the stationary inner cylinder measures torque. Both cylinders have vertical ribs to reduce slip. The inner and outer cylinder sizes can be changed based on the size of the aggregate in the concrete being tested. At a constant angular velocity, the shear rate in the concrete is non-uniform at the bottom of the outer cylinder. Therefore, in order to more accurately measure torque, the inner cylinder is split into three parts so that only the middle section of the inner cylinder measures torque.

The BML rheometer is intended for flowable concretes with slump greater than 12 cm and can be used for self-consolidating concrete. The device has also been used successfully for low slump concretes with slumps of 5 ~ 6 cm. For lower slump concretes the inner cylinder can be replaced with blade impeller system.

■ **The BTRHEOM Rheometer**

The BTRHEOM rheometer [2,3] is a parallel plate that measures the yield stress and plastic viscosity of soft-to-fluid concrete (slump higher than 10 cm, up to self-consolidating concrete). The device consists of a 240 mm diameter, 100 mm tall cylindrical container with blades mounted at the top and bottom of the container. The bottom blade is fixed while the top blade rotates and measures torque. The motor is housed below the container and is connected to the top blade through a 40 mm diameter inner shaft in the concrete container. The device includes a vibrator to consolidate the concrete and to measure the effect of vibration on the rheological parameters. The test is conducted by turning the top blade at different speeds and recording the resulting torque.

Different versions of the BTRHEOM rheometer have been developed to eliminate several drawbacks of the original device. The motor is located above the skirts in Ref. [4]. The top blade is fixed and the bottom blade is driven by the motor and measures torque in Ref. [5].

■ **The Tattersall Two-Point Rheometer**

The Tattersall two-point device [6] was one of the earliest attempts to measure the rheology of concrete based on the Bingham model and one of the fires devices to use impeller geometry. The device has been refined over the years by Tattersall and other researchers and continues to be widely used in research [7].

The above rheometers all assume that fresh concrete is a homogeneous material, and cannot reflect the non-uniformity of the material, especially after segregation.

2.2.2 Prediction of rheological properties

■ **Prediction Based on Consistency Tests**

Rheological properties of fresh concrete are mostly often associated with the slump result. Many investigations have been done to predict the rheological properties of fresh concrete based on the result of slump test.

Based on numerous experiments, Murata et al. [8] proposed a relationship between the yield stress and the slump flow S_f with slump ranging from 12.5 cm to 26 cm, as shown in the follow:

$$\tau_b = 714 - 473\log\left(S_f/10\right) \tag{2.2}$$

Considering the density of concrete, Sedran and de Larrard [9] established equations predicting the yield stress and the plastic viscosity with slump flow above 500 mm, as:

$$\tau_b = \left(808 - S_f\right)\frac{\rho g}{11740} \tag{2.3}$$

$$\mu_b = \frac{\rho g}{10000}\left(0.026S_f - 2.39T_{500}\right) \tag{2.4}$$

where, T_{500} is time required for the concrete to spread to a diameter of 500 mm.

There are many other prediction formulas based on slump test. However, the scope of application of different prediction formulas is different, and there are discrepancies between the prediction results. Moreover, these prediction formulas also assume concrete as a homogeneous material. Once the concrete segregates, the reliability of the prediction results is low.

■ **Prediction Based on Constituents**

Concrete is a sort of composite material containing cement, mineral admixtures, water, aggregates and chemical admixtures. Some researchers considered fresh concrete as a concentrated suspension in which solids are dispersed in the fluid phase water [10,11] while others regarded fresh concrete as a two-phase system that coarse aggregates are dispersed in the mortar [12,13]. Its rheological properties depend on the quality of each constituent used in the concrete mixture and their interactions. So that, it is possible to predict the rheological properties based on the constituents of the concrete mixture.

If the system is considered as homogenous suspension, the Krieger and Dougherty equation [14,15] can be used to calculate the plastic viscosity from the volume fraction of solid particles. The Krieger and Dougherty equation is:

$$\frac{\mu}{\mu_0} = \left(1 - \frac{\varphi}{\varphi_m}\right)^{-[\mu]\varphi_m} \tag{2.5}$$

where, μ_0 is viscosity of the medium, φ is volume fraction of aggregate, φ_m is maximum packing volume fraction of aggregate, $[\mu]$ is intrinsic viscosity.

Many researchers imitated the Krieger and Dougherty equation, and derived the plastic viscosity prediction model of fresh concrete based on the constituents. Considered fresh concrete as a suspension with multiple sizes of particle, assuming the relative size are sufficient to have the condition of zero interaction, the viscosity can be calculated from the unimodal viscosity of each size, namely Farris model [16]:

$$\mu = \mu_0\left(1 - \frac{\varphi_1}{\varphi_{m1}}\right)^{-[\mu_1]\varphi_{m1}}\left(1 - \frac{\varphi_2}{\varphi_{m2}}\right)^{-[\mu_2]\varphi_{m2}} \tag{2.6}$$

If aggregates in fresh concrete are divided into coarse and fine aggregates, the Farris model can be used in the following form [17]:

$$\mu = \mu_0 \left(1 - \frac{\varphi_S}{\varphi_{S,m}}\right)^{-[\mu_S]\varphi_{S,m}} \left(1 - \frac{\varphi_G}{\varphi_{G,m}}\right)^{-[\mu_G]\varphi_{G,m}} \tag{2.7}$$

where, φ_S and $\varphi_{S,m}$ are sand volume fraction and maximum solid volume, respectively. φ_G and $\varphi_{G,m}$ are sand volume fraction and maximum gravel solid volume. $[\mu_S]$ and $[\mu_G]$ are intrinsic viscosity of fine coarse aggregate, respectively.

Mahaut et al. [18] stated that the relationship between the yield stress of suspensions and the particle volume fraction fitted well with the Chateau-Ovarlez-Trung model [19], as shown in the following:

$$\tau = \tau_0 \cdot \sqrt{(1-\varphi)\cdot\left(1 - \frac{\varphi}{\varphi_m}\right)^{-[\tau]\varphi_m}} \tag{2.8}$$

where, τ_0 is yield stress of the medium, φ is volume fraction of aggregate, φ_m is maximum packing volume fraction of aggregate, $[\tau]$ is intrinsic yield stress.

The prediction models of viscosity and yield stress of fresh concrete mentioned above are functions relate to the concertation of aggregate in fresh concrete. These models allow to considering the heterogeneity of concrete materials, which may be caused by segregation.

2.3 Segregation of Fresh Concrete

2.3.1 Segregation Measurement Methods

■ **Column Segregation Test**

In the column segregation method, fresh concrete is poured in an PVC mold in one lift and allow the specimen to stand for 15 min. Concrete from top and bottom portions of the PVC pipe are then collected and washed out. The mass of coarse aggregate in the top section and bottom section are used to calculate the segregation index.

■ **V-funnel Test**

V-funnel method was developed by Japan Society of Civil Engineers. The test measures the variation of flow times following different periods of resting after filling the SCC in the V-funnel. The segregation index is equal to $(T_5\text{-}T_0)/T_0$, where T_5 and T_0 are flow times for filling the V-funnel after 5 and 0 minutes resting.

■ **Slump Flow Test**

Segregation resistance can be evaluated by observing the periphery of the concrete after the slump flow test. Spangenberg et al. [20] investigated the segregation in slump test and found that slump in

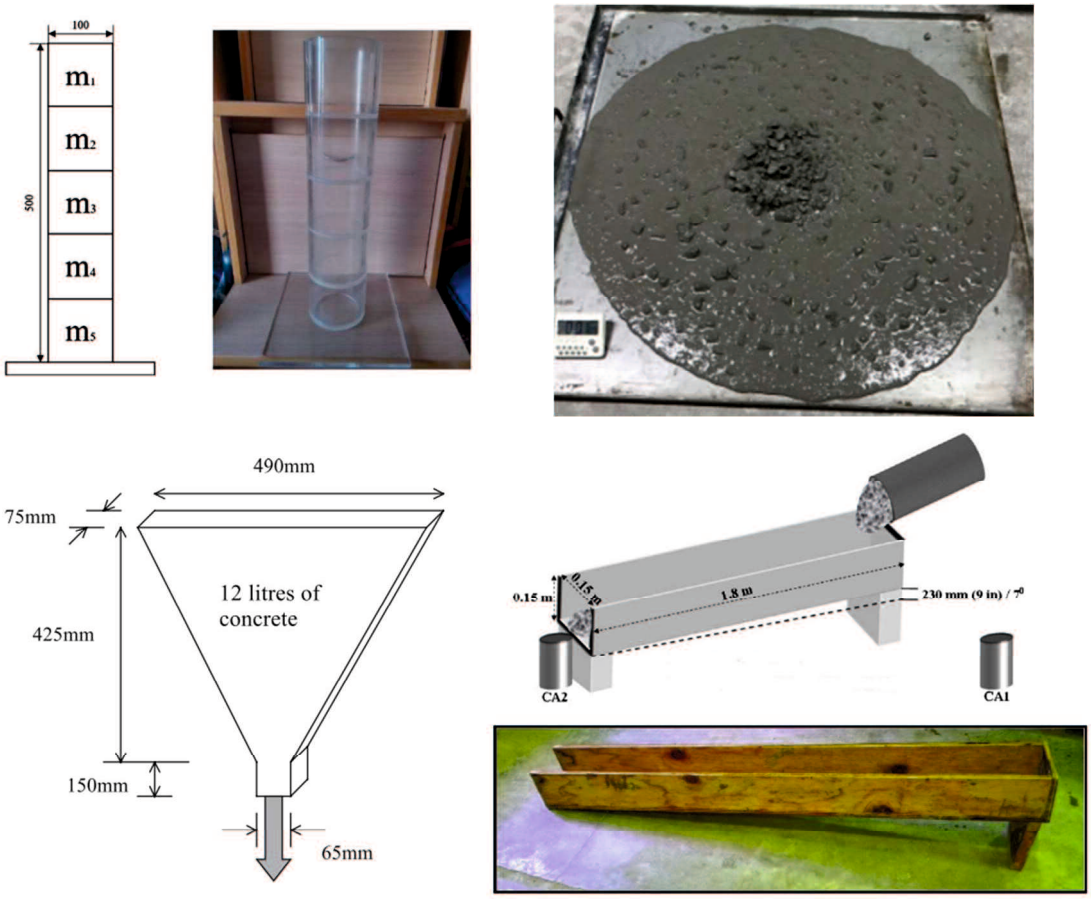

Fig. 2.2 Segregation measurement methods

the case of conventional concrete is only weakly affected by flow induced particle migration, slump flow for self-compacting concrete is affected by both a potential gravity induced particle migration and wall effects. When there is no border of water, the concrete is regarded as having good dynamic segregation resistance. A Visual Stability Index (VSI) ranging from 0 to 3 is used to rate the SCC [21]. This method is going to be part of ASTM standard for slump flow.

- **Flow Trough Test**

The flow trough mold [22] is made by assembling 25 mm thick wood boards to form a 0.15 m by 0.15 m by 0.18 m trough. The 0.23 m height difference between two ends gives a 7° angle of inclination, which allows the SCC to flow to the lower end. Fresh concrete has a volume of 13.5 L is poured onto the trough from the higher end and collected from the lower end in the two 100 mm by 200 mm molds. One collected at the beginning of the test, and the other collected at the end of the test. The coarse aggregates are wash out and weighed. The dynamic segregation index is calculated as (CA1-CA2)/CA1, where CA1 is the weight of coarse aggregate in the first mold and CA2 is the weight of coarse aggregate in the second mold.

2.3.2 Influencing Factors of Segregation

Safawi et al. [23] observed the segregation tendency in the vibration of high fluidity concrete, and got the results that concrete with lower viscosity has a higher segregation tendency. Besides, larger-sized aggregate is more dominant in determining the segregation pattern as compared with smaller ones.

Pan et al. [24] measured the rheological properties and vibration segregation of quite amount of fresh concrete with various fluidities, concluded the effect of rheological properties of matrix mortar on the segregation of fresh concrete, as shown in **Fig. 2.3**. It is shown that fresh concrete with low yield stress easily has severe segregation. The segregation of fresh concrete also increases with the decrease of plastic viscosity. Sand ratio and high range water reducer also have significant influences on segregation since they can change the yield stress of concrete.

Gao et al. [25] yield the results that the plastic viscosity plays a main role than yield stress in controlling vibration-induced segregation, fresh concrete with a higher yield stress had a better resistance to vibrating duration.

Spangeberg et al. [20] divided particle migration in fresh concrete into two types: shear induced particle migration and gravity induced particle migration. From Stoke's law for dilute spheres in Newtonian fluids, neglecting any other non-Newtonian features of the yield stress of the surrounding fluid, the vertical settling velocity can be written as:

$$V_{set} = g\Delta\rho a^2 / 18\mu_0 \tag{2.9}$$

where, $\Delta\rho$ is density difference between the aggregates and the suspending phase, a is radius of sphere particle.

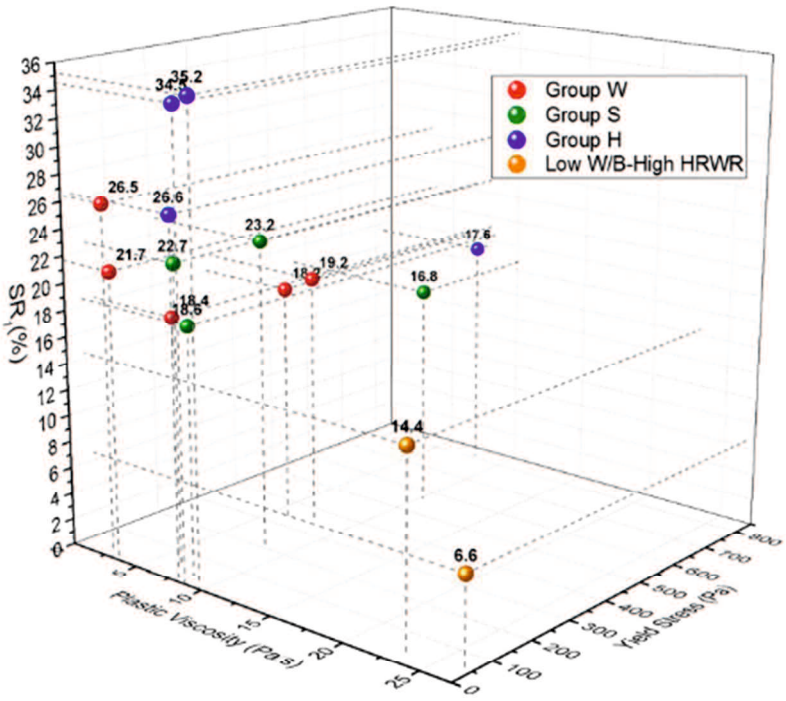

Fig. 2.3 3D segregation-rheology relationship

In addition, shape and texture on coarse aggregate also play a role on the behavior of fresh concrete. Shape and texture affect the demand for sand. Flaky, elongated, angular, and rough particles have high voids and require more mortar to fill the voids and provide a good workability. So that, poorly shaped aggregates may also increase segregation.

Based on the previous researches mention above, it can be concluded that the influencing factors of segregation are yield stress and viscosity of matrix mortar, density difference between the aggregates and the suspending phase, and size and shape of coarse aggregate. Low yield stress, low viscosity, large density difference, large aggregate size and poor shaped aggregate can lead to a severe segregation.

2.3.3 Segregation in Pipe Flow

Segregation is an additional factor that can influence flow properties of fresh concrete. During pumping of concrete, two types of coarse aggregate dynamic segregation can be considered: a particle migration radially (from the wall to the center), a longitudinal motion of particles to the front of the flow. The slip layer is formed by that large aggregate particles tend to migrate towards the low shear zone. It is considered that coarse aggregates undergo the shear-induced migration towards the inner, while cement paste and a fraction of finer material move towards the pipe wall [26–28]. Thus, the slip layer is composed of cement paste and a limited fraction of fine aggregate, aggregates are not evenly distributed in diameter direction. Also, in front of the concrete, the concentration of coarse aggregate is high, even a plug of coarse aggregates is formed [29,30], as shown in **Fig. 2.4**.

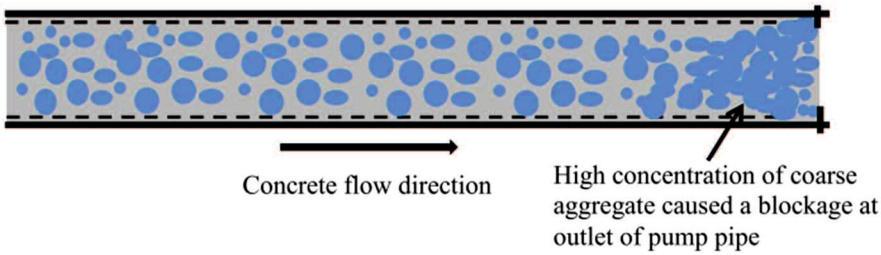

Fig. 2.4 Dynamic segregation in pumping pipe

As stated above, dynamic segregation plays an important role in characterizing concrete flow in a pipe. Once the segregation takes place, the concentration of aggregate in different parts of the concrete would become uneven, resulting in changes in yield stress and viscosity of rheological properties. So that leads to hose blockage during pumping and damage of workability after pumping. Thus, the segregation prediction of pumped concrete is an important issue.

The current research on segregation of fresh concrete is almost all based on experimental research. Experiments, especially large-scale construction experiments, require a lot of time, material and labor. In addition, the experimental results have large errors and poor repeatability. Limited by experimental conditions and insufficient measurement methods, the observable results in the experiment are limited. It is impossible to analyze the segregation movement of coarse aggregates in fresh concrete, and the changes in the flow velocity distribution and rheological properties of the concrete during the segregation process cannot be measured in the experiment. However, these problems can be easily solved in numerical simulation. Therefore, it is an urgent issue to conduct numerical simulation studies on the segregation behaviors of fresh concrete.

2.4 Concrete Flow in Pipeline

2.4.1 Pipe Flow of Fresh Concrete

Pumped concrete is often considered as Bingham fluid flowing along the pump pipe under pressure. Generally, when viscosity fluid flows in a cylinder pipe, assuming that no slippage occurs between the fluid and the pipe wall, the shear stress of the fluid varies linearly from the maximum value at the pipe wall to 0 Pa at the center, which can be expressed by the following:

$$\tau = \frac{\pi r^2 P}{2\pi r L} = \frac{r}{2} \cdot \frac{P}{L} \tag{2.10}$$

where, τ is shear stress, r is radius, L is length of pipeline, P is pumping pressure.

Combing the shear rate with the rheological model of concrete and dividing it along the cross-section area of the pipe, the flow velocity profile of the concrete in the cross-section of the pipe can be obtained. However, the fresh concrete is generally regarded as a Bingham fluid, rather than a Newtonian fluid. It has a distinct flow characteristic from Newtonian fluid [31]. Fresh concrete will only deform when the shear stress is greater than the yield stress. Based on this, it is believed that there will be a no-shearing zone around the symmetry axis in [32]. So that, the velocity profile of fresh concrete in pipe cross-section is shown in **Fig. 2.5** and velocity V at radius of r can be expressed by:

$$V = \frac{P(R^2 - r^2)}{4L\mu_b} - \frac{\tau_0 (R - r)}{\mu_b} \quad r \in [R, r_0] \tag{2.11}$$

where, V is flow velocity, R is inner radius of pumping pipe, τ_0 is yield stress (Pa), μ_b is plastic viscosity (Pa·s). r_0 is radius of plug flow, which equals to $2\tau_b \cdot L/P$.

Kaplan suggested that at low velocities, the concrete moves as a block in the pipe, with only a small thickness of slip layer near the pipe wall (often identified as plug flow). As the velocity increases, the pressure imposed on bulk concrete is sufficient to initiate shear flow in the bulk concrete (the applied shear stress is greater than the yield stress), accordingly generating a viscous flow in the concrete [29]. Thus, concrete flow in a pipe typically occurs in three layers or regions, as shown in **Fig. 2.6**: (i) slip layer or lubrication layer, (ii) shearing layer, (iii) plug flow layer. Total of the shearing layer and the plug flow layer is referred to as bulk concrete.

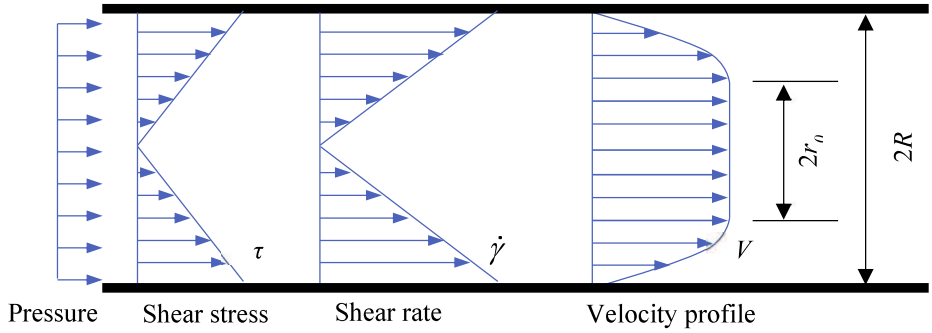

Fig. 2.5 Pipe flow of fresh concrete (no slippage)

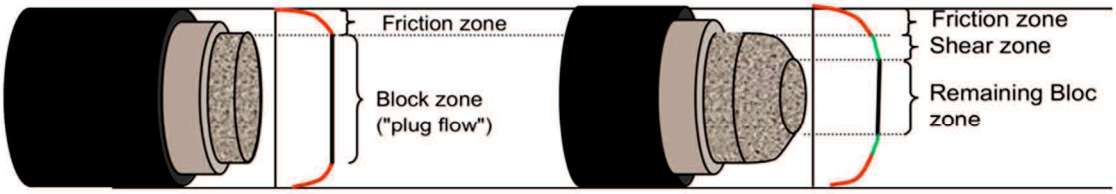

Fig. 2.6 Kaplan's model along with a representation of the flow in the pipe for both portion of the model

2.4.2 Formation of Slip Layer

Fresh concrete is a kind of heterogeneous composite mixture containing water, cement and filler, and aggregates with a wide range of sizes. Forming of a slip layer is mostly related to the flow-induced particle migration [33,34]. During pumping, shear deformation concentrates at the pipe wall, and the magnitudes of shear rate can reach over 100 s^{-1} [26]. The high shear rate can involve the phenomena that aggregates move slightly towards the pipe center where the shear rate is lower. As a consequence, cement paste and a fraction of finer material move towards the pipe wall, forming the slip layer (also known as lubrication layer) [27]. The schematic representation [28] is shown in **Fig. 2.7**. The process strongly depends on the magnitude of the induced shear stress. Shear stress increases as a function of particle size, and the particle movement is most pronounced on the scale of the coarse aggregates [20].

The movement of concrete without a sufficiently formed slip layer is immediately marked by a severe increase on pumping pressure and may even result in blockage [32]. Hence, overall pumping behaviors depend mainly on not only rheological properties of the bulk concrete but also properties of the slip layer.

2.4.3 Properties of Slip Layer

Depending on the scale of observation, either a slip layer or a slip velocity may be observed [35]. At large scales of observation (macroscopic level), an apparent slip velocity may be measured whereas, at smaller scales of observation, a fine material, slip layer appears, in which the velocity evolves from zero at the wall to the apparent slip velocity at the boundary of the slip layer (see **Fig. 2.8**).

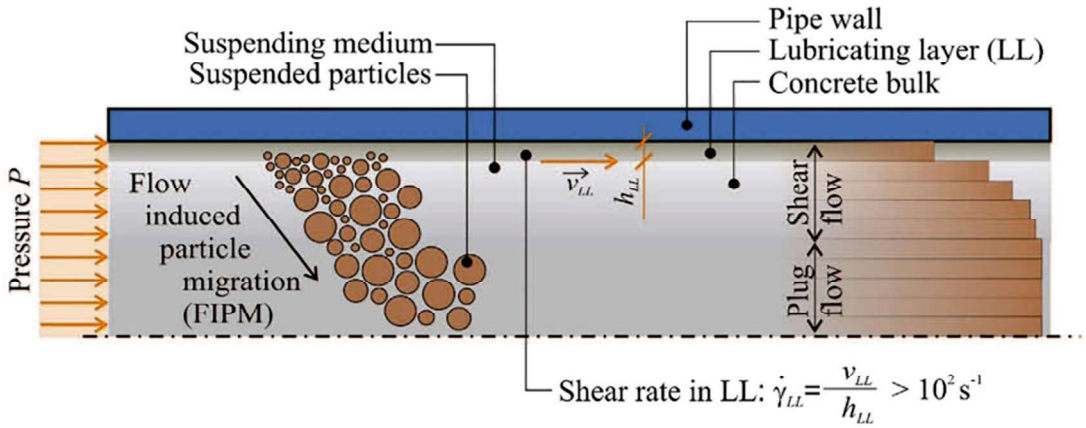

Fig. 2.7 Schematic representation of lubricating layer formation in a pipeline due to flow-induced particle migration in a pumped concrete

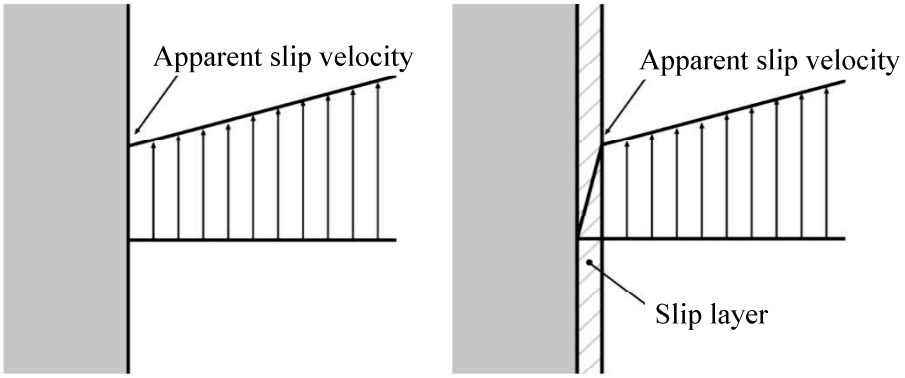

Fig. 2.8 Apparent slip velocity and slip layer: velocity in the fluid at the fluid –solid interface. Macroscopic scale (left) microscopic scale (right)

■ **Microscopic Properties of Slip Layer**

Aleekseev [36] and Weber [37] first proposed the existence of slip layer, and it was confirmed and investigated widely by both experiments and numerical simulations [8,14,32]. The slip layer contains more liquid and fine particles and has a lower value of the maximum aggregate size, accordingly with lower yield stress and lower viscosity than the bulk concrete, is highly sheared [38]. The size of the slip layer has been widely debated and there is no consensus in the literature as to its thickness (as shown in **Table 2.1**). Ngo et al. [40] found that the thickness of slip layer is proportional to the volume of the cement paste, the water-to-cement ratio, and the dosage of superplasticizer. The slip layer thickness also decreases with a higher amount of fine sand. The length and diameter of pipeline are also considered to change the thickness of the slip layer. Ngo et al. [40] observed that the slip-layer is between 1 mm to 9 mm thick, by visualizing the material flow in the rheometer. However, Choi et al. [26] found that the thickness of the slip layer is around 2 mm for the concretes, not depending on flow rate, but varying with sand and gravel particle's initial volume fractions and pipe diameter. Le et al. [38] found that the thickness of the slip layer is not constant in space and time, varying from 0 to 3 mm by the PIV velocity measuring technique. Jo et al. [39] proposed that the slip

Table 2.1 Summarization of the thickness of slip layer given in literatures

Authors	Thickness of slip layer	Influencing factors
T. T. Ngo et al. [40]	1mm ~ 9mm	volume of the cement paste, water-to-cement ratio, dosage of superplasticizer, amount of fine sand, length and diameter of pipeline
Myoungsung Choi et al. [26]	2mm	independent on flow rate, but varying with sand and gravel particle's initial volume fractions and pipe diameter
H. D. Le et al. [38]	0mm ~ 3mm	not constant in space and time
Seon Doo Jo et al. [39]	1mm ~ 5mm	particle concentrations of cement, sand, gravel, as well as pipe size

layer ranges from about 1 mm to 5 mm based on the numerical analysis of shear-induced particle migration, depending particle concentrations of cement, sand, gravel, as well as pipe size. For special types of concrete, e.g. ultra-high performance concrete (UHPC), the formation of a slip layer is not induced by shear-induced particle migration [27].

For conventional concrete, several kinds of tribometer (as shown in **Fig. 2.9**) have been developed to measure the rheological properties (viscous constant and yield stress) of slip layer [28,29,40,41]. Although design parameters of each tribometer are different, the underlying principle of these devices is identical: a smooth cylinder is spun in a container containing fresh concrete mixture, allowing formation of the slip layer. Since no information on the thickness of slip layer is available [27], it is impossible to obtain its plastic viscosity using the rotational velocity-torque to shear rate-stress transformation. Viscous constant (Pa.s/m) is viscosity (Pa.s)-to-thickness (m) ratio of the slip layer. When measuring the rheological properties of the slip layer, it is desirable that only slip layer is sheared in tribometer. However, other two flow conditions may be observed in tribometer for fresh concretes with different fluidity: i) Both slip layer and bulk concrete are completely sheared; ii) slip layer is sheared while concrete is partially sheared. In these two cases, a correction must be made to the measured rotational velocity value for removing the effect of sheared concrete. That is to say, accurate measurement of rheological properties of slip layer is still an issue for different concretes.

■ **Macroscopic Properties of Slip Layer**

From a macroscopic view of the slip layer, the apparent slip velocity is used to represent the flow of the slip layer, and the thickness is ignored. Le et al. [38], Suzuki et al. [42], and Feys et al. [43]

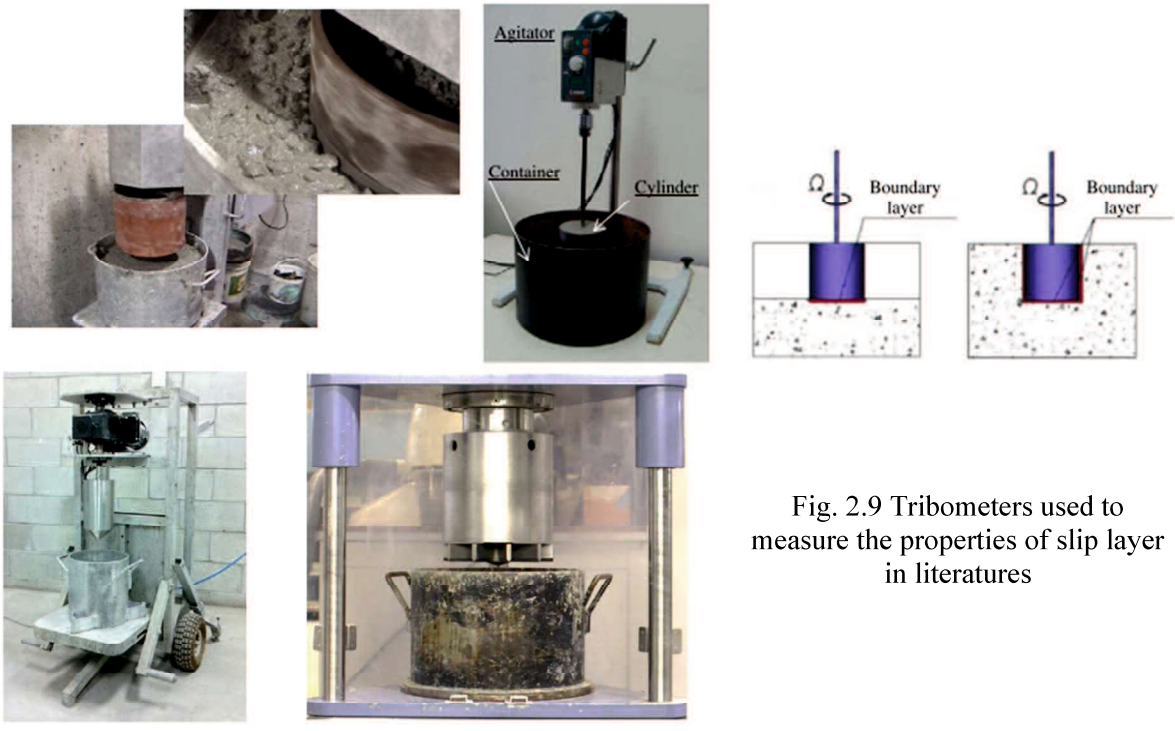

Fig. 2.9 Tribometers used to measure the properties of slip layer in literatures

focus on the macro effect of the slip layer, and use a tribological behavior model to calculate the slip resistance. The flow velocity of outer surface of slip layer to be zero [26], and the slip layer is regarded as part of the pipe wall. In the tribological behavior model, the shear stress is a linear function of the slip velocity and has a slip yield stress, as follow:

$$\tau_L = \eta_L \cdot V_L + \tau_{L0}. \tag{2.12}$$

where, τ_L is slip resistance stress, η_L is viscous constant of slip layer (Pa·s/m), τ_{L0} is slip yield stress of slip layer (Pa), V_L is apparent slip velocity of slip layer (m/s).

Suzuki et al. [42] develop a slip resistance measurement device (as shown in **Fig. 2.10**) to measure the macroscopic rheological parameters of slip layer. Mechtcherine et al.[44] developed a sliding pipe rheometer (as shown in **Fig. 2.11**) to mimic pumping at various speeds. This rheometer can also be used to measure the macroscopic properties of slip layer in pipe flow.

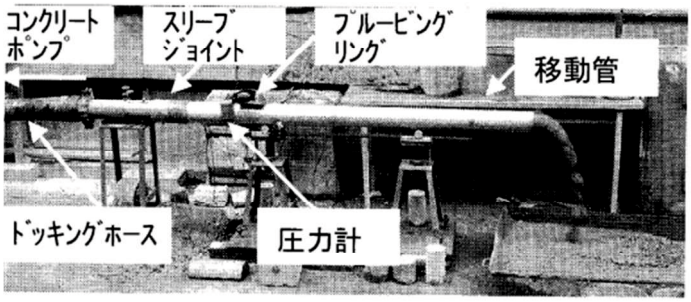

Fig. 2.10 Slip resistance measurement device for fresh concrete

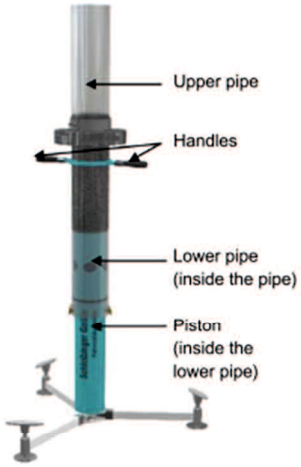

Fig. 2.11 Slid pipe rheometer

2.4.3 Prediction of Pumping Pressure

Fresh concrete is generally regarded as a Bingham fluid with a yield stress. For this reason, the Buckingham-Reiner equation [45] is used to predict pressure required for concrete to flow through a pipeline. However, it is found that the Buckingham-Reiner equation leads to overestimation of pumping pressures at certain flow rates [43]. This is primarily due to the fact that a slip layer forms along the pipe wall, and therefore, the material does not remain homogenous during pumping. To address the inhomogeneous nature of concrete in the pipeline, several pressure prediction models were recently developed, such as Kwon's model [46], Choi's model [26], Kaplan's model [47], and Mechtcherine's model [44], etc. These models incorporate not only the rheological properties of bulk concrete, but also the rheological properties of slip layer.

■ **Kwon's Model and Choi's Model**

Kwon et al. [46] divides the concrete in the pipeline into three parts: the lubricating layer, the shear layer and the plug layer. The thickness of the lubricating layer is assumed to be 2 mm. Integrate the three parts of concrete to obtain the prediction formula of concrete pumping flow and pressure as follows:

$$Q = 3600\frac{\pi}{24\mu_{ll}\mu_b}\begin{bmatrix} 3\mu_b\left(R^4 - R_L^4\right) - 8\tau_{ll}\mu_b\left(R^3 - R_L^3\right) \\ + 3\mu_{ll}\Delta P\left(R^4 - R_G^4\right) - 8\tau_b\mu_{ll}\left(R^3 - R_G^3\right) \end{bmatrix} \tag{2.13}$$

where, Q is pumping flow rate of fresh concrete, μ_{ll} is plastic viscosity of lubrication layer, μ_b is plastic viscosity of bulk concrete, τ_{ll} is yield stress of lubrication layer, τ_b is yield stress of bulk concrete, ΔP is pressure loss, R is radius of pipe, R_L is total radius of shear layer and plug layer, R_G is radius of plug layer.

Choi et al. [26] also uses a similar model to predict the concrete pumping pressure, but Choi equates the rheological properties of the mortar to the rheological properties of the lubricating layer.

■ **Kaplan's Model and Mechtcherine's Model**

Based on the rheological properties of concrete and its flow characteristics in pipelines, Kaplan et al. [47] deduced the formula for calculating the pressure loss of concrete in horizontal pipelines:

$$\Delta P = \frac{2}{R}\left(\frac{\dfrac{Q}{\pi R^2} - \dfrac{R}{4\pi\mu_b}\tau_{L0} + \dfrac{R}{3\mu_b}\tau_b}{1 + \dfrac{R}{4\mu_b}\eta_L}\eta_L + \tau_{L0}\right) \tag{2.14}$$

where, η_L is viscous constant of slip layer, τ_{L0} is slip yield stress of slip layer.

Based on the characteristics of the sliding tube instrument, Mechtcherine et al. [44] modified the above formula and obtained the pressure prediction formula of the sliding pipe rheometer:

$$\Delta P = \frac{4}{R}\tau_{L0} + \frac{16Q}{\pi R^3}\eta_L + \rho g \tag{2.15}$$

2.5 Numerical Methods for Fresh Concrete

With the development of computer technology, the numerical simulation becomes a novel and important tool to solve the practical problems in engineering. Based on it, the geometry of concrete structures, the mixture proportions can be optimized. Since 1992 Mori and Tanigawa firstly used numerical approach for concrete flow [48], there were a lot of simulations conducted for concrete test, e.g. slump [49], L-flow [50], V-funnel test [51], etc. and concrete production and construction e.g. mixing [52], transportation [53], pumping [54] and casting [55], etc. The numerical methods of fresh concrete that can be found in the literature may be divided into three main series [56]: single fluid methods, discrete particle flow methods and suspension flow methods.

2.5.1 Computational Fluid Dynamics (CFD) Methods

- **Viscoplastic Finite Element Method and Viscoplastic Divided Element Method**

Viscoplastic Finite Element Method (VFEM) is developed based on FEM by introducing a frictional interface law. In VFEM, the fresh concrete is divided into discrete elements, then the individual elements are connected together by a topological map, which is usually called a mesh. The interpolation functions are built upon the mesh, the displacements of nodal points of mesh represent the deformation of fresh concrete. In Viscoplastic Divided Element Method (VDEM), space is divided into elements and cells, which are either empty or full, and the flow is described by the displacement of virtual markers. The fixed position of nodal points allows reinforcement and complicated structure to be simulated.

Mori and Tanigawa [48] used the VFEM and VDEM to simulate flow of fresh concrete, both of these two numerical methods can simulate various concrete tests. Kurokawa et.al [57] used the VFEM to study the effect of volume fraction of coarse aggregate on Bingham's parameters of fresh concrete. Theane et.al [58] assuming that the fresh concrete is a continuum fluid, using the Bingham model describing the rheological behavior, simulated the L-flow based on Galerkin FEM formulation of the Navier-Stokes equation. The BML rheometer was used to measure the Bingham parameters When blockage does not occur, it is possible to simulate the flow in the L-box with reinforce steel bars by a continuum mechanical approach and the Bingham model. It is not reasonable to simulate the plane of symmetry in a 3D model (8-node brick elements) by that of a 2D (4-node quadrilateral elements) model due to the effect of viscous. It is necessary to take the effect of lifting rate of gate and slid at the boundary into account in numerical simulation, otherwise, the numerical simulation does not seem to correspond to the experimental results, as shown in **Fig. 2.12**. However, it cannot assess the blocking resistance due to the absence of particles in a continuum approach.

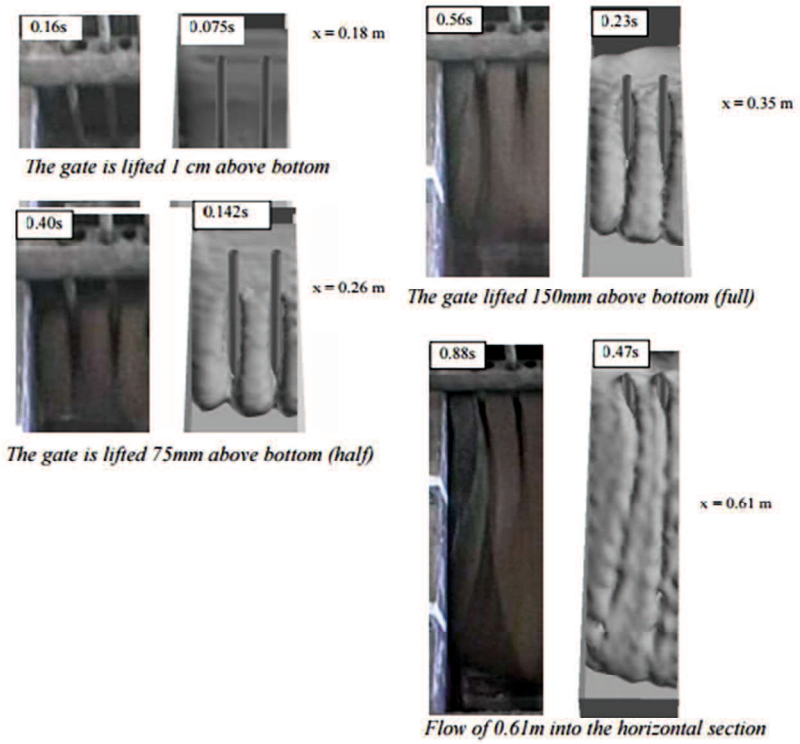

Fig. 2.12 Experimental results (left) and numerical simulations (right) at the same flow distance but different times

■ **CFD-Particle Finite Element Method**

A single fluid approach has been employed, using Poly flow, a CFD code developed by ANSYS, by Ferrara to assess the correlation between fundamental rheological properties of cementitious suspensions acquired through rheometer tests and field test parameters, a wide set of numerical simulations of both the mini-slump flow and the EN445 cone tests have been performed [59]. The Bingham model had been employed to describe the rheology behavior of fresh concrete. With reference to the mini-slump flow test, both the final slump diameter (**Fig. 2.13** (a)) and the time to final spread (**Fig. 2.13** (b)) of numerical and experimental results were compared. With reference to EN445 cone test, the flow times corresponding to different volumes of fluid cement paste flown out

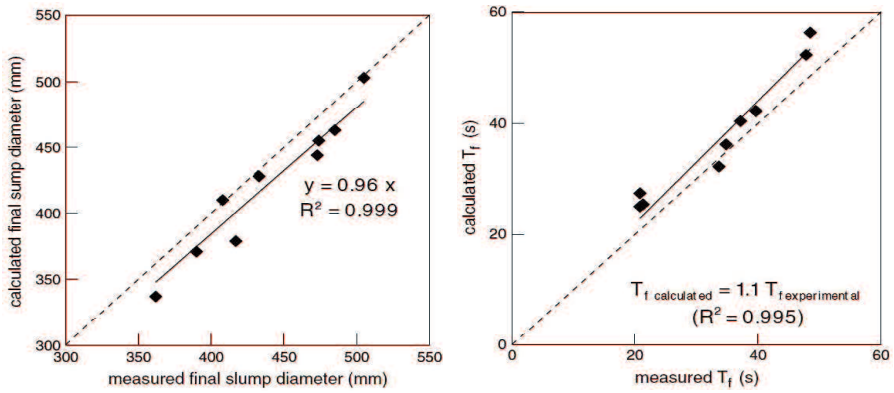

(a) final slump diameter (b) the time to final spread

Fig. 2.13 Experimental results and numerical simulation of min-slump flow test

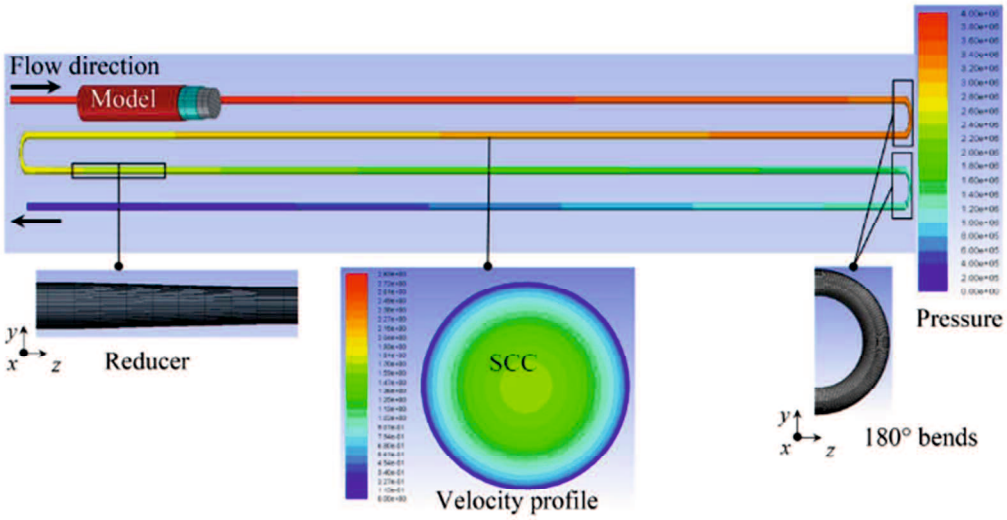

Fig. 2.14 Pressure distribution and velocity profile in pumping simulated by ANSYS

of the cone nozzle of numerical and experimental results were compared. The FEM method based ANSYS commercial software can also be used to simulate the pressure distribution and velocity profile in pumping, as shown in **Fig. 2.14**.

■ **CFD-Volume of Fluid Method**

Flow 3D code [60] is a general purposed computer program and is user friendly when dealing with complex free surface transient flow of non-Newtonian fluids. Rouseel [61] performed 3D simulations of different slump test methods using the computational fluid mechanics code Flow 3D. The materials were assumed to behave as an incompressible elastic solid before yield, beyond which it behaves as a Bingham fluid. The invariant generalization of fresh concrete was the one proposed by Oldroyd [62] based on the three dimensional von Mises yield criterion. The numerical simulation performed for two asymptotic cases (**Fig. 2.15**): when there is a very small slump value (purely extensional flow, yield stress is equal to 2600pa) and when there is a large spread diameter (purely shearing flow, yield stress is equal to 2000pa). Inertia effects were neglected, that is to say, the influence of lifting speed or the plastic viscosity was not taken into consideration. Tatersall and Banfill [63] experimentally concluded that the slump of fresh concrete is indeed highly correlated with yield stress but is not significantly affected by the plastic viscosity. The numerical results of mini cone test and ASTM slump test were in agreement with corresponding experimental results. Le et al. [38] simulated the pipe flow in the half open pipe using the Volume of Fluid method to track the shape and position of the interface between concrete and the air above the free surface of the concrete. The open channel simulated with the boundary conditions is shown in **Fig. 2.16**.

In CFD, concrete is modeled as a single continuum phase or as multiple continuum phases, while the modeled domain is discretized as interconnected mesh elements. This means that the rheological

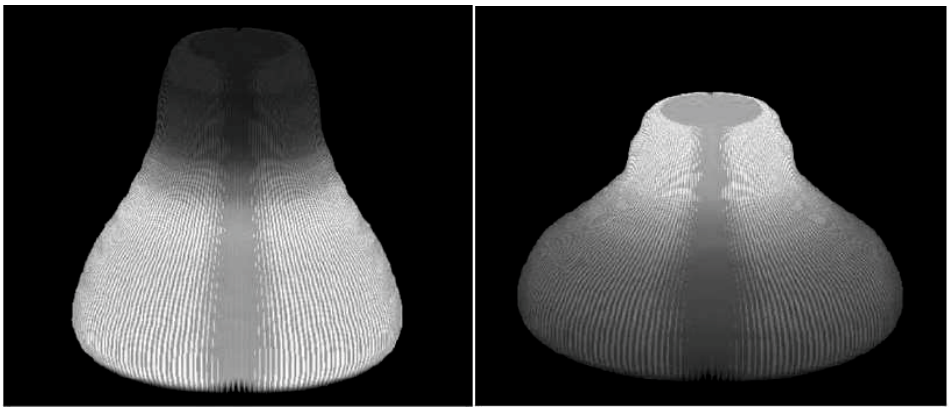

(a) yield stress= 2600Pa (b) yield stress=2000Pa

Fig. 2.15 Examples of obtained shapes of numerical results of ASTM slump test

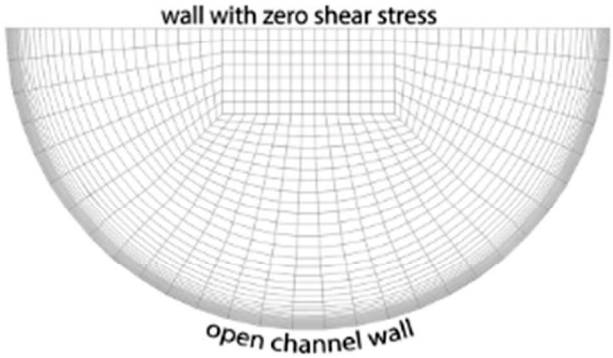

Fig. 2.16 Pipe flow in the half open channel simulated by VOF

properties of concrete in a phase are constant throughout the modeled geometry. Numerical solution for fresh concrete's rheological behaviors is then made possible by adding apparent viscosity, commonly following the Bingham or Herschel-Bulkley models, to the Navier-Stokes equations. Though CFD has proven to be a useful tool for simulating macroscopic phenomena such as pressure and flow rate during pumping. Nevertheless, this method excludes the interactions among solid particles from the simulation and, hence, is not appropriate to simulate heterogeneous phenomena and provide information about the dynamic segregation of concrete in pipe for predicting blockage during pumping [64].

2.5.2 Discrete Particle Flow Methods

When fresh concrete is of high fluidity and the content of coarse aggregate is low, it flows like a fluid. Whereas, in case of low fluidity and large amount of coarse aggregate, the interaction between coarse aggregate is obvious, that is to say, the behavior is dominated by the granular nature. Therefore, it is natural advantages to simulate the flow of fresh concrete using the discrete particle method. The numerical simulation of fresh concrete based on discrete particle flow are summarized as follows.

■ **Discrete Element Method (DEM)**

The DEM is a particle approach, of which a fundamental assumption is that the analyzed material consists of separate discrete particles: circular particles (2D) or spherical particles (3D). The boundary is represented by the wall. At every calculation cycle includes two steps: according to Newton's second law to calculate the motion of each particle and deciding the contact forces by the force-displacement law [65–67]. The contact force at each contact point is divided into normal and shear direction. Spring, dashpot, and slip are used to express the elastic, viscous and plastic component, as shown in **Fig. 2.17**. As a complement to laboratory experiments, discrete particle numerical simulation applied to granular materials gives access to microstructure or even microstructure at the scale of the grains and contacts, and improves our understanding of macroscopic mechanical behavior from the microscopic point.

Based on the work in Ref. [68], Noor and Uomoto [69] used the PFC3D code to simulated behaviors of SCC under various states. Various consistency and rheology tests of SCC were performed using this numerical method. In DEM calculation, the increase of phase numbers and small particle sizes like sand and cement extremely time and calculation consuming. Hence, the double-phase model: coarse aggregate and mortar were used. The contact parameters, such as contact stiffness and bond strength both for normal and tangential direction were verified by the lifting sphere viscometer test. The method proposed by Noor and Uomoto was also adopted by Petersson [70] and Hakami and Petersson [71] to simulate the flow in L-box. It proves that the 3D model and 2D model (depending on type of simulation) are very suitable for the simulation of SCC flow and simulation of tests for passing ability.

Many DEM-based flow simulations of fresh concrete have been reported so far, but the input parameters, e.g., viscosity coefficient of dash-pot, stiffness of spring, representing interactions of imaginary rigid particles need to be calibrated, thus for different concrete mixtures, the setup of the input parameters is not easy.

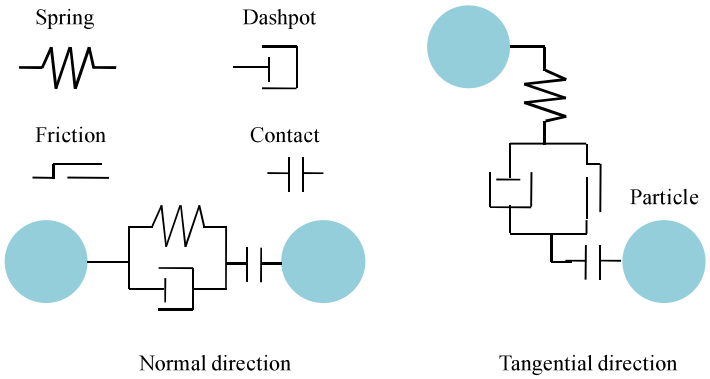

Fig. 2.17 Standard contact model between particles in DEM

■ **Smoothed Particle Hydrodynamics (SPH) Method**

The SPH was originally developed in 1977 by Lucy [72] and, Monaghan and Gingold [73] for astrophysical applications (here called standard SPH). The method uses a purely Lagrangian approach

and has been successfully employed in compressible viscous fluid problems. The state of a system is represented by a set of particles, which possess materials properties and interact with each other within the range controlled by a weight function or smoothing function. The discretization of the governing equations is based on these discrete particles, and a variety of particle-based formulations have been used to calculate the local density, velocity and acceleration of the fluid.

Later, Monaghan [74] further developed the new SPH algorithm for simulating the slightly compressible flows by introducing a virtual speed of sound and attaining a very low Mach number to control density variation within 1%, which is usually called weakly compressible SPH (WCSPH). The fluid pressure is calculated from the density using an equation of state, the particle acceleration is then calculated from the pressure gradient and the density. In many SPH approaches, incompressible fluids are treated as slightly compressible fluids for using WCSPH method. Cummins & Rudman [75] realized the incompressibility in SPH in 1999 by solving a pressure Poisson equation at every time step to satisfy the divergence-free velocity condition, which is called pressure or projection - based incompressible SPH (ISPH). Later after, the pressure-based ISPH algorithm was improved for satisfying the constant density condition besides the divergence-free velocity condition [76,77]. However, these ISPH methods need the iterative solution of the pressure Poisson equation. This makes implementing them in parallel and on GPUs fairly difficult. The WCSPH implementations are generally more popular as they are much easier to implement and parallelize, and the WCSPH implements boundary relatively easily and this is harder to do with the pressure-based ISPH [78]. Lee et al. [79] compared the pressure-based ISPH and the WCSPH on various incompressible flow test cases and concluded that the WCSPH method exhibits strong spurious oscillations especially in pressure and produces unreliable results particularly on coarse particle resolutions.

Huang et.al [80] adopted the WCSPH method to simulate and investigate the fiber orientation in UHPC beams with different placements, as shown in **Fig. 2.18**. Dhaheer et. al [81] investigated the capabilities of the method to predict the flow of SCC mixes through gaps in reinforxing bars, the J-ring test was simulated by using the ISPH method and a suitable Bingham-type constitutive model, as shown in **Fig. 2.19**.

- **Moving Particle Semi-implicit (MPS) Method**

Moving Particle Semi-implicit (MPS) method is presented by Koshizuka and Oka for incompressible fluid [82]. The motion of each particle is calculated through interactions with neighboring particles covered with the kernel function. Deterministic particle interaction models representing gradient, Laplacian, and free surfaces are proposed. Fluid density is implicitly required to be constant as the incompressibility condition, and a pressure Poisson equation is solved at every time step to ensure the incompressibility of particle, while the other terms are explicitly calculated. Hence, general MPS is called semi-implicit algorithm.

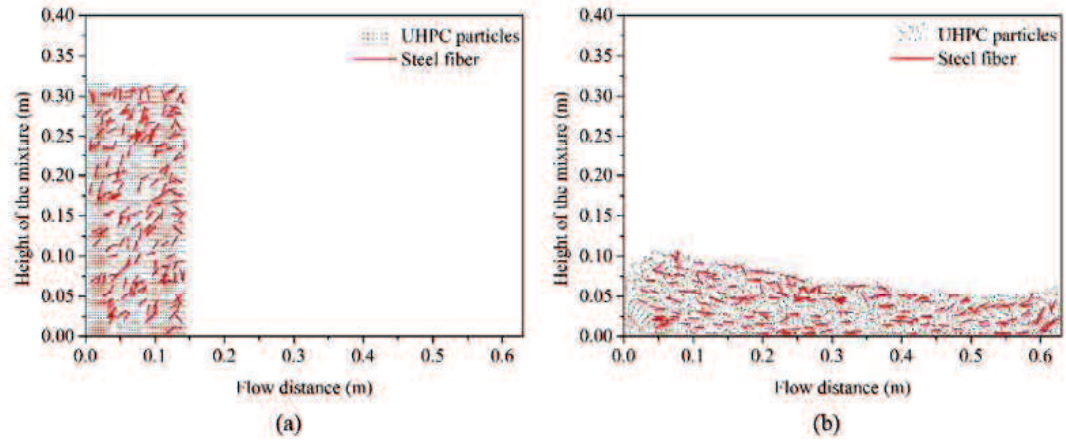

Fig. 2.18 SPH simulation of fiber orientation in UHPC beams

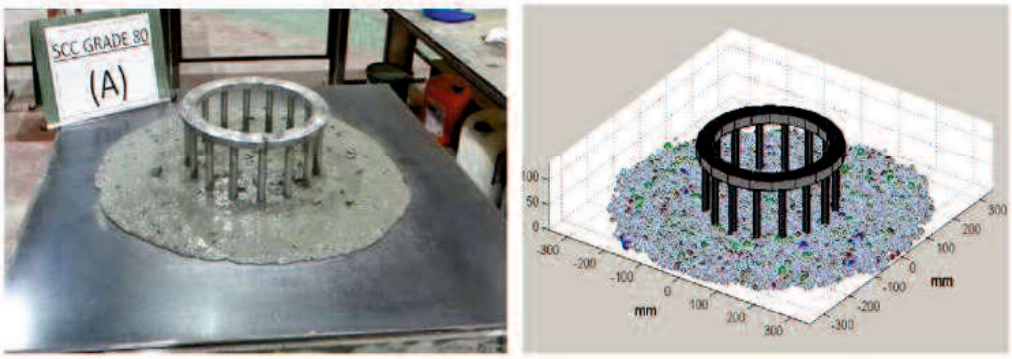

Fig. 2.19 Simulation of self-compacting concrete flow in the J-ring test using SPH

Cho et.al [83] develop a numerical approach using the MPS and a viscous-plastic flow constitutive law to simulate the flow analysis of fresh concrete. Uehara et. al [84] confirmed that the flow determination of fresh concrete to be unstable, and investigated the slump analysis by s high accuracy MPS for fresh concrete.

Since an explicit algorithm is used for the viscous item in the original MPS, for a fluid with high viscosity, such as fresh concrete, the calculation time step needs to be set very small to stabilize the calculation results [85], accordingly the calculation efficiency is reduced. Therefore, the MPS algorithm needs to be improved for the flow simulation of fresh concrete.

Particle methods, SPH and MPS, can simulate the interactions among solid particles have the potential to simulate heterogeneous properties of concrete and provide information about the dynamic segregation of concrete in pipe. Nevertheless, using the same shape, uniform size, uniform density particles cannot simulate segregation. Moreover, almost all current particle method based numerical analyses of fresh cementitious materials are for slump flow, L-flow or flow behaviors in rheometer. There is no meshless particle method that can predict pressure loss together with segregation behavior of pumped concrete now.

2.5.3 Suspension Flow Methods

■ **Viscoplastic Suspension Element Method**

A Viscoplastic Suspension Element Method (VSEM) was used by Mori and Tanigawa to simulate the flow of concrete in various tests [48]. Two phases: mortar and coarse aggregates (monosize spheres) was used. A viscoplastic equation was introduced to describe the viscoplastic interactions between particles.

■ **Finite Element Method with Lagrangian Integration Points**

A finite element method with Lagrangian integration points (FEMLIP) [86] is a code based on an Eulerian grid of finite element and a set of Lagrangian particles or tracers inside the mesh. The different point of FEMLIP and FEM, SPH and DEM is that the materials points and computational points do not coincide, as shown in **Fig. 2.20**. The grid is usually kept fixed except in the case of moving boundary conditions. The retained approach uses a Eulerian finite element grid (fixed) as a computational set of points and a set of Lagrangian particles embedded in the mesh which are used as integration points for any given configuration. Material properties are initially set on particles. The nodal unknowns of grid are computed using the integration over particles, then the velocity of particles was calculated by interpolated of nodal information. The position of particles will be undated according their velocities.

When using FEMLIP modeling concrete as a heterogeneous material made of mortar and aggregate (see **Fig. 2.21** (top)), the scale should be smaller than the form scale since aggregates must be discretized by several finite elements in order to be properly modeled as rigid compared to mortar.

FEMLIP was used by Dufour and Cabot to simulate flow of fresh concrete [87]. Three types of fresh concrete, ordinary concrete, high performance concrete and SCC were used. The constitutive relationship of fresh concrete was described by a Bingham-type model and friction was not considered

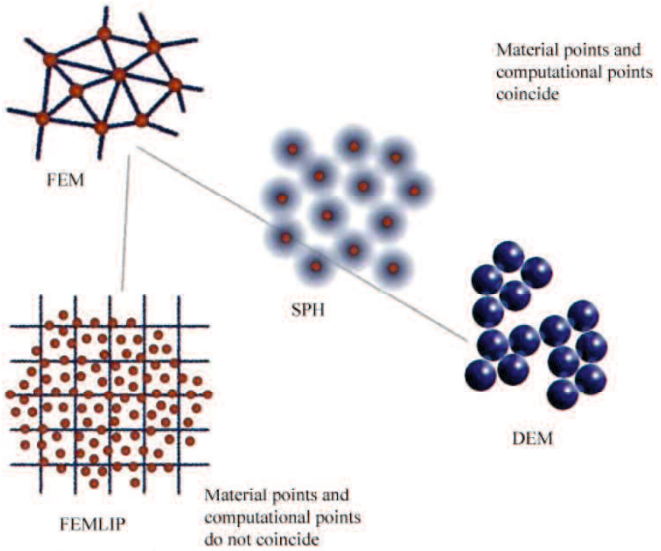

Fig. 2.20 Different ways to discretize a system with particles and/or grid

at the boundary. They fitted the two Bingham parameters from the slump test with flow time to calibrate the model parameters, as shown in **Fig. 2.21** (bottom). Then the final shape of L-flow of 2D numerical simulation and experiment were compared.

It is worthy of note that it is possible to couple CFD calculations, rep- resenting the fluid phase, with DEM, which represents the particle phase, but such calculation procedures are very complex, very time-consuming, and still in the early stages of their development [59].

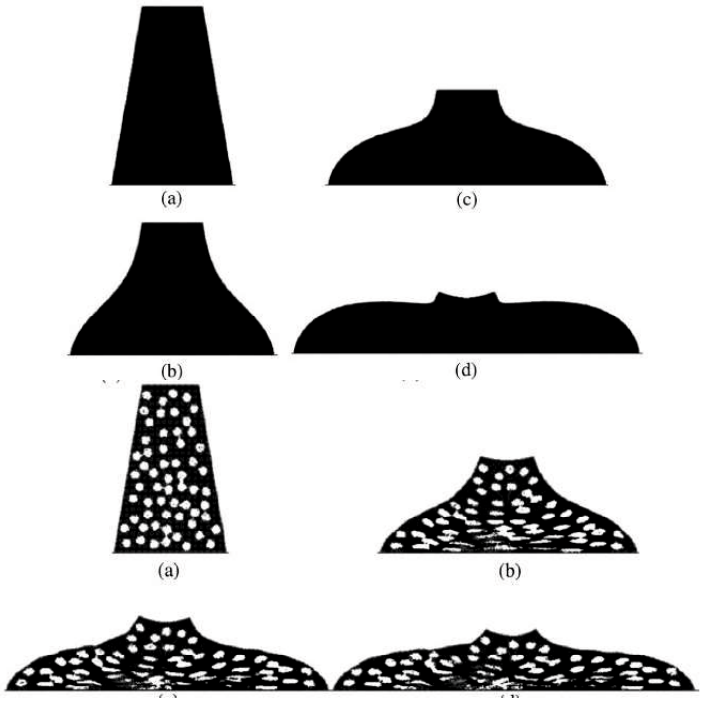

Fig. 2.21 Numerical simulation of the slump flow test using a homogeneous approach (top) and using a heterogeneous approach (bottom)

2.6 Summary

In this chapter, previous researches relevant to the pipe flow model of fresh concrete are reviewed. The development and application of numerical methods for flow simulation of fresh concrete are discussed. The prediction methods of rheological properties of fresh concrete materials are investigated. The segregation of fresh concrete and its influencing factors are summarized. At last, the important results of concrete pumping research and future research needs have been concluded. The main summaries are stated as follows:

1. Among the existing numerical simulation methods, SPH and MPS methods are suitable for simulating pipe flow of fresh concrete. Moreover, they have the potential to simulate heterogeneous properties of concrete and provide information about the dynamic segregation of concrete in pipe. However, some necessary improvements need to be done to make them more suitable for concrete flow simulation.

2. It is important to evaluate the pumpability of concrete. The formation of slip layer and the segregation of aggregates have a great influence on the pumping behavior and need to be further studied. The existing research on the concrete pumping is mostly limited to theory and experiment, and relevant numerical simulation is urgently needed to deepen the research.

3. The rheological properties (viscosity and yield stress) of fresh concrete is reported can be predicted according to the material constituent. These prediction models allow to considering the heterogeneity of concrete materials and investigating the segregation behaviors in a numerical approach.

4. It is urgent and feasible to establish a proper numerical model for concrete pumping based on particle method. In addition, this numerical model should be able to predict the flow behaviors and segregation behaviors of fresh concrete in pipe flow.

Reference

[1] O.E. Gjørv, Workability: a new way of testing, Concr. Int. 20 (1998) 57–60.

[2] B.P. Ferraris C F, Brower L E, Comparison of concrete rheometers: international test at LCPC, US Department of Commerce, 2000.

[3] F. De Larrard, C. Hu, T. Sedran, J.C. Szitkar, M. Joly, F. Claux, F. Derkx, A new rheometer for soft-to-fluid fresh concrete, Mater. J. 94 (1997) 234–243.

[4] L. Struble, R. Szecsy, G. Salinas, Rheology of fresh concrete, in: Int. Purdue Conf. Concr. Pavement Des. Mater. High Performance, 6th, 1997, Indianapolis, Indiana, USA, 1997.

[5] Z. Li, Rheological model and rheometer of fresh concrete, J. Struct. Constr. Eng. (Transactions AIJ). 80 (2015) 527–537.

[6] G.H. Tattersall, S.J. Bloomer, Further development of the two-point test for workability and extension of its range, Mag. Concr. Res. 31 (1979) 202–210.

[7] O.H. Wallevik, O.E. Gjørv, Modification of the two-point workability apparatus, Mag. Concr. Res. 42 (1990) 135–142.

[8] J. Murata, H. Kukawa, Viscosity equation for fresh concrete, Mater. J. 89 (1992) 230–237.

[9] T. Sedran, F. De Larrard, Optimization of self compacting concrete thanks to packing model, in: Self-Compacting Concr. (Stockholm, 13-14 Sept. 1999), 1999: pp. 321–332.

[10] F. De Larrard, Concrete mixture proportioning: a scientific approach, CRC Press, 1999.

[11] C.F. Ferraris, F. DeLarrard, Testing and modeling of fresh concrete rheology, (1998).

[12] A.W. Saak, H.M. Jennings, S.P. Shah, New methodology for designing self-compacting concrete, Mater. J. 98 (2001) 429–439.

[13] J. Hu, K. Wang, Effect of coarse aggregate characteristics on concrete rheology, Constr. Build. Mater. 25 (2011) 1196–1204.

[14] L. Struble, G.-K. Sun, Viscosity of Portland cement paste as a function of concentration, Adv. Cem. Based Mater. 2 (1995) 62–69.

[15] I.M. Krieger, T.J. Dougherty, A mechanism for non-Newtonian flow in suspensions of rigid spheres, Trans. Soc. Rheol. 3 (1959) 137–152.

[16] R.J. Farris, Prediction of the viscosity of multimodal suspensions from unimodal viscosity data, Trans. Soc. Rheol. 12 (1968) 281–301.

[17] M.A. Noor, T. Uomoto, Rheology of high flowing mortar and concrete, Mater. Struct. 37 (2004) 513–521.

[18] F. Mahaut, S. Mokéddem, X. Chateau, N. Roussel, G. Ovarlez, Effect of coarse particle volume fraction on the yield stress and thixotropy of cementitious materials, Cem. Concr. Res. 38 (2008) 1276–1285.

[19] X. Chateau, G. Ovarlez, K.L. Trung, Homogenization approach to the behavior of suspensions of noncolloidal particles in yield stress fluids, J. Rheol. (N. Y. N. Y). 52 (2008) 489–506.

[20] J. Spangenberg, N. Roussel, J.H. Hattel, H. Stang, J. Skocek, M.R. Geiker, Flow induced particle migration in fresh concrete: Theoretical frame, numerical simulations and experimental results on model fluids, Cem. Concr. Res. 42 (2012) 633–641.

[21] L. Shen, L. Struble, D. Lange, Testing static segregation of SCC, in: SCC2005, Proc. 2nd North Am. Conf. Des. Use SCC, Novemb., 2005: pp. 1–3.

[22] L. Shen, H. Bahrami Jovein, Z. Sun, Q. Wang, W. Li, Testing dynamic segregation of self-consolidating concrete, Constr. Build. Mater. 75 (2015) 465–471.

[23] M.I. Safawi, I. Iwaki, T. Miura, The segregation tendency in the vibration of high fluidity concrete, Cem. Concr. Res. 34 (2004) 219–226.
[24] J. Pan, X. Gao, H. Ye, Influence of Rheological Behavior of Mortar Matrix on Fresh Concrete Segregation and Bleeding, Iran. J. Sci. Technol. - Trans. Civ. Eng. (2020) 1–15.
[25] X. Gao, J. Zhang, Y. Su, Influence of vibration-induced segregation on mechanical property and chloride ion permeability of concrete with variable rheological performance, Constr. Build. Mater. 194 (2019) 32–41.
[26] M. Choi, N. Roussel, Y. Kim, J. Kim, Lubrication layer properties during concrete pumping, Cem. Concr. Res. 45 (2013) 69–78.
[27] G. De Schutter, D. Feys, Pumping of fresh concrete: insights and challenges, RILEM Tech. Lett. 1 (2016) 76.
[28] E. Secrieru, J. Khodor, C. Schröfl, V. Mechtcherine, Formation of lubricating layer and flow type during pumping of cement-based materials, Constr. Build. Mater. 178 (2018) 507–517.
[29] M. Jolin, D. Burns, B. Bissonnette, F. Gagnon, L.-S. Bolduc, B. Bissonnette, Understanding the pumpability of concrete, in: Shotcrete Undergr. Support XI, 2009.
[30] M. Choi, C.F. Ferraris, N.S. Martys, V.K. Bui, H.R.T. Hamilton, D. Lootens, Research needs to advance concrete pumping technology, Gaithersburg, MD, 2015.
[31] I.R. Siqueira, P.R. de Souza Mendes, On the pressure-driven flow of suspensions: Particle migration in apparent yield-stress fluids, J. Nonnewton. Fluid Mech. 265 (2019) 92–98.
[32] R.D. Browne, P.B. Bamforth, Tests to establish concrete pumpability, ACI J. Proc. 74 (1977) 193–203.
[33] R.J. Phillips, R.C. Armstrong, R.A. Brown, A.L. Graham, J.R. Abbott, A constitutive equation for concentrated suspensions that accounts for shear-induced particle migration, Phys. Fluids A Fluid Dyn. 4 (1992) 30–40.
[34] M.S. Choi, Y.J. Kim, S.H. Kwon, Prediction on pipe flow of pumped concrete based on shear-induced particle migration, Cem. Concr. Res. 52 (2013) 216–224.
[35] F. De Larrard, N. Roussel, Flow simulation of fresh concrete under a slipform machine, Road Mater. Pavement Des. 12 (2011) 547–566.
[36] S.N. Alekseev, On the calculation of resistance in pipe of concrete pumps, Mekhanizatia Storit. 9 (1952) 8–13.
[37] R. Weber, The transport of concrete by pipeline, London,UK Cem. Concr. Assoc. (1968).
[38] H.D. Le, E.H. Kadri, S. Aggoun, J. Vierendeels, P. Troch, G. De Schutter, Effect of lubrication layer on velocity profile of concrete in a pumping pipe, Mater. Struct. 48 (2015) 3991–4003.
[39] S.D. Jo, C.K. Park, J.H. Jeong, S.H. Lee, S.H. Kwon, A computational approach to estimating a lubricating layer in concrete pumping, Comput. Mater. Contin. (2012).
[40] T.T. Ngo, E.H. Kadri, R. Bennacer, F. Cussigh, Use of tribometer to estimate interface friction and concrete boundary layer composition during the fluid concrete pumping, Constr. Build. Mater. 24 (2010) 1253–1261.
[41] D. Feys, A. Perez-Schell, R. Khatib, Development of a tribometer to characterize lubrication layer properties of self-consolidating concrete, Cem. Concr. Compos. 54 (2014) 40–52.
[42] K. Suzuki, S. Koshikawa, Y. Itoh, Studies on pipe flow of concrete, Concr. Res. Technol. 15 (2004) 47–57.
[43] D. Feys, G. De Schutter, R. Verhoeven, Parameters influencing pressure during pumping of self-compacting concrete, Mater. Struct. Constr. 46 (2013) 533–555.

[44] V. Mechtcherine, V.N. Nerella, K. Kasten, Testing pumpability of concrete using Sliding Pipe Rheometer, Constr. Build. Mater. 53 (2014) 312–323.
[45] E. Buckingham, On plastic flow through capillary tubes, Proc. Am. Soc. Test. Mater. (1921) 1154–1156.
[46] H. Kwon, C.K. Park, J.H. Jeong, S.D. Jo, S.H. Lee, Prediction of concrete pumping : part II — analytical prediction and experimental verification, ACI Mater. J. 110 (2013) 657–668.
[47] T. Kaplan, D., De Larard, F., & Sedran, Design of concrete pumping circuit, ACI Mater. J. 102 (2005) 110–117.
[48] Y.T. H. Mori, Simulation methods for fluidity of fresh Concrete, Nagoya University, 1992.
[49] R. Deeb, S. Kulasegaram, B.L. Karihaloo, 3D modelling of the flow of self-compacting concrete with or without steel fibres. Part I: slump flow test, Comput. Part. Mech. 1 (2014) 373–389.
[50] G. Cao, Z. Li, Numerical flow simulation of fresh concrete with viscous granular material model and smoothed particle hydrodynamics, Cem. Concr. Res. 100 (2017) 263–274.
[51] W.S. Alyhya, S. Kulasegaram, B.L. Karihaloo, Simulation of the flow of self-compacting concrete in the V-funnel by SPH, Cem. Concr. Res. 100 (2017) 47–59.
[52] X. Xiao, Y. Tan, H. Zhang, R. Deng, S. Jiang, Experimental and DEM studies on the particle mixing performance in rotating drums: Effect of area ratio, Powder Technol. 314 (2017) 182–194.
[53] R. Deng, Y. Tan, H. Zhang, X. Xiao, S. Jiang, Experimental and DEM studies on the transition of axial segregation in a truck mixer, Powder Technol. 314 (2017) 148–163.
[54] Y. Tan, H. Zhang, D. Yang, S. Jiang, J. Song, Y. Sheng, Numerical simulation of concrete pumping process and investigation of wear mechanism of the piping wall, Tribol. Int. 46 (2012) 137–144.
[55] H. Kitaoji, Y. Tanigawa, H. Mori, Y. Kurokawa, S. Urano, Flow simulation of fresh concrete cast into wall structure by viscoplastic divided space element method, Trans. Japan Concr. Inst. 18 (1997) 45–52.
[56] N. Roussel, M.R. Geiker, F. Dufour, L.N. Thrane, P. Szabo, Computational modeling of concrete flow: General overview, Cem. Concr. Res. 37 (2007) 1298–1307.
[57] Y. Kurokawa, Y. Tanigawa, H. Mori, K. Nishinosono, Analytical study on effect of volume fraction of coarse aggregate on Bingham's constants of fresh concrete, Trans. Japan Concr. Inst. 18 (1997) 37–44.
[58] L.N. Thrane, P. Szabo, M. Geiker, M. Glavind, H. Stang, Simulation of the Test Method "L-box" for Self-compacting Concrete, in: Annu. Trans. Nord. Rheol. Soc., 2004.
[59] N. Roussel, A. Gram, M. Cremonesi, L. Ferrara, K. Krenzer, V. Mechtcherine, S. Shyshko, J. Skocec, J. Spangenberg, O. Svec, Numerical simulations of concrete flow: A benchmark comparison, Cem. Concr. Res. 79 (2016) 265–271.
[60] T.C. Papanastasiou, Flows of materials with yield, J. Rheol. (N. Y. N. Y). 31 (1987) 385–404.
[61] N. Roussel, Correlation between yield stress and slump: comparison between numerical simulations and concrete rheometers results, Mater. Struct. 39 (2006) 501.
[62] J.G. Oldroyd, A rational formulation of the equations of plastic flow for a Bingham solid, in: Proc. Camb. Philos. Soc, 1947: p. 5.
[63] G.H. Tattersall, P.F.G. Banfill, The rheology of fresh concrete, Pitman Advanced Pub. Program, 1983.
[64] N. Roussel, A. Gram, Simulation of fresh concrete flow, RILEM State-of-the-Art Reports. 15 (2014).

[65] S. Shyshko, V. Mechtcherine, Developing a Discrete Element Model for simulating fresh concrete: Experimental investigation and modelling of interactions between discrete aggregate particles with fine mortar between them, Constr. Build. Mater. 47 (2013) 601–615.
[66] R. Pieralisi, S.H.P. Cavalaro, A. Aguado, Discrete element modelling of the fresh state behavior of pervious concrete, Cem. Concr. Res. 90 (2016) 6–18.
[67] V. Mechtcherine, S. Shyshko, Simulating the behaviour of fresh concrete with the Distinct Element Method - Deriving model parameters related to the yield stress, Cem. Concr. Compos. 55 (2015) 81–90.
[68] H. CHU, M. A, Numerical simulation of fluidity behavior of fresh concrete by 2d distinct element method, Trans. Japan Concr. (1997) 1–8.
[69] N. M.A, U. T, Three-dimensional discrete element simulation of rheology tests of self-compacting concrete - Search results - Pascal and Francis Bibliographic Databases, in: Proc. 1rd Int. RILEM Symp. SCC, 1999: pp. 35–46.
[70] Ö. Petersson, H. Hakami, Simulation of SCC-laboratory experiments and numerical modeling of slump flow and L-box tests, in: Proc. 2nd Int. RILEM Symp. SCC, Coms Engineering Corporation Tokyo, 2001: pp. 79–88.
[71] O. Petersson, H. Hakami, Simulation of self-compacting concrete-laboratory experiments and numerical modelling of testing methods, slump flow, J-ring and L-box tests, in: 2nd Int. SCC Conf. Tokyo, Japan, 2001.
[72] L.B. Lucy, A numerical approach to the testing of the fission hypothesis, Astron. J. 82 (1977) 1013–1024.
[73] R.A. Gingold, J.J. Monaghan, Smoothed particle hydrodynamics: Theory and application to non-spherical stars, Mon. Not. R. Astron. Soc. 181 (1977) 375–389.
[74] J.J. Monaghan, Simulating free surface flows with SPH, J. Comput. Phys. 110 (1994) 399–406.
[75] S.J. Cummins, M. Rudman, An SPH projection method, J. Comput. Phys. 152 (1999) 584–607.
[76] P. Jacek, W. Arkadiusz, SPH computation of incompressible viscous flows, J. Theor. Appl. Mech. 40 (2002) 917–937.
[77] S. Shao, E.Y.M. Lo, Incompressible SPH method for simulating Newtonian and Non-Newtonian flows with a free surface, Adv. Water Resour. 26 (2003) 787–800.
[78] A. Muta, P. Ramachandran, P. Negi, An efficient, open source, iterative ISPH scheme, Comput. Phys. Commun. (2020).
[79] E.S. Lee, C. Moulinec, R. Xu, D. Violeau, D. Laurence, P. Stansby, Comparisons of weakly compressible and truly incompressible algorithms for the SPH mesh free particle method, J. Comput. Phys. 227 (2008) 8417–8436.
[80] H. Huang, X. Gao, Y. Li, A. Su, SPH simulation and experimental investigation of fiber orientation in UHPC beams with different placements, Constr. Build. Mater. 233 (2020) 117372.
[81] M.S. Abo Dhaheer, S. Kulasegaram, B.L. Karihaloo, Simulation of self-compacting concrete flow in the J-ring test using smoothed particle hydrodynamics (SPH), Cem. Concr. Res. 89 (2016) 27–34.
[82] S. Koshizuka, Y. Oka, Moving-Particle Semi-implicit method for fragmentation of incompressible fluid, Nucl. Sci. Eng. 123 (1996) 421–434.
[83] C.-G.W.-J.Y. Cho, Model for Flow Analysis of Fresh Concrete Using Particle Method with Visco-Plastic Flow Formulation, J. Korea Concr. Inst. 20 (2008) 317–323.
[84] Y. Uehara, K. Sakihara, Y. Yamada, S. Urano, A basic study on slump analysis of high accuracy MPS for fresh concrete, Cem. Sci. Concr. Technol. 67 (2013) 626–633.

[85] J.J. Monaghan, J. J., On the problem of penetration in particle methods, J. Comput. Phys. 82 (1989) 1–15.
[86] L. Moresi, F. Dufour, H.B. Mühlhaus, A Lagrangian integration point finite element method for large deformation modeling of viscoelastic geomaterials, J. Comput. Phys. 184 (2003) 476–497.
[87] F. Dufour, G. Pijaudier-Cabot, Numerical modelling of concrete flow: Homogenous approach, Int. J. Numer. Anal. Methods Geomech. 29 (2005) 395–416.

Chapter 3 Comparison and Selection of Numerical Analysis Methods

3.1 Introduction

3.2 WCSPH and I-MPS Methods

3.3 Constitutive Models

3.4 Boundary Conditions

3.5 Experiment

3.6 Numerical Simulation of the L-Flow Tests of Fresh Mortar

3.7 Conclusions

Chapter 3
Comparison and Selection of Numerical Analysis Methods

3.1 Introduction

With the development of high-rise and sustainable concrete structures, the performance demand for concrete has been increasing. Various chemical and mineral admixtures, especially high-range water reducing agent provide great opportunity for the property improvement of concrete. As a result, the performances of fresh concrete present complexity and diversity. In many cases, slump test and slump flow test are even less accurate in evaluating the workability of fresh concrete, which are only related to yield stress of fresh concrete. Also, the workability of fresh concrete is dependent on construction method, structural condition, and environmental condition. Large-scale construction experiment may confirm the workability of fresh concrete, but it requires a lot of time, material and labor. With the advance of computational technology, the numerical analysis technology of fresh concrete has been gaining much attention and a great development due to its high efficiency and environmental friendliness. Workability evaluation and design based on numerical flow simulation has become an important subject.

In computational fluid dynamics (CFD), many grid-based numerical methods have been developed for solving and studying different fluid problems. Although these methods have shown their ability in simulating many problems, the existence of some fairly complicated problems with free surfaces, large deforming boundaries, etc., makes modeling of them very difficult when using grid-based numerical methods. Also, the generation of a suitable mesh in grid-based methods for complex geometries is not an easy task and it usually involves a complicated and time-consuming procedure. In addition, the precise calculation of free surfaces and deforming boundaries cannot be easily performed by applying these methods. The flow of fresh concrete is a large deformation problem with a free surface, the application of grid-based numerical methods is obviously difficult.

Now there are mainly three particle methods, so-called meshless method, which are Discrete Element Method (DEM), Smoothed Particle Hydrodynamics (SPH), and Moving Particle Semi-Implicit (MPS), respectively. In addition to the advantage that large deformation can be calculated because of unnecessity of computational grid generation, the particle methods have the possibility of

analyzing the segregation behavior of fresh concrete. Hence, the development of flow simulation methodology of fresh concrete based on the particle methods is an issue. Many DEM-based flow simulations of fresh concrete have been reported so far [1–3], dealing with large deformation problem by representing concrete with imagined particles, but the input parameters, e.g. viscosity coefficient of dash-pot, stiffness of spring, representing interactions of imaginary rigid particles need to be calibrated, thus for different concrete mixtures, the setup of the input parameters is not easy.

The SPH was originally developed in 1977 by Lucy [4] and, Monaghan and Gingold [5] for astrophysical applications (here called standard SPH). The method uses a purely Lagrangian approach and has been successfully employed in compressible viscous fluid problems. Later, Monaghan [6] further developed the new SPH algorithm for simulating the slightly compressible flows by introducing a virtual speed of sound and attaining a very low Mach number to control density variation within 1%, which is usually called weakly compressible SPH (WCSPH). In many SPH approaches, incompressible fluids are treated as slightly compressible fluids for using WCSPH method. To completely solve this particle compression problem, the MPS algorithm was developed in 1996 in Japan [7], which solves a pressure Poisson equation at every time step to ensure the incompressibility of particle. In the MPS method, the particles are incompressible, the viscous effect between fluid particles is calculated by an explicit algorithm, but the particle pressure is calculated by an implicit algorithm. Hence, general MPS is called semi-implicit algorithm. After the birth of the MPS, Cummins & Rudman [8] realized the incompressibility in SPH in 1999 by solving a pressure Poisson equation at every time step like as the MPS to satisfy the divergence-free velocity condition, which is called pressure or projection - based incompressible SPH (ISPH). Later after, the pressure-based ISPH algorithm was improved for satisfying the constant density condition besides the divergence-free velocity condition [9,10]. However, these ISPH methods need the iterative solution of the pressure Poisson equation. This makes implementing them in parallel and on GPUs fairly difficult. The WCSPH implementations are generally more popular as they are much easier to implement and parallelize, and the WCSPH implements boundary relatively easily and this is harder to do with the pressure-based ISPH [11]. Lee et al. [12] compared the pressure-based ISPH and the WCSPH on various incompressible flow test cases and concluded that the WCSPH method exhibits strong spurious oscillations especially in pressure and produces unreliable results particularly on coarse particle resolutions. However, Muta et al. [11] pointed out that both the WCSPH and the ISPH schemes suffer from inaccuracies when the particles become disordered. In flows with significant shear, the particles can become significantly disordered leading to poor accuracy and particle clumping in extreme cases. Recently, many other ISPH approaches, differentiating from the traditional pressure-based ISPH, have been developed, for example, by using full explicit algorithm [13], enforcing a kinematic constraint that the volume of the fluid particles is constant [14], and employing the artificial compressibility method [15], etc., but there is no generally accepted ISPH now.

So far, many flow simulation studies of fresh concrete have been found, using WCSPH method [16–19], ISPH method [20–22], or MPS method [23–25]. Almost all current numerical analyses of fresh cementitious materials are for slump flow, L-flow or flow behaviors in rheometer. The numerical results were roughly confirmed by comparing with the experimental results of flow shape or/and distance. However, in these flow tests, the thickness of concrete sample is limited and accordingly small weight-induced pressure acts on the concrete sample. The low pressure may contribute to the accuracy of SPH analysis. On the contrary, fresh concrete suffers from great pressure in actual construction due to pumping or high casting height. On the other hand, during casting or pumping, the densification of fresh concrete, caused by air loss and water evaporation, slightly reduce the volume of concrete. Thus, there may be no problem to treat fresh concrete as a weakly compressible fluid. Moreover, there is a lack of constitutive law to accurately describe the flow behaviors of fresh concrete that is a complicated fluid, and because concrete has large dimension and coarse aggregate is included, the requirement of flow simulation accuracy of fresh concrete may be low, not like other non-Newtonian fluids. At this time, there is still a lack of detailed discussion on respective applicability and practicality of SPH and MPS in the concrete field. Therefore, despite of some problems with WCSPH compared to ISPH, we do not yet rule out that WCSPH can be applied to fresh concrete as well.

In this study, we tried to clarify the applicability of weakly compressible SPH and complete implicit MPS methods for the flow simulations of fresh cementitious materials under high pressure. Since traditional semi-implicit MPS is not efficient for high viscosity fluid such as fresh concrete, we used a complete implicit MPS (I-MPS) in this study. Since the experiment accuracy of fresh concrete is easily reduced by the random distribution of coarse aggregate particles than fresh mortar, and the boundary slippage resistance model of fresh concrete has not been established now. Also, for the same numerical method (SPH or MPS), there is no difference in the calculation procedure between fresh concrete and fresh mortar. Hence, in this study flow behaviors of fresh mortars in the L-box were observed experimentally and simulated by WCSPH and I-MPS, respectively. Then we discussed quantitatively the effects of various factors on the applicability of two numerical methods, including mortar's fluidity, constitutive law used, boundary slippage resistance, and initial gravity-induced pressure.

3.2 WCSPH and I-MPS Methods

3.2.1 Governing Equations

In the simulation of fluid motion, the governing equations mainly include continuity equation and motion equation. The continuity equation considers the conservation of mass of the fluid, and the motion equation considers the conservation of momentum during the fluid movement. For viscos fluids, the fluid motion caused by gravity, viscosity, and pressure, the governing equations are shown as following:

$$\begin{cases} \dfrac{1}{\rho}\dfrac{d\rho}{dt} + \nabla \cdot \vec{u} = 0 \\ \dfrac{d\vec{u}}{dt} = \vec{g} + \dfrac{\mu}{\rho}\nabla^2 \vec{u} - \dfrac{1}{\rho}\nabla P \end{cases} . \tag{3.1}$$

where, ρ is density of fluid, $\vec{u}$ is velocity, t is time, P is pressure, $\vec{g}$ is gravitational acceleration, and μ is dynamic viscosity of fluid, the ratio of dynamic viscosity to fluid density is kinematic viscosity.

3.2.2 Kernel Function

The kernel function is only a weight function for MPS, whereas for SPH, it is not only used as a weight function, but also its derivative is used to calculate the differential operator such as a gradient of velocity.

For SPH, there are many kinds of kernel functions, the following cubic spine function [26] is generally adopted, as shown in Eq. (3.2).

$$W(r,h) = \begin{cases} \dfrac{1}{4\pi h^2}\left(1 - \dfrac{3}{2}q^2 + \dfrac{3}{4}q^3\right) & 0 \le q \le 1 \\ \dfrac{1}{4\pi h^2}(2-q)^3 & 1 \le q \le 2, \quad q = \dfrac{r}{h} \\ 0 & q \ge 2 \end{cases} \tag{3.2}$$

where, r is distance between two particles, and h is smoothing length.

The kernel function used in MPS is proposed by Koshizuka and Oka [7], as shown in Eq. (3.3).

$$w(r) = \begin{cases} \dfrac{r_e}{r_{ij}} - 1 & 0 < r_{ij} < r \\ 0 & r_{ij} \ge r_e \end{cases}, \quad r_{ij} = \left|\vec{r}_j - \vec{r}_i\right| \tag{3.3}$$

where, r_{ij} is distance between two particles, and r_e is radius of influence area.

As shown in Eq. (3.3), the closer the particle distance r_{ij}, the greater the interaction weight $w(r)$ for preventing particles from agglomeration.

3.2.3 Particle Density

The particles in SPH are permitted to be weakly compressed, and their mean density is obtained by averaging the densities of all particles in each influential domain. The change of fluid density is expressed by Eq. (3.4) [27].

$$\frac{d\rho_i}{dt} = \sum_{j \neq i} m_j \vec{u}_{ij} \cdot \nabla_i W(r,h), \quad \vec{u}_{ij} = \vec{u}_i - \vec{u}_j \tag{3.4}$$

where, m_j is mass of particle j.

In MPS, particle number density n is used instead of the particle density used in SPH. Since the particles are assumed to be incompressible, the n should be a constant. The n of particle i and its derivation with respect to time are expressed as follows [7, 28]:

$$n_i = \sum_{j \neq i} w(|\vec{r}_j - \vec{r}_i|), \quad \frac{dn_i}{dt} = \sum_{j \neq i} \frac{-r_e}{r_{ij}^3} (\vec{r}_{ij} \cdot \vec{u}_{ij}) \tag{3.5}$$

where, n^0 is initial value of particle number density.

3.2.4 Viscous Term Calculation

In SPH, the viscous stress term is simplified, as shown in Eq. (3.6) [27].

$$\left\langle \frac{\mu}{\rho} \nabla^2 \vec{u} \right\rangle_i = -\sum_{j \neq i} m_j \left[\frac{4\mu_i \mu_j}{(\mu_i + \mu_j)(\rho_i + \rho_j)} \frac{\vec{r}_{ij} \vec{u}_{ij}}{|\vec{r}_{ij}|^2} \right] \nabla_i W_{ij} \tag{3.6}$$

In MPS, the higher order discretization expression of the viscosity term is shown in Eq. (3.7) [28].

$$\left\langle \frac{\mu}{\rho} \nabla^2 \vec{u} \right\rangle_i = \frac{5-d}{n^0} \sum_{i \neq j} \left[\frac{4\mu_i \mu_j}{(\mu_i + \mu_j)(\rho_i + \rho_j)} \frac{\vec{u}_{ij} r_e}{r_{ij}^3} \right] \tag{3.7}$$

where, μ is dynamic viscosity of particle, d is model dimension (here, d is equal to 3).

The semi-implicit MPS is not suitable for high viscosity fluids because large viscosity makes the time-step Δt to be a small value according to Eq. (3.7) and Eq. (3.26) mentioned late. Since fresh cementitious materials have large viscosity, using implicit calculation to solve the viscous term would make it possible to use a large time-step Δt to improve the calculation efficiency. The implicit expression is shown in Eq. (3.8). Hence, the MPS used in this study is a complete implicit algorithm, hereafter called implicit MPS (I-MPS).

$$\langle \vec{u}_t \rangle_i + dt \cdot \left\langle \frac{\mu}{\rho} \nabla^2 \vec{u}_{t+1} \right\rangle_i = \langle \vec{u}_{t+1} \rangle_i \tag{3.8}$$

3.2.5 Pressure Solution

In WCSPH, the fluid is treated to be weakly compressible, and the equation of state (EOS) is used to determine fluid pressure. The pressure-density relationship [29,30] is assumed to follow Eq. (3.9).

$$P = B\left[\left(\frac{\rho}{\rho_0}\right)^{\gamma} - 1\right] \tag{3.9}$$

where, ρ_0 is initial density of fluid, and $B=\rho_0 c_0^2/\gamma$, in which γ is a constant and equals to 7, and c_0 is sound speed under the initial density ($c_0 = c(\rho_0) = \sqrt{(\partial P/\partial \rho)}|_{\rho_0}$).

In the MPS, the particle pressure is obtained by solving the pressure Poisson equation [7] shown in Eq. (3.10).

$$\left\langle \frac{\Delta t}{\rho}\nabla^2 P \right\rangle_i^{k+1} = \frac{1}{n^0}\left(\frac{dn}{dt}\right)^* \tag{3.10}$$

where, * indicates the temporary value of the variables after considering gravity and viscous force.

The Laplacian in Eq. (3.10) is discretized by higher order Laplacian (HL) scheme [28] as:

$$\left\langle \frac{\Delta t}{\rho}\nabla^2 P \right\rangle_i = \frac{5-d}{n^0}\sum_{i\neq j}\left[\frac{r_e}{r_{ij}^3}\left(P_j - P_i\right)\right] \tag{3.11}$$

3.2.6 Pressure Term Calculation

In the SPH, the pressure gradient term is calculated by a derivation of the kernel function and discretized in symmetrical form, as shown in Eq. (3.12) [27].

$$\left(-\frac{1}{\rho}\nabla P\right)_i = -\sum_j m_j\left(\frac{P_i}{\rho_i^2} + \frac{P_j}{\rho_j^2}\right)\nabla_i W_{ij} \tag{3.12}$$

However, the pressure gradient of the MPS is independent on the kernel function. For stabilizing the numerical calculation, $P_{i,\min}$ is used in place of P_i, as the configuration of neighboring particles is not isotropic in general. The value of $P_{i,\min}$ is the minimum value among the neighboring particles within a distance of r_e. the pressure gradient is calculated by the following discrete formula [7]:

$$\langle \nabla P \rangle_i^{k+1} = \frac{d}{n^0}\sum_{j\neq i}\left[\frac{P_j^{k+1} - P_{i,\min}^{k+1}}{\left|\vec{r}_j^{\,*} - \vec{r}_i^{\,*}\right|^2}\left(\vec{r}_j^{\,*} - \vec{r}_i^{\,*}\right)w\left(r_{ij}^*\right)\right] \tag{3.13}$$

The main differences between WCSPH and I-MPS are summarized in **Table 3.1**.

Table 3.1 Comparison of WCSPH and I-MPS

Item	WCSPH	I-MPS
Kernel function	$W(r,h)=\begin{cases}\frac{10}{7\pi h^2}(1-\frac{3}{2}q^2+\frac{3}{4}q^3) & 0\le q\le 1\\ \frac{10}{28\pi h^2}(2-q)^3 & 1\le q\le 2,\quad q=\frac{r}{h}\\ 0 & q\ge 2\end{cases}$	$w(r)=\begin{cases}\frac{r_e}{r_{ij}}-1 & 0<r_{ij}<r\\ 0 & r_{ij}\ge r_e\end{cases},\quad r_{ij}=\left\|\vec{r}_j-\vec{r}_i\right\|$
Particle density	$\frac{d\rho_i}{dt}=\sum_{j\neq i}m_j\vec{u}_{ij}\cdot\nabla_i W(r,h),\quad \vec{u}_{ij}=\vec{u}_i-\vec{u}_j$	$\frac{dn_i}{dt}=\frac{1}{n_0}\sum_{j\neq i}\frac{-r_e}{r_{ij}^3}(\vec{r}_{ij}\cdot\vec{u}_{ij})$
Viscous term	$\left\langle\frac{\mu}{\rho}\nabla^2\vec{u}\right\rangle_i=-\sum_{j\neq i}m_j\left[\frac{4\mu_i\mu_j}{(\mu_i+\mu_j)(\rho_i+\rho_j)}\frac{\vec{r}_{ij}\vec{u}_{ij}}{\left\|\vec{r}_{ij}\right\|^2}\right]\nabla_i W_{ij}$	$\left\langle\frac{\mu}{\rho}\nabla^2\vec{u}\right\rangle_i=\frac{5-d}{n^0}\sum_{i\neq j}\left[\frac{4\mu_i\mu_j}{(\mu_i+\mu_j)(\rho_i+\rho_j)}\frac{\vec{u}_{ij}r_e}{r_{ij}^3}\right]$
Pressure calculation	$P=B\left[\left(\frac{\rho}{\rho_0}\right)^{\gamma}-1\right]$	$\left\langle\frac{\Delta t}{\rho}\nabla^2 P\right\rangle_i^{k+1}=\frac{1}{n^0}\left(\frac{dn}{dt}\right)^*$
Pressure term	$\left(-\frac{1}{\rho}\nabla P\right)_i=-\sum_j m_j\left(\frac{P_i}{\rho_i^2}+\frac{P_j}{\rho_j^2}\right)\nabla_i W_{ij}$	$\left\langle\nabla P\right\rangle_i^{k+1}=\frac{d}{n^0}\sum_{j\neq i}\left[\frac{P_j^{k+1}-P_{i,\min}^{k+1}}{\left\|\vec{r}_j^{\,*}-\vec{r}_i^{\,*}\right\|^2}\left(\vec{r}_j^{\,*}-\vec{r}_i^{\,*}\right)w\left(r_{ij}^*\right)\right]$

3.3 Constitutive Models

The Bingham model has been generally used to describe the rheological behaviors of FCM [31]. However, FCM is a special viscous granular material, there are flocculation and dispersion of binder particles, inter-particle friction, and interlocking of aggregate particles. Hence, their rheological behaviors are so complicated that they may not be exactly expressed by the Bingham model. Li proposed the VGM model based on a series of theoretical analyses [32, 33] and experimental investigations [34, 35]. It has been verified that this model is able to simultaneously describe the pressure-dependence, shearing time dependence, thixotropy and nonlinear characteristic of flow behaviors of FCM [36]. In this study, we also discussed the effects of using different constitutive models on the WCSPH and I-MPS simulations.

3.3.1 Bingham Model

Bingham model is shown in Eq. (3.14). The effective viscosity μ (also called dynamic viscosity in section 2.4) for numerical computation is represented by Eq. (3.15).

$$\tau = \tau_b + \mu_b \cdot \dot{\gamma} \tag{3.14}$$

$$\mu = \mu_b + \frac{\tau_b}{\dot{\gamma}} \tag{3.15}$$

where, τ_b is yield stress, μ_b is plastic viscosity, $\dot{\gamma}$ is shear strain rate defined by the second invariant of the deformation rate tensor as:

$$\dot{\gamma} = \sqrt{2\mathrm{II}_\mathrm{D}}, \quad \mathrm{II}_\mathrm{D} = \frac{1}{2} D : D, \quad D = \frac{1}{2}\left[(\nabla \vec{u}) + (\nabla \vec{u})^T\right] \tag{3.16}$$

where, $\boldsymbol{D}$ is deformation rate tensor, II_D is the second invariant of $\boldsymbol{D}$.

But the constitutive law shown in Eq. (3.15) is discontinuous when shear stress τ approaches to the yield stress τ_0. Moreover, the effective viscosity attains an infinite value in case of $\tau \leqq \tau_0$, which leads to a numerical divergence. Hence, a regularized Bingham model [37] is generally used, as shown in Eq. (3.17). Two models are illustrated in **Fig. 3.1**.

$$\mu = \mu_b + \tau_b \frac{1 - e^{\beta\dot{\gamma}}}{\dot{\gamma}} \tag{3.17}$$

where, β is a parameter related to the transition between solid and fluid regimes, and the larger the β, the sharper the transition.

3.3.2 VGM Model

The relationship between shear stress and shear strain rate in the VGM model is shown in **Fig. 3.2** [32]. The VMG model not only describes the flow behaviors of fresh concrete in the shear failure state (see Part III in **Fig. 3.2**) but also provides the information about the deformation behaviors before shear failure (yield) (see Part I and Part II in **Fig. 3.2**). Since fresh concrete may quickly enter into the shear failure state during pumping or casting, a precise calculation of the shear deformation before

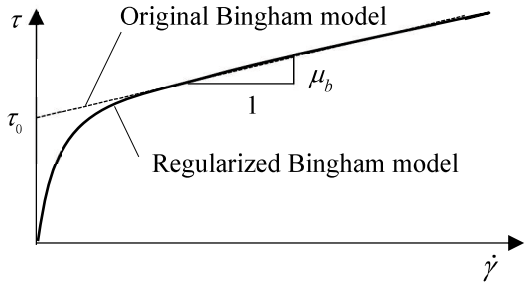

Fig. 3.1 Original and regularized Bingham models

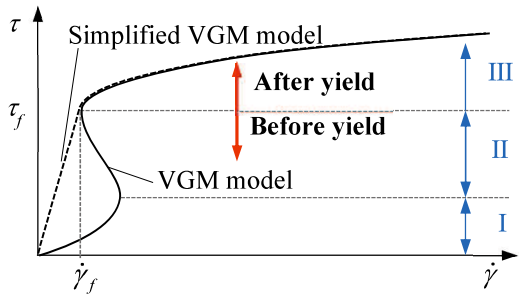

Fig. 3.2 VGM model and simplified VGM model

yield is not necessary. Therefore, we simplified the flow curve before yield with a straight line. The simplified VGM model equations are shown in Eqs. (3.18) and (3.19).

$$\begin{cases} \mu = \dfrac{\tau_f}{\dot{\gamma}_f} & \dot{\gamma} < \dot{\gamma}_f \\ \mu = \dfrac{\mu_0}{\cos(\theta_f \cdot e^{-\kappa \cdot \dot{\gamma} \cdot (t - t_f)})} + \dfrac{\tau_f}{\dot{\gamma}} & \dot{\gamma} \geq \dot{\gamma}_f \end{cases} \tag{3.18}$$

$$\tau_f = \sigma_n \tan(\theta_f \cdot e^{-\kappa \cdot \dot{\gamma} \cdot (t - t_f)} + \varphi) + C_{w1} \tag{3.19}$$

where, σ_n is normal stress, θ_f is mean particle contact angle, κ is a parameter related to shearing time-dependence, t_f is shearing time before shear failure, φ is mean inter-particle frictional angle, C_{w1} is shear resistance related to mixing water's surface tension, τ_f is shear failure limit stress, $\dot{\gamma}_f$ is shear strain rate at the shear failure point, μ_0 is basic viscosity not related to temperature and particle arrangement.

When shear stress τ and shear strain rate $\dot{\gamma}$ are smaller than the shear failure stress limit τ_f and the strain limit rate $\dot{\gamma}_f$, respectively, fresh concrete is in viscose-elastic-plastic state (before yield). When $\tau > \tau_f$ and $\dot{\gamma} > \dot{\gamma}_f$, fresh concrete enters into the shear failure state (after yield). The shear failure limit stress τ_f is mainly dependent on normal stress σ_n, mean particle contact angle θ_f, mean inter-particle frictional angle φ, and the mixing water-induced shear resistance C_{w1}.

3.4 Boundary Conditions

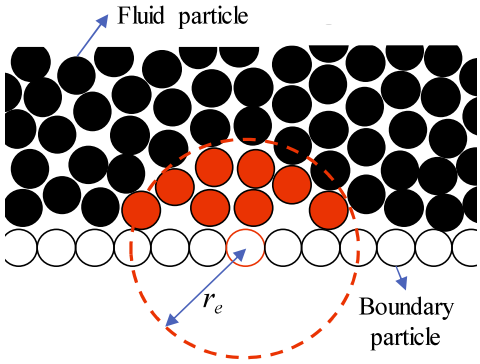

Fig. 3.3 Influence area of boundary particle

In this study, the flow fields considered were confined within solid boundaries over which a non-slip condition was applied. The solid boundaries were represented by boundary particles. Hence, the interaction between boundary and fluid is treated with the interactions between the boundary particles and fluid particles within a spherical domain, as shown in **Fig. 3.3**. The radius (r_e) of influence range of a boundary particle was set as 2.1 times of inter-particle distance [7, 26]. However, the r_e of spherical domain was set as 4.1 times of interparticle distance when calculating Laplacian operator of the MPS [7].

Numerous approaches have been proposed to handle the solid boundary conditions in SPH. In this study, the repellent-particle approach [6] has been adopted, in which fixed boundary particles lie at the wall surfaces and exert an artificial repulsive force on approaching fluid particles to prevent them from penetrating the solid walls. The repellent particle approach has greater flexibility in handling boundary conditions with complex geometry. Although it is reported that the densities of the particles approaching to the boundary will decrease to about half of them in the bulk material [19], this problem has been solved by solving Eq. (3.4) and using Shepard filter to modify the density field in every 30 time-steps, instead of using a weighted summation of mass term [27].

Fluid particles in the MPS are also subjected to a pressure from motionless boundary particles (see Eq. (3.13)). Since the implicit algorithm was used in the I-MPS to calculate the pressure term, the Dirichlet boundary condition [38] was adopted to solve the pressure Poisson equation. The pressure on the free surface was set to be zero, and the boundary particles should satisfy the same pressure calculation equations (see Eq. (3.10)) as fluid particles.

Besides the interaction (repulsive force or pressure) between boundary and fluid particles described above, fresh cementitious materials also suffer from a boundary slippage resistance (BSR) in the same time. Different BSR models were adopted in previous numerical analyses. Deeb et al. [22] considered the BSR with dynamic friction coefficient. Dhaheer et al. [20] handled the effect of BSR by a kinetic friction coefficient. Murata et al.[39] performed a series of pipe flow experiments of fresh mortars with different fluidity, then concluded that the BSR of fresh mortar is a linear function of slippage velocity and has a minimum value, as shown in Eq. (3.20). Considering that there is not only a friction between boundary and fluid, but also a viscous force caused by rotational motion or relative displacement of particles near the boundary, we adopted the Murata model in this study.

$$\tau_R = \alpha \cdot V_S + A \tag{3.20}$$

where, τ_R is boundary slippage resistance, V_S is slippage velocity, α and A are constants.

3.5 Experiment

Since the rheological behaviors of fresh concrete are greatly affected by random distribution and segregation of coarse aggregate particles, so that the rheological test of fresh concrete usually has larger error, compared to fresh mortar or cement paste. For ensuring the reliability of comparison of experimental result and numerical result, in this study we took fresh mortar as an object of experimental and numerical investigation. Other reason is that there is no suitable method to measure the parameter α, A of fresh concrete at this time.

3.5.1 Mortar Mixtures and Rheological Parameters Type

To compare the experimental and simulation results of fresh mortar with different fluidity, three series of mortars were used, of which mix proportions are presented in **Table 3.2**, and bulk densities were 2039 kg/m^3, 2065 kg/m^3, and 2091 kg/m^3, respectively. Ordinary Portland cement with specific surface area of 3500 cm^2/g and density of 3.16 g/cm^3 was used. Fine aggregate was sea sand with 2570 kg/m^3 of density in saturated surface dry state, 1.36% of water absorption ratio, and 2.9 of fineness modulus. As bleeding would worsen the uniformity of mortar and further affect the rheological properties, AE water reducing agent was added to reduce water content.

Right after the mortars were mixed, the parameters of Bingham model and VGM model were measured by the RSNS rheometer (see in **Fig. 3.4**). The upper blade was fixed, but the lower blade was rotated by the motor's driving. The thickness of the mortar sample between the two blades was 100mm. The rotating speed was increased firstly and then decreased to obtain the up and down-curves of shear stress-shear rate relationship. The down-curve was used to calculate the constants of Bingham model. Then, the normal stress was increased by two air cylinders via the aluminum plate placed on the top surface of mortar sample, the rheological parameters of VGM model were measured. The

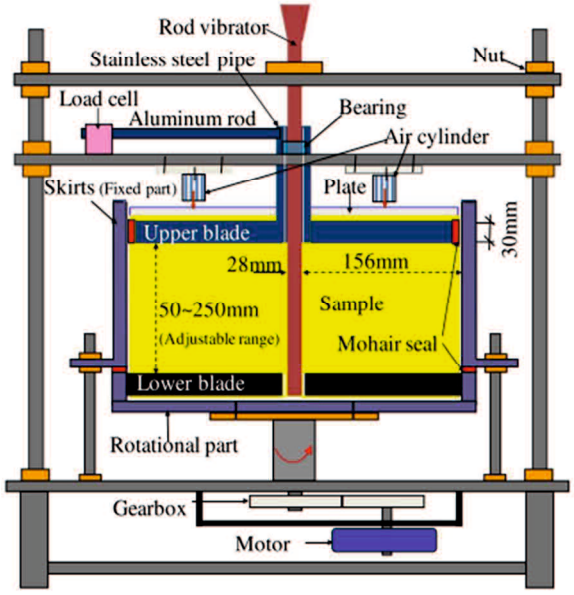

Fig. 3.4 The RSNS rheometer

Table 3.2 Mix proportions of fresh mortar

Series No.	*W/C*	*WR*	*S/C*	Unit mass (kg/m^3)				*Flow* (mm)
				W	*C*	*S*	*WR*	
1	0.50			254				102
2	0.55	0.5×*C*%	2.5	280	509	1273	2.5	159
3	0.60			306				200

Notes: *W/C*: water-cement ratio, *WR*: AE water reducing agent, *S/C*: sand-cement ratio by mass, *W*: water, *C*: cement, *S*: sand, *Flow*: flow table spread with non-dropping.

detailed calculation methods of rheological parameters can be found in Ref. [32]. It should be noted that when measuring the constants of Bingham model, the aluminum plate and the two air cylinders were not used, thus no external pressure was applied to the sample.

There is no doubt that boundary slippage resistance (BSR) affects the flow behavior of fresh concrete. However, the measurement of BSR has still been an issue for fresh concrete. In this study, we tried to measure the BSR of fresh mortar with a B-type viscometer. B-type viscometer is originally designed to measure yield stress and viscosity of Bingham fluid, supposing that no slippage occurs between fluid and rotor. However, for granular materials, the occurrence of slippage cannot be avoided when the rotating speed of rotor is large. Taking Series No.3 as an example, as shown in **Fig. 3.5**, the rotational speed of rotor was first increased and then decreased to get up-curve and down-curve of $\tau - \dot{\gamma}$ relationship. In the up-curve, when the shear rate was beyond 1.33s^{-1} (rotating speed: 0.26deg./s), shear stress got very less increase, the slope of the up-curve became very small. This is usually considered to be due to the breakdown of flocculent structure of cement particles. However, even if the flocculent structure of cement particles was completely broken down, the shear stress should continue to increase provided that the shear rate is raised because the viscous resistance increases with the shear rate. Thus, we thought that the slippage between the mortar sample and the rotor resulted in the almost changeless shear stress in the shear rate range of 1.33 ~ 2.66s^{-1}, though we have no method to confirm this supposition at this time.

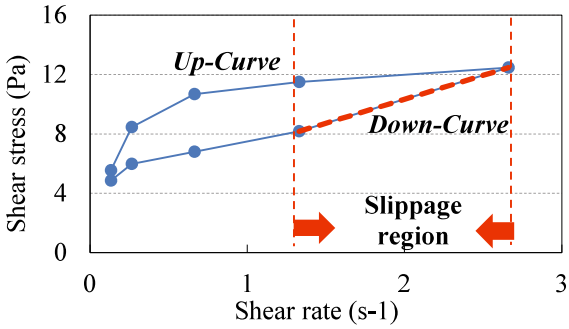

Fig. 3.5 Shear stress-shear rate relationship of Series No.3 measured by B-type viscometer

On the other hand, the mean stress τ_m that the rotor acts on the mortar sample is obtained on basis of Eq. (3.21), as shown in Eq. (3.22).

$$M = \int_0^R 2\pi r \cdot r \cdot \tau_m dr = \frac{2}{3}\pi R^3 \tau_m \tag{3.21}$$

$$\tau_m = \frac{3M}{2\pi R^3} \tag{3.22}$$

where, M is rotor's torque, R is radius of rotor.

And the position r_m, where the stress is equal to the mean stress, is obtained on basis of Eqs. (3.21) and (3.23), as shown in Eq. (3.24) and **Fig. 3.6**.

$$M = \pi R^2 \cdot \tau_m \cdot r_m \tag{3.23}$$

$$r_m = \frac{2}{3}R \tag{3.24}$$

Thus, if the slippage occurs when the rotating speed is high, the mean slippage velocity V_S is expressed by Eq. (3.25).

$$V_S = \frac{2}{3} R \cdot \theta_r \tag{3.25}$$

where, θ_r is rotating speed of rotor (deg./s).

For Series No.3, if considering it in slippage state on the rotor surface when the shear rate is over 1.33 s^{-1}, the relationship between mean slippage resistance stress τ_m and mean slippage velocity V_s is shown in **Fig. 3.7**. In the shear stress-shear rate relational plots, the hysteresis loop of up -curve and down-curve is caused by the breakdown of flocculent structure of particles. Likewise, when the slippage occurs, the contact point angles of the particles of mortar and the rotor change with the slippage, i.e., destruction of contact structure of particles and rotor, which results in a continuous reduction of the slippage resistance. Hence, the slope of the up-curve is small, and the down-curve is lower than the up-curve, as shown in the **Fig. 3.7**.

In this study, the B-type viscometer was employed to measure the parameter α, A of the BSR model of fresh mortar. The down-curve in the slippage region is used to determine the α and the A, which are the intercept and the slope of the regressive line of down-curve, respectively. Measured rheological parameters of Bingham model, VGM model, and the BSR model are shown in **Table 3.3**.

3.5.2 L-Flow Test

The geometry of L-box used in the L-flow test is shown in **Fig. 3.8**. The section and height of vertical room was 120mm×100mm, and 750mm, respectively, and the length of horizontal room was 600mm. A scale with 1 mm accuracy was attached to the L-box bottom.

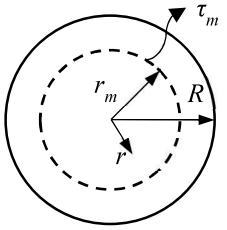

Fig. 3.6 Position of mean stress τ_m on the

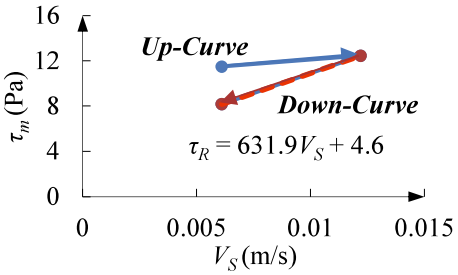

Fig. 3.7 Relationship between slippage stress τ_m and slippage velocity V_S (series No.3)

Table 3.3 Mix proportions of fresh mortars and rheological parameters

Series No.	Bingham model		VGM model						BSR Model	
	μ_b (Pa·s)	τ_b (Pa)	μ_0 (Pa·s)	$\dot{\gamma}_f$ (s^{-1})	κ	θ_f (rad)	φ (rad)	C_{w1} (Pa)	α (Pa·s·m^{-1})	A (Pa)
1	267.6	1112.6	240.8	0.222	2.7	0.326	0.187	660	1315.7	7.1
2	85.7	296.1	85.4	0.192	1.9	0.132	0.096	198	1218.5	6.1
3	47.1	256.1	46.8	0.183	1.5	0.085	0.064	156	631.9	4.6

Notes: μ_b: plastic viscosity of fresh mortar, τ_b: yield stress of fresh mortar, μ_0: basic viscosity, θ_f: mean particle contact angle, κ: a parameter related to shearing time-dependence, t_f: shearing time before shear failure, φ: mean inter-particle frictional angle, C_{w1}: shear resistance related to water surface tension, $\dot{\gamma}_f$: shear strain rate at the shear failure point, α and A are constants of BSR model.

Right after mixing, fresh mortar was cast into the vertical room of the L-box for a height of 25cm (Height-25cm), 50cm (Height-50cm), or 75cm (Height-75cm), following by quickly lifting upward the sliding gate to allow the mortar to flow under its own gravity. The flow distance in the horizontal room was recorded by a video camera. L-flow distance-time relational curves were shown in **Fig. 3.9**. The final flow shapes and the flow times until stop are shown in **Fig. 3.10**.

As shown in **Fig. 3.9**, in case of Height-1, Series No.1, which had the smallest flow table spread, flowed for only 3.0 seconds until it stopped, and the flow distance was the shortest of only 6.3 cm. Series No.2 flowed 41.9cm and stopped at 5.5 seconds. And Series No.3 had the highest fluidity and its flow did not stop until it reached the end of the horizontal room of L-box after 6.5 seconds. From **Fig. 3.10**, it can be found that the higher the initial height, the faster the flow of mortar. The sample with 75cm of initial height was the fastest to reach the end of the horizontal room of L-box at 1.5 seconds.

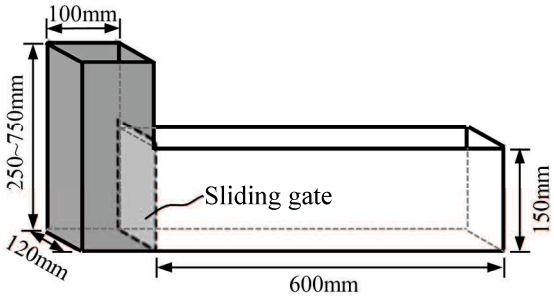

Fig. 3.8 Geometry of L-box

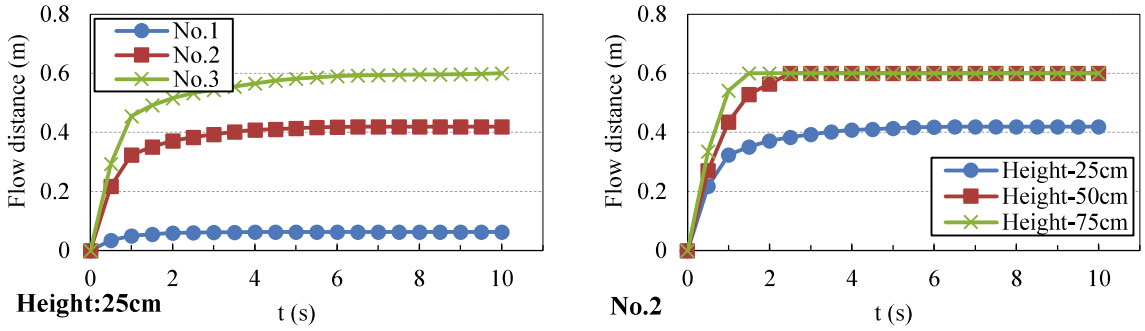

Fig. 3.9 Experimental results of L-flow distance-flow time relationship

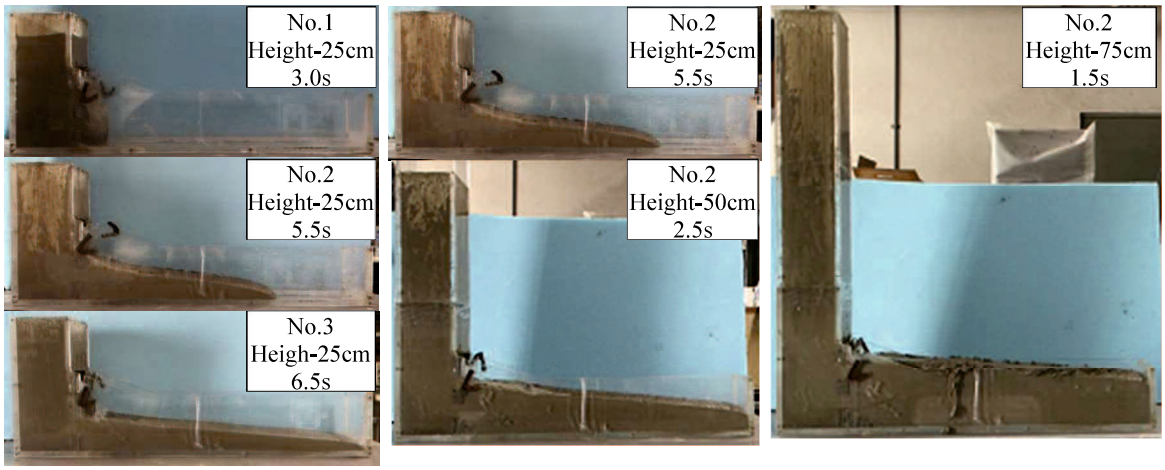

Fig. 3.10 Final flow shape and total flow time of mortars with different initial heights

3.6 Numerical Simulation of the L-flow Tests of Fresh Mortar

3.6.1 Numerical Analysis Conditions

Spherical particles were used to represent fresh mortar and flow boundary of the L-box. In the WCSPH, the L-box's bottom and walls were expressed by one layer of particles, while in the I-MPS three layers of particles were used in order to ensure the accuracy of particle density. Next, we conducted the resolution convergence study by using different inter-particle distances (*dis*), which were 20mm, 10mm and 5mm, respectively, for determining suitable size of fluid particles used in the L-flow simulations. Mortar's height in the vertical room of L-flow box was 25cm, and Murata's BSR model and Bingham model were employed. Taking Series No.2 as example, flow distance - elapse time relational curves were shown in **Fig. 3.11**. The calculated results using the three inter-particle distances were close, especially when *dis* was 10mm and 5mm. That is to say, when the *dis* is smaller than 10mm, the simulation result will be independent of inter-particle distance. And, the calculated results were almost the same within 5 seconds of flow time. According to **Fig. 3.10**, the L-flow almost finished in just a few seconds. Thus, there is almost no bad effect of large *dis* on L-flow simulation. Moreover, although smaller interparticle distance can yield a better output, more particles are required so that the calculation will be less efficient. Therefore, the inter-particle distance *dis* was set to be 10mm in the following simulations. The summary of analytical models was shown in **Table 3.4**.

The time-step of SPH was dependent on the Courant-Friedrichs-Lewy (CFL) condition, the force term, and the viscous diffusion term. A variable time-step Δt is determined according to Ref. [40] by using Eqs. (3.26) ~ (3.28).

$$\Delta t = 0.1 \cdot \min(\Delta t_f, \Delta t_{cv}) \tag{3.26}$$

$$\Delta t_f = \min\left(\sqrt{h/|f_i|}\right) \tag{3.27}$$

$$\Delta t_{cv} = \min \frac{h}{c_s + \max\left|\frac{h\vec{u}_{ij} \cdot \vec{r}_{ij}}{\vec{r}_{ij}^2}\right|} \tag{3.28}$$

where, Δt_f is based on the force acting on per unit mass $|f_i|$, Δt_{cv} combines the Courant and the viscous time-step, and i, j represents particles.

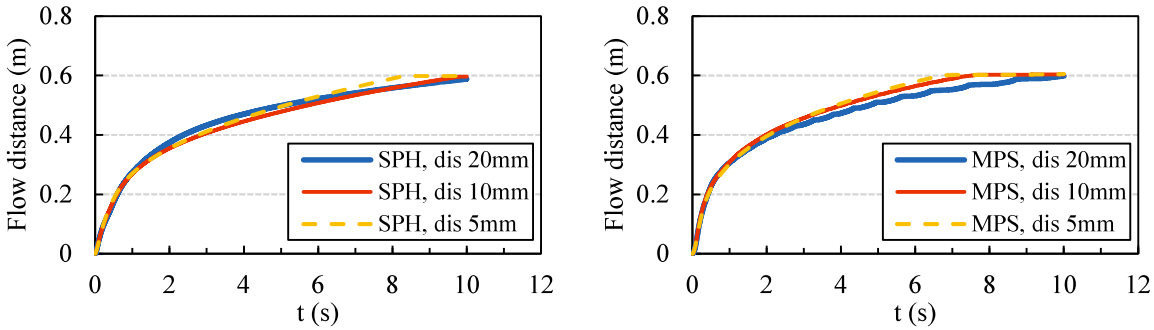

Fig. 3.11 Flow distance - elapse time relationship for different particle resolutions (Series No.2)

Table 3.4 Outline of analytical models

Method	Particle center distance *dis* (m)	Particle Number						Time-step (s)
		Height-25cm		Height-50cm		Height-75cm		
		Boundary	Mortar	Boundary	Mortar	Boundary	Mortar	
WCSPH	0.01	3834	2475	4934	4950	6034	7425	Variable (see Eq.(26)) (Initial value: 0.00005)
I-MPS		13158		17058		20958		0.001

The WCSPH method uses explicit algorithms to calculate particle motion, the time-step Δt is variable. To prevent excessive agglomeration or escape of particles, the initial value of Δt was set to be small, being 0.00005s in this study. However, since the I-MPS method uses implicit algorithms in this study, the Δt is a constant, and large time-step can be used. The used Δt was 0.001s for the I-MPS simulation in this study.

In addition, the L-flow simulations were run on a desktop computer with Windows 10 Education version (64 bit) operating system, using a single Inter Core i3-4130 CPU and memory of 8 GB. The compiler used was Visual Studio Community 2013. The compiler optimization directives selected the maximum optimization (Favor Speed, /O2).

3.6.2 Time Consumption of Numerical Simulation

During the L-flow test, the flow speed of mortar gradually decreased with the flow time, and eventually became zero. However, in numerical simulation, particle velocity becomes smaller and smaller, but it never reaches zero [18]. Since the start and the stop of flow are dependent on the yield stress (τ_0) of mortar, it was supposed that when the particle velocity reduced to $\Delta t \cdot \tau_0/(\rho \cdot dis)$, the particles were considered to stop moving, and the numerical calculation was finished. Calculating time of each L-flow simulation is recorded and shown in **Fig. 3.12**, when the initial filling height was 25cm and the Bingham model was employed as the constitutive model.

For the mortars in this study, the time-step Δt in the WCSPH was mainly controlled by the CFL condition and limited to 0.000046s, the length of time-step in I-MPS was fixed as 0.001s. As shown in **Fig. 3.12**, for different mortars, the necessary simulation times were almost the same for either the WCSPH method or the I-MPS method. For the same mortar, the WCSPH method required a longer calculating time than the I-MPS method. Simulation time of the WCSPH was approximately 2 times as long as the I-MPS. This is because that the I-MPS method in this study used implicit algorithms so that large time-step could be used, as stated in Section 6.1. Though

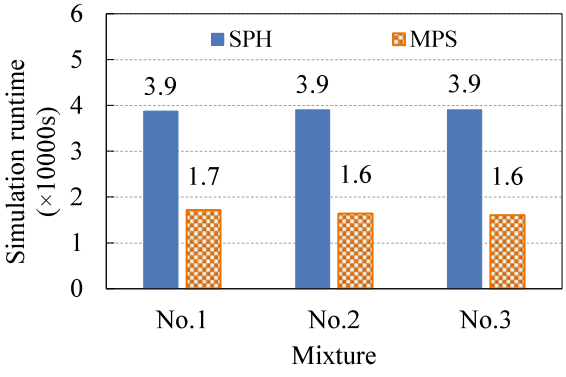

Fig. 3.12 Simulation runtime of different numerical methods

much time is needed to solve the Poisson equations, large time-step is able to significantly improve calculation efficiency of the I-MPS.

3.6.3 Discussion of Calculation Accuracy

In order to clarify respective calculation accuracy of WCSPH and I-MPS in the numerical flow simulation of FCM, the results of L-flow simulation were compared to the experimental results. Taking Series No.2 as example, the particle distributions and pressure fields of the numerical simulations at different times are shown in **Fig. 3.13**. The flow distance of mortar gradually increased with the elapsed time, at the same moment the height of the mortar remaining in the vertical room in the WCSPH is higher than that in the I-MPS. Correspondingly, the flow distance in the WCSPH was smaller than that in the I-MPS. In both the WCSPH and the I-MPS methods, the pressure was low on the free surface and high at the bottom of L-flow box. However, due to the compression of particles, the pressure was largely calculated for the particles at the bottom of the vertical room in the WCSPH, compared to the I-MPS.

In the following, the calculation accuracies of SPH and MPS were discussed under different boundary conditions, mortar fluidities, constitutive models, and initial pressures.

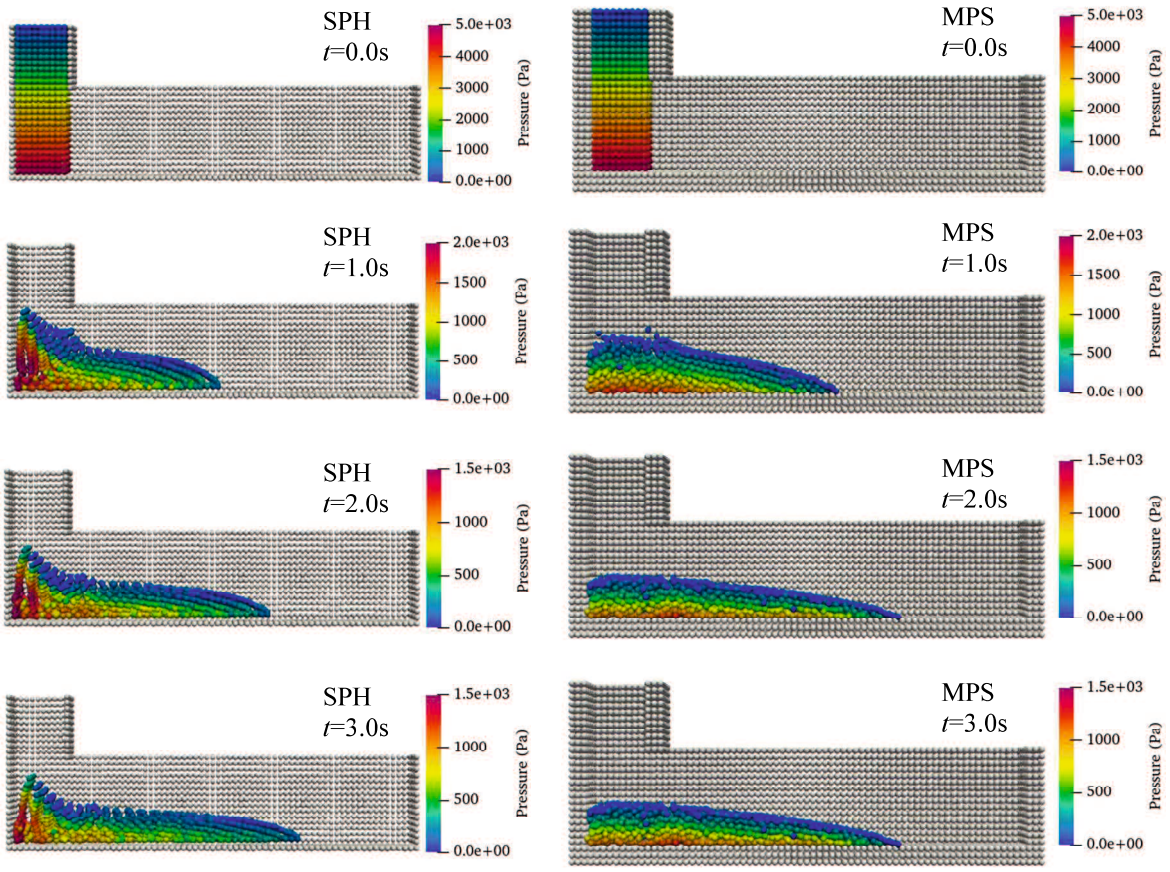

Fig. 3.13 Particle distributions and pressure fields
(Series No.2, initial height of 25cm, Murata's BSR and Bingham models)

■ **Influence of Boundary Slippage Resistance (BSR)**

The numerical results of L-flow distance-elapsed time relationships of three mortars with and without BSR are shown in **Fig. 3.14**, and final flow distance and calculation errors were listed in **Table 3.5**. Calculation method of the error is shown in Eq. (3.29)

$$\delta = \frac{\left| x_{num} - x_{\exp} \right|}{x_{\exp}} \times 100\% \tag{3.29}$$

where, δ is calculation error, x_{num} is numerical result, and x_{exp} is experimental result.

The simulation results of two numerical methods were different under whether the BSR was considered or not. Without the BSR, the mortar flowed rapidly, and the final flow distance was larger than the experimental value. However, when considering the BSR, the mortar flowed fast at the beginning, but the flow rapidly stopped. This flow behavior was coincident with the experiment, and the numerical results of final flow distance were close to the experimental results. As shown in **Table 3.5**, if considering the BSR, the calculation error δ in the final flow distance of Series No.1~No.3 reduced 53%, 13% and 0% in the WCSPH, and reduced 241%, 35% and -13% in the I-MPS, respectively. It should be noticed that due to the high fluidity of Series No.3 and the length limitation

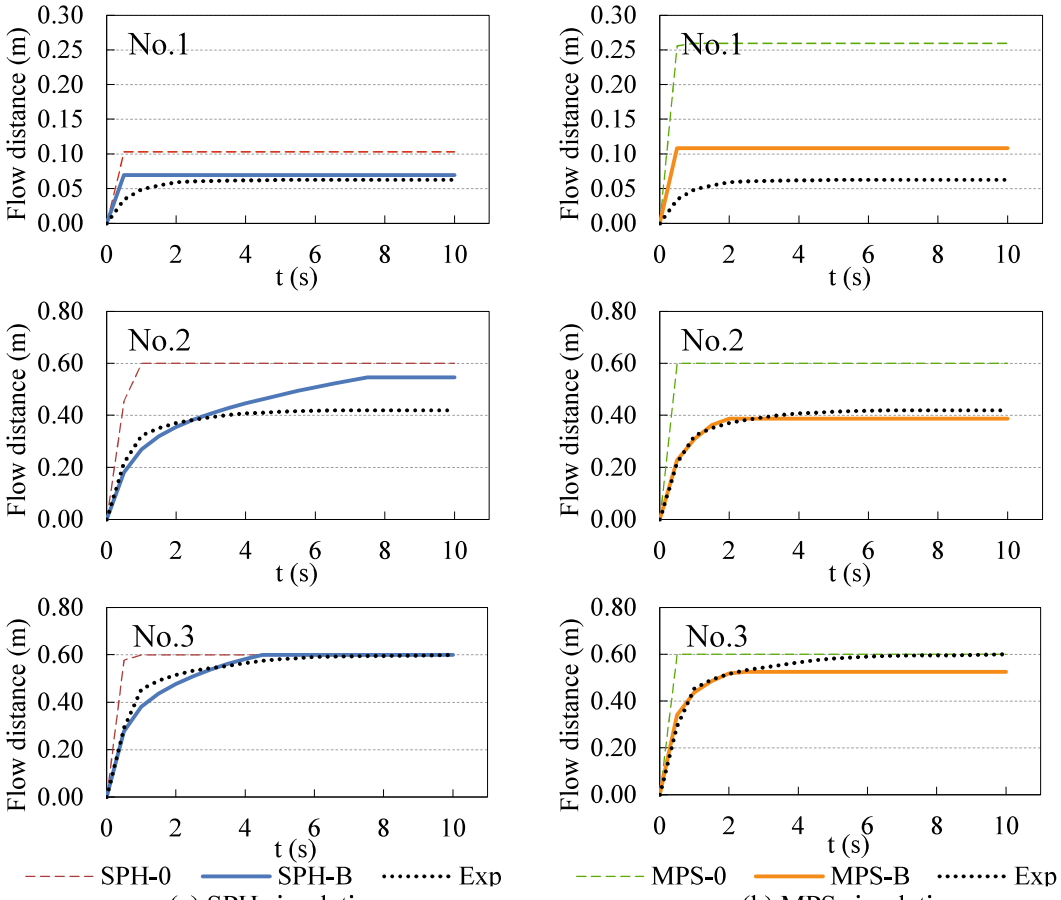

(a) SPH simulation (b) MPS simulation

Fig. 3.14 Influence of BSR on the numerical flow distance
(In the legends, "0" represents no BSR, "B" represents the BSR was considered, and "Exp" represents the experimental result)

Table 3.5 Numerical results and calculation errors of final flow distance with and without BSR

Series	Final flow distance (m)								
	Exp	SPH-0	Error δ	SPH-B	Error δ	MPS-0	Error δ	MPS-B	Error δ
No.1	0.063	0.103	64%	0.070	11%	0.259	313%	0.108	72%
No.2	0.419	0.600	43%	0.546	30%	0.600	43%	0.387	8%
No.3	0.600	0.600	0%	0.600	0%	0.600	0%	0.524	13%

Notes: "SPH-0"/"SPH-B" and "MPS-0"/"MPS-B" represent the numerical results, in which "0" represents no BSR, "B" represents the BSR was considered. "Exp" represents the experimental results.

of the horizontal room of L-box, the mortar sample flowed to the end of the horizontal room, no matter the BSR was considered or not. Therefore, the numerical result of Series No.3 could not truly reflect the influence of BSR. It can be concluded that the boundary slippage resistance has great effect on the numerical simulation, especially for the mortar with low fluidity. In order to accurately conduct numerical flow simulation of fresh cementite materials, the BSR should be considered.

■ **Influence of Mixture's Fluidity**

The numerical results and their errors of different fresh mortars are shown in **Fig. 3.15**. The BSR was considered in the calculation and Bingham model was used. **Fig. 3.16** shows the statistical errors of numerical results against the experimental results. Calculation method of the statistical error is shown in Eq. (3.30), which can intuitively reflect the deviating degree of the numerical results from the experimental results. The smaller the statistical error, the higher the simulation accuracy.

$$\delta_{sta} = \sqrt{\frac{1}{N}\sum_{t=0.5}^{T}\delta_t^2} \times 100\%,$$
$$\delta_t = \left(\frac{\left|x_{num} - x_{\exp}\right|}{x_{\exp}}\right)_t \times 100\% \qquad (30)$$

where, δ_{sta} is statistical error, δ_t is calculation error at time t, T is stop-time, N is number of 0.5s interval from 0.5s to T.

The final flow distance of Series No.1 calculated by the WCSPH was much closer to the experimental value, compared to the

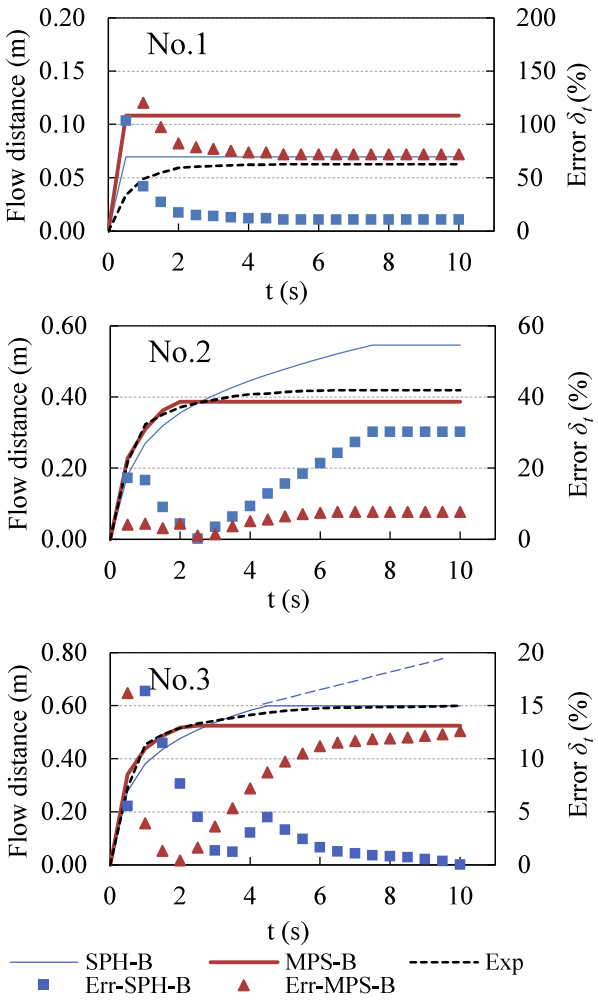

Fig. 3.15 Numerical results and calculation errors for different mortars, considering boundary slippage resistance

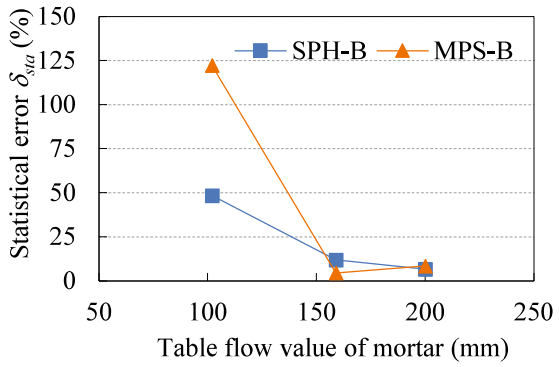

Fig. 3.16 Effect of fluidity on calculation error of flow distance

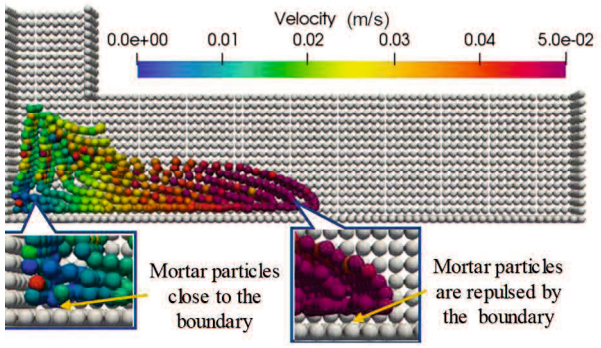

Fig. 3.17 Effect of boundary repulsive force

use of the I-MPS. The statistical error of the WCSPH results was also smaller than that of the I-MPS. For Series No.2, the I-MPS method gave more accurate results as the δ_{sta} was smaller, whereas in the WCSPH simulation, the flow of mortar did not stop until it reached 54.6 cm. For Series No.3, if the length of the L-box was no limited, the flow simulated by the WCSPH would not stop, and was supposed to last along the thin dashed line shown in **Fig. 3.15**. But the flow, simulated by the I-MPS, stopped before it reached to the end of the L-box, the δ_{sta} was less than 10%. Hence, for the fresh mortar with low fluidity, the simulation accuracy of the WCSPH is higher. But for the mortars with middle fluidity or high fluidity, the simulation accuracy of the I-MPS is higher.

As can be seen from **Fig. 3.15**, in case of the WCSPH simulation, the higher the fluidity of the fresh mortar, the more hardly its flow stopped, and the greater the error of the numerical result of final flow distance against experimental value. This is because that the repulsive force of boundary increases as the flow speed increases, and large repulsive force of boundary makes the fluid particles of SPH not close to the boundary, as shown in **Fig. 3.17**. The flow speeds of Series No.2 and No.3 were higher than that of Series No.1, This is because that higher flow speed of Series No.2 and No.3 results in a greater boundary repulsive force, which makes the fluid particles of SPH far from the boundary, correspondingly reduces the BSR of Series No.2 and No.3. For the I-MPS simulation, in the slowdown phase of flow, as the effective viscosity of fresh mortar, used in the regularized Bingham model, was much greater than its actual plastic viscosity, as shown in **Fig. 3.1**, the stop of numerical flow is earlier than the experiment. But since the final flow distance is dependent on yield stress other than effective viscosity, the I-MPS results of final flow distance are well consistent with the experiments, as shown in **Fig. 3.15**.

Hence, due to the combined influence of fluidity and BSR, the WCSPH is roughly appliable to fresh cementitious materials with low fluidity, whereas the I-MPS is of wide application, especially it is applied to high/middle fluidity FCM. Detailed discussion on the scope of application of the WCSPH method will be described in Section 6.4, which shows that it is inappropriate to use the level of fluidity to indicate the scope of application of the WCSPH method.

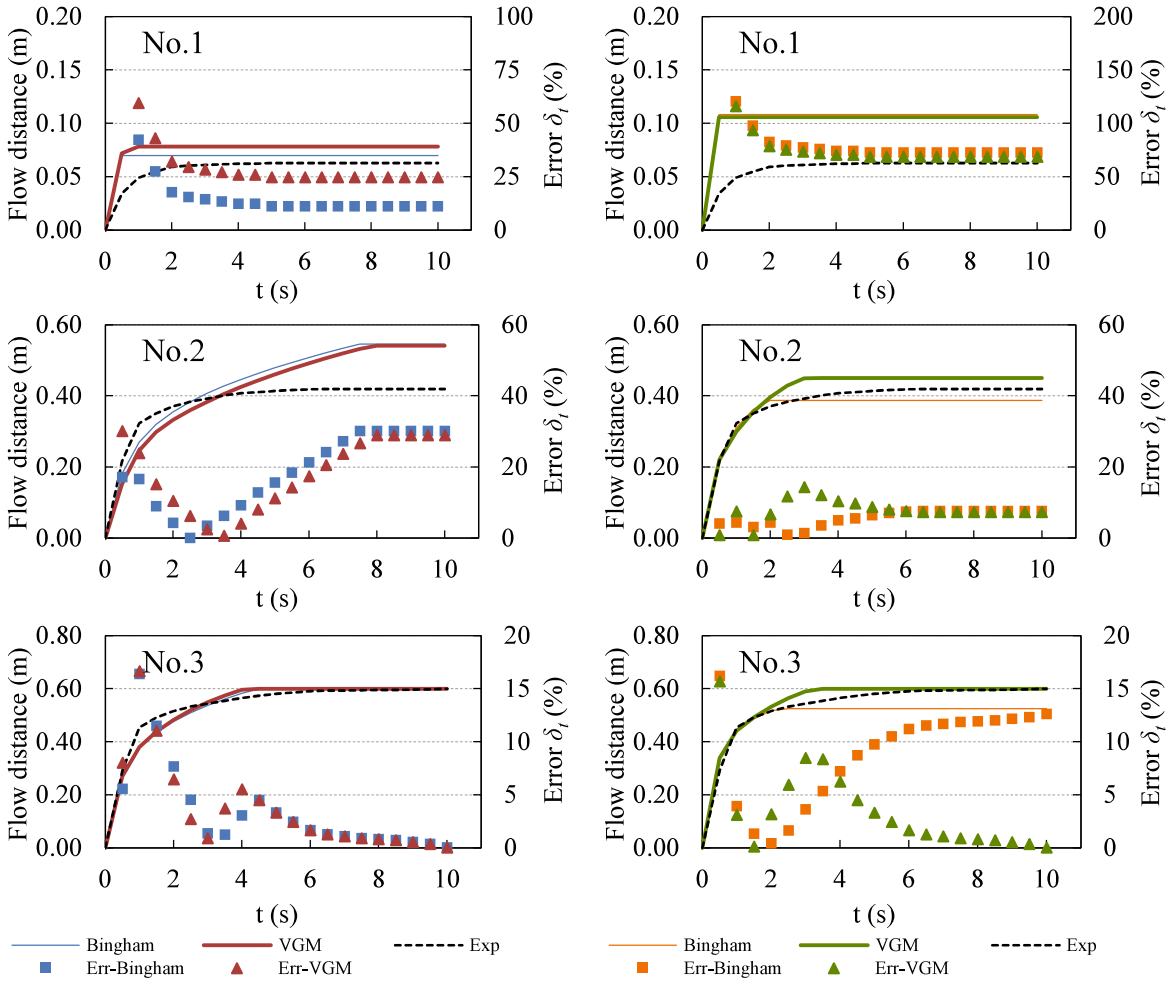

(a) SPH simulation (b) MPS simulation

Fig. 3.19 Numerical results and calculation errors, using different constitutive models

■ Influence of Constitutive Model

The numerical results of flow distance-elapsed time relationship, using different constitutive models, and the calculation errors are shown in **Fig. 3.19**. And the statistical errors of the numerical results are shown **Fig. 3.18**. As the mortar flows, its height in the vertical room decreases, accordingly the vertical pressure acting on the mortar by its gravity gradually decreases. In the VGM model, the pressure-dependent characteristic of rheological property is treated, the shear failure limit stress τ_f gradually decreases with the decrease of vertical pressure. Therefore, as shown in **Fig. 3.19**, the final flow distance calculated by using the VGM model was longer than that of the Bingham model, especially in the I-MPS simulations of Series No.2 and No.3, which were closer to the experimental results. However, due to the combined influences

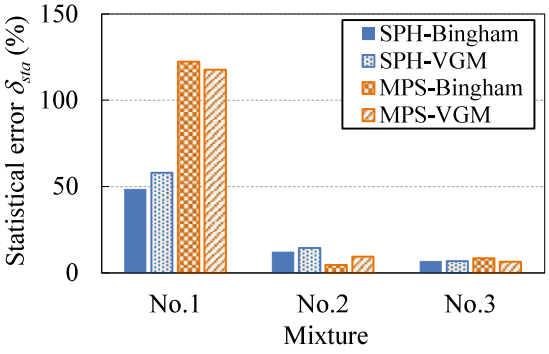

Fig. 3.18 Effect of constitutive model on the error of numerical analysis

of fluidity of mortar and boundary repulsive force in the WCSPH simulation, the influence of constitutive model on the numerical results was not clearly found in case of fresh mortar.

Fig. 3.18 shows that in either SPH or MPS simulations, the statistical errors of the calculation results are almost the same, no matter which constitutive model was used. That is to say, in the flow simulation of fresh mortar subjected to low external pressure, there is no great difference between the Bingham model and the VGM model. The VGM model has an advantage of describing the granular feature of fresh cementitious materials. Fresh concrete has more pronounced granular characteristics than fresh mortar due to the inclusion of coarse aggregate, thus fresh mortar is closer to Bingham fluid. In the case of the mortar, the advantage of the VGM model might not be demonstrated. Hence, further numerical investigation is needed for fresh concrete.

■ **Influence of Initial Pressure**

The flow simulations were conducted under different initial heights (25cm, 50cm and 75cm) of mortar in the vertical room, the numerical results and calculation errors are shown in **Fig. 3.20**. In case of relatively high pressure (initial height: 50cm and 75cm), the fluid particles in the WCSPH

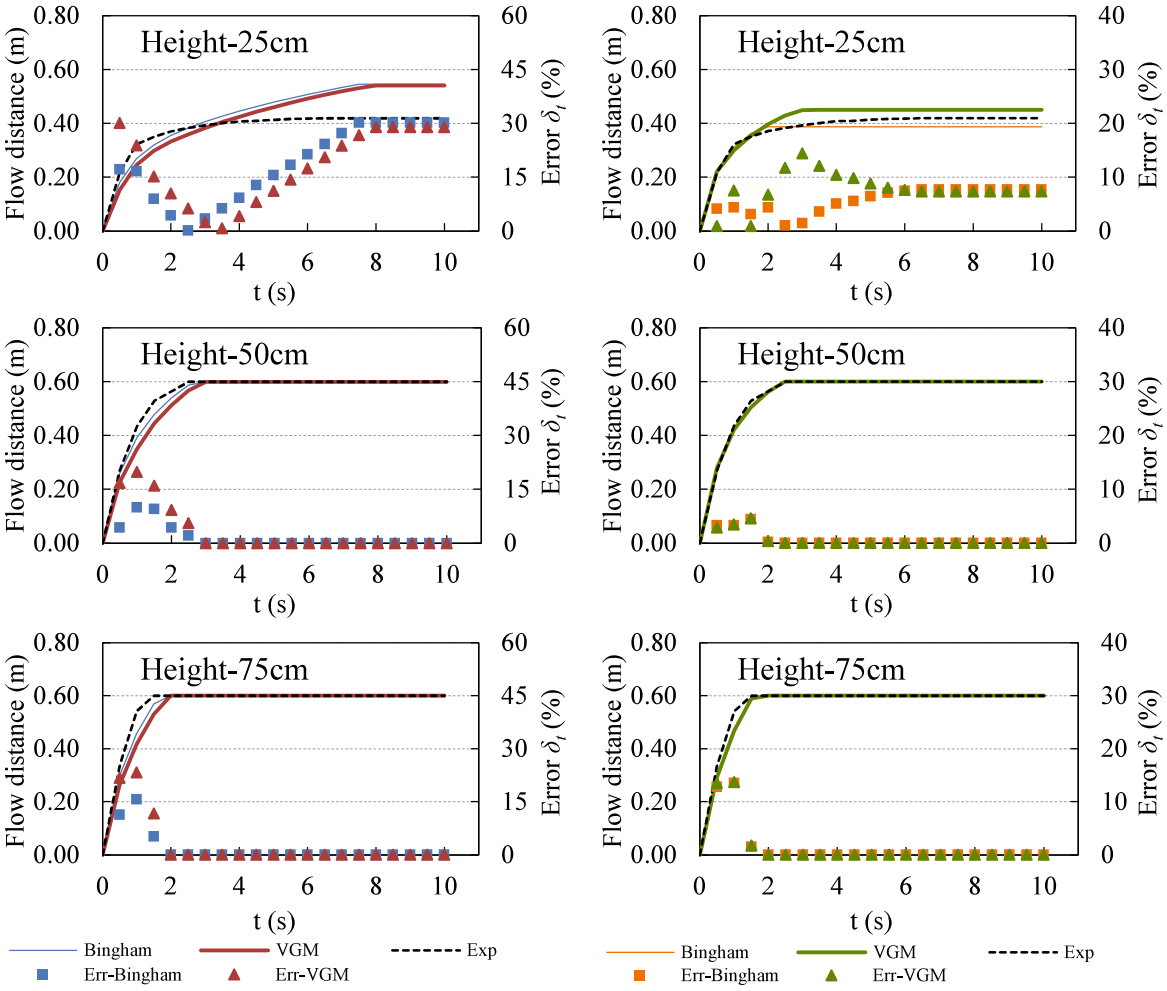

(a) SPH simulation (b) MPS simulation

Fig. 3.20 Numerical results and their errors for different initial heights of mortar in the vertical room

simulations were compressed and consequently cause a pressure increase. But the fluid particles in the I-MPS simulations were not compressed, and the implicit algorithms yielded a more precise inter-particle pressure (see in **Fig. 3.21**). Since the VGM model can describe the pressure-dependent characteristics of mortar's rheological behaviors, the effective viscosity for the WCSPH analysis gotten by the VGM model was overestimated due to higher pressure. But the effective viscosity of the Bingham model was a constant, not varying with the pressure. Therefore, the flow distance calculated by using the VGM model was shorter than that using the Bingham model for the same flow time in the WCSPH simulations. In the I-MPS simulation, the numerical results of the Bingham and VGM models were almost the same. The statistical errors of numerical results are shown in **Fig. 3.22**. As seen in **Fig. 3.22**, in the WCSPH simulations, the analysis accuracy using the VGM model was lower than that using the Bingham model. The higher the initial pressure, the lower the accuracy. But the simulation accuracy by either the Bingham model or the VGM model was the same when the I-MPS method was used or the initial height was high, i.e., the initial pressure was high. Moreover, due to the use of implicit algorithm in the I-MPS simulation, which makes the particle velocity to be accurately simulated, the I-MPS has a higher precision in case of high pressure.

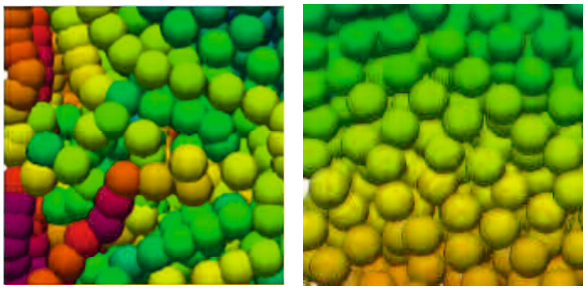

(a) WCSPH (b) I-MPS

Fig. 3.21 Compression situations of fluid particles in the two simulations (initial height of mortar is

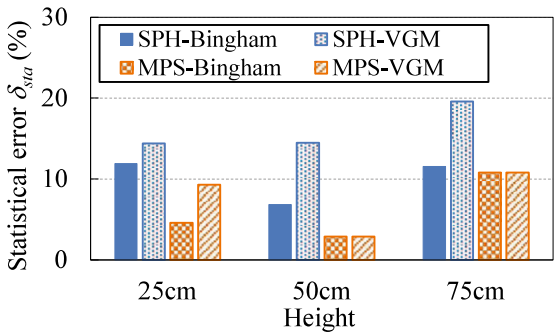

Fig. 3.22 Statistical errors of numerical results for different initial heights of mortar in the vertical

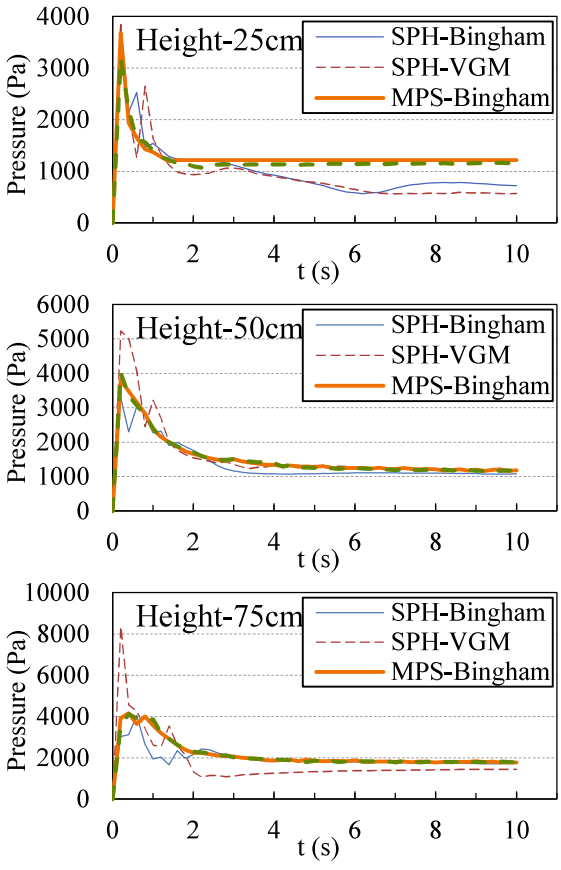

Fig. 3.23 The pressure acting on the center of the vertical room's bottom

Fig. 3.23 shows the pressure acting on the center of the bottom of the vertical room. For the initial height of 25cm (Height-25cm), since the final flow distance in the WCSPH simulation was larger than the experimental value, the final height of the mortar left in the vertical room was smaller, the pressure was underestimated. Moreover, during the flow, the numerical results of pressure in the WCSPH simulation fluctuated until the flow slowed down. However, in the I-MPS simulation, the pressure fluctuation was very small. In the I-MPS algorithm, based on the temporary positions and moving velocities of the fluid particles, accurate pressure values in the next time step can be obtained by solving the pressure Poison equations. Thus, the particle pressure in the I-MPS simulation was more stable and accurate.

3.6.4 Applicable Condition of WCSPH

As discussed in Subsection 3.6.3, the WCSPH method may be applied to fresh cementitious materials with low fluidity or subjected to low initial pressure, i.e. the Bingham constants are large, or the initial height is low when the initial pressure is caused by only gravity. On the contrary, the calculation accuracy becomes low. The reasons are discussed as follows:

It is generally thought that when the Mach number (a ratio of flow velocity of fluid to virtual speed of sound) is no more than 0.1, the fluid is in a weakly incompressible or quasi-incompressible state in the SPH simulation [6]. If the fluidity of fresh mortar is low or the initial pressure is low, the flow of the fresh mortar becomes slow, resulting in a smaller Mach number (≤0.1). The fresh mortar in the WCSPH simulation is in an incompressible state, so that the analysis accuracy can be improved. On the contrary, if the fluidity or the initial pressure is high, the WCSPH calculation has a poor accuracy because the Mach number increases to result in a larger compression degree.

According to Ref. [6], the virtual speed of sound c_0 in the EOS can be calculated by Eq. (3.31).

$$c_0 = \sqrt{200gL} \tag{3.31}$$

where, L is the maximum fluid height.

When the initial height of fresh mortar in the vertical room of the L-box is 0.25m, the virtual speed of sound c_0 is about 22.1m/s according to Eq. (3.31). In order to ensure the Mach number to be less than 0.1, the flow velocity of fresh mortar should be less than 2.2 m/s. When a fresh cementitious material (FCM) is subjected to only self-gravity and it is regarded as a Bingham fluid, the flow velocity of the FCM can be estimated by Eq. (3.32):

$$\rho g l - \tau_b = \mu_b \dot{\gamma} = \mu_b \frac{\Delta u}{\Delta l} \tag{3.32}$$

where, u is flow velocity, l is fluid height.

In case of gravity-induced flow of FCM, the flow velocity in the beginning is the maximum because the height of FCM is the greatest. The maximum flow velocity (u_{max}) can be obtained by integrating Eq. (3.32), as shown in Eq. (3.33). It should be noted that when the shear stress is less than the yield stress τ_b, the flow does not occur.

$$u_{\max} = \int_{\tau_b/\rho g}^{L} \frac{\rho g l - \tau_b}{\mu_b} dl = \frac{1}{2\rho g \mu_b}(\rho g L - \tau_b)^2, \quad \rho g L > \tau_b \tag{3.33}$$

Substituting the Bingham constants of fresh mortar into Eq. (3.33), the maximum flow velocities of Series No.1~3, i.e. initial flow velocities, can be gotten, which are 1.4m/s, 6.5m/s, and 12.3m/s, respectively. The $u_{\max}$ of Series No.1 is less than 2.2m/s, but the $u_{\max}$ of Series No.2 and No.3 are greater than 2.2m/s. This result can explain theoretically the reason why the WCSPH simulations of series No.2 and No.3 had low accuracy and, in turn, confirmed that the suggestion of Monaghan [6] is suitable, which the Mach number should be no more than 0.1 for ensuring the reliability of the WCSPH method.

Based on the above analysis, an applicable condition of the WCSPH method was proposed for flow simulation of FCM, as shown in Eq. (3.34). That is to say, the maximum fluid velocity $u_{\max}$ should be no more than 0.1 times of virtual speed of sound.

$$\frac{1}{2\rho g \mu_b}(\rho g L - \tau_b)^2 \le \sqrt{2gL}, \quad \rho g L \ge \tau_b \tag{3.34}$$

For a given initial height or thickness (L), the larger the Bingham constants (τ_b, μ_b) of FCM, i.e. the lower the fluidity of FCM, the more easily the Eq. (3.34) is satisfied. Hence, as discussed above, the WCSPH method is more likely applicable to the flow simulation of FCM with low fluidity. However, for high fluidity FCM, e.g., self-consolidation concrete (SCC), even if it has small Bingham constants, if the initial height L is also enough small, the WCSPH method is possibly applicable. Therefore, in some past studies, the use of WCSPH to simulate the slump flow or the L-flow of SCC should be not debated because the initial height or thickness of concrete was small. On the other hand, with the increase of initial height L of FCM, the increase of the value of the left side in Eq. (3.34) is greater than that of the right side, which may result in a failure of Eq. (3.34). Hence, when the initial height of FCM is too large, i.e. FCM is subjected a high gravity-induced pressure, the WCSPH may become inapplicable. Overall, as shown in **Fig. 3.24**, when using the WCSPH method to simulate the gravity-induced flow of FCM, fluidity and initial height of FCM must be well matched to ensure that the u_{max} is smaller than the root value of $2gL$. Either way, if the Eq. (3.34) is not met, it is recommended to use the MPS method.

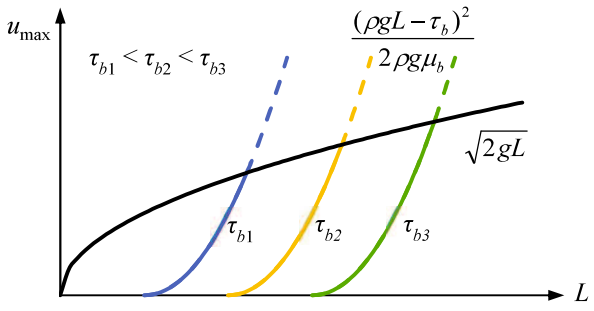

Fig. 3.24 Permitted maximum flow velocity range (blue, orange, green solid line) for reliable WCSPH simulation

3.7 Conclusions

This chapter discussed the calculation efficiency and the applicability of WCSPH, and I-MPS methods for the flow simulation of fresh cementitious materials (FCM), respectively, under the specific computer conditions. The L-flow tests of fresh mortars were performed for comparing with the numerical results. In addition, in these investigations we considered the effects of boundary slippage resistance, mortar's fluidity, constitutive law of FCM used, and initial gravity-induced pressure. Main conclusions are as follows.

The I-MPS method has a higher efficiency than the WCSPH method. Although the implicit algorithm in the I-MPS method needs much time to solve the Poison equations, large time-step is allowed, so that the calculation time is greatly saved. In the case of high viscosity of FCM and high pressure subjected, small time-step is required to ensure the accuracy of the WCSPH simulation, which significantly reduces the calculation efficiency.

For properly simulating the flow behaviors of fresh cementitious materials, it is necessary to take the boundary slippage resistance into account, especially when fresh cementitious materials have low fluidity.

VGM (viscous granular material) model can well describe the effect of vertical pressure on the rheological behaviors of fresh cementitious materials. In the I-MPS simulation of fresh mortar, Bingham model and VGM model yield almost the same calculation accuracy, whereas the WCSPH simulation using the VGM model has high accuracy in case of small gravity-induced pressure. The effects of constitutive model need to be further investigated for fresh concrete because fresh concrete has more obvious granular characteristic.

When the fresh cementitious materials have low fluidity or they are subjected to low pressure, so that the Mach number is no more than 0.1 or Eq. (3.34) is satisfied, the WCSPH method would be suitable for their flow simulation, whereas the I-MPS method is of a wide application. Especially for the fresh cementitious materials with high fluidity or subjected to a high pressure, the I-MPS method has a great advantage, provided that the boundary slippage resistance is exactly considered.

Reference

[1] X. Zhang, Z. Zhang, Z. Li, Y. Li, T. Sun, Filling capacity analysis of self-compacting concrete in rock-filled concrete based on DEM, Constr. Build. Mater. 233 (2020).

[2] V. Mechtcherine, S. Shyshko, Simulating the behaviour of fresh concrete with the Distinct Element Method - Deriving model parameters related to the yield stress, Cem. Concr. Compos. (2015).

[3] Y. Zhan, J. Gong, Y. Huang, C. Shi, Z. Zuo, Y. Chen, Y. Zhan, J. Gong, Y. Huang, C. Shi, Z. Zuo, Y. Chen, Numerical study on concrete pumping behavior via local flow simulation with Discrete Element Method, Materials (Basel). 12 (2019) 1415.

[4] L.B. Lucy, A numerical approach to the testing of the fission hypothesis, Astron. J. 82 (1977) 1013–1024.

[5] R.A. Gingold, J.J. Monaghan, Smoothed particle hydrodynamics: Theory and application to non-spherical stars, Mon. Not. R. Astron. Soc. 181 (1977) 375–389.

[6] J.J. Monaghan, Simulating free surface flows with SPH, J. Comput. Phys. 110 (1994) 399–406.

[7] S. Koshizuka, Y. Oka, Moving-Particle Semi-implicit method for fragmentation of incompressible fluid, Nucl. Sci. Eng. 123 (1996) 421–434.

[8] S.J. Cummins, M. Rudman, An SPH projection method, J. Comput. Phys. 152 (1999) 584–607.

[9] P. Jacek, W. Arkadiusz, SPH computation of incompressible viscous flows, J. Theor. Appl. Mech. 40 (2002) 917–937.

[10] S. Shao, E.Y.M. Lo, Incompressible SPH method for simulating Newtonian and Non-Newtonian flows with a free surface, Adv. Water Resour. 26 (2003) 787–800.

[11] A. Muta, P. Ramachandran, P. Negi, An efficient, open source, iterative ISPH scheme, Comput. Phys. Commun. (2020).

[12] E.S. Lee, C. Moulinec, R. Xu, D. Violeau, D. Laurence, P. Stansby, Comparisons of weakly compressible and truly incompressible algorithms for the SPH mesh free particle method, J. Comput. Phys. 227 (2008) 8417–8436.

[13] S.M. Hosseini, M.T. Manzari, S.K. Hannani, A fully explicit three-step SPH algorithm for simulation of non-Newtonian fluid flow, Int. J. Numer. Methods Heat Fluid Flow. 17 (2007) 715–735.

[14] M. Ellero, M. Serrano, P. Español, Incompressible smoothed particle hydrodynamics, J. Comput. Phys. (2007).

[15] F. Rouzbahani, K. Hejranfar, A truly incompressible smoothed particle hydrodynamics based on artificial compressibility method, Comput. Phys. Commun. 210 (2017) 10–28.

[16] H. Huang, X. Gao, Y. Li, A. Su, SPH simulation and experimental investigation of fiber orientation in UHPC beams with different placements, Constr. Build. Mater. 233 (2020) 117372.

[17] G. Cao, Z. Li, Numerical flow simulation of fresh concrete with viscous granular material model and smoothed particle hydrodynamics, Cem. Concr. Res. 100 (2017) 263–274.

[18] H. Lashkarbolouk, M.R. Chamani, A.M. Halabian, A.R. Pishehvar, Viscosity evaluation of SCC based on flow simulation in the L-box test, Mag. Concr. Res. 65 (2013) 365–376.

[19] H. Zhu, N.S. Martys, C. Ferraris, D. De Kee, A numerical study of the flow of Bingham-like fluids in two-dimensional vane and cylinder rheometers using a smoothed particle hydrodynamics (SPH) based method, J. Nonnewton. Fluid Mech. 165 (2010) 362–375.

[20] M.S. Abo Dhaheer, S. Kulasegaram, B.L. Karihaloo, Simulation of self-compacting concrete flow in the J-ring test using smoothed particle hydrodynamics (SPH), Cem. Concr. Res. 89 (2016) 27–34.

[21] R. Deeb, S. Kulasegaram, B.L. Karihaloo, 3D modelling of the flow of self-compacting concrete with or without steel fibres. Part I: slump flow test, Comput. Part. Mech. 1 (2014) 373–389.
[22] R. Deeb, S. Kulasegaram, B.L. Karihaloo, 3D modelling of the flow of self-compacting concrete with or without steel fibres. Part II: L-box test and the assessment of fibre reorientation during the flow, Comput. Part. Mech. 1 (2014) 391–408.
[23] Y. Uehara, K. Sakihara, Y. Yamada, S. Urano, A basic study on slump analysis of high accuracy MPS for fresh concrete, Cem. Sci. Concr. Technol. 67 (2013) 626–633.
[24] S. Urano, H. Nemoto, K. Sakihara, Application of flow simulation for evaluation of filling-ability of self-compacting concrete, J. Japan Soc. Civ. Eng. Ser. E2 (Materials Concr. Struct. 68 (2012) 38–48.
[25] I. Tsunakiyo, I. Shigeo, Y. Yoshitomo, T. Jun, Three-dimensional flow analysis of fresh concrete considering coarse aggregate by MPS method, Proc. Japan Concr. Inst. 26 (2004) 1161–1166.
[26] J.J. Monaghan, J.C. Lattanzio, A refined particle method for astrophysical problems, Astron. Astrophys. 149 (1985) 135–143.
[27] M. Gomez-Gesteira, B.D. Rogers, A.J.C. Crespo, R.A. Dalrymple, M. Narayanaswamy, J.M. Dominguez, SPHysics - development of a free-surface fluid solver - Part 1: Theory and formulations, Comput. Geosci. 48 (2012) 289–299.
[28] A. Khayyer, H. Gotoh, A 3D higher order Laplacian model for enhancement and stabilization of pressure calculation in 3D MPS-based simulations, Appl. Ocean Res. 37 (2012) 120–126.
[29] J.J. Monaghan, R.A.F. Cas, A.M. Kos, M. Hallworth, Gravity currents descending a ramp in a stratified tank, J. Fluid Mech. 379 (1999) 39–69.
[30] G.K. Batclielor, An introduction to fluid dynamics, Cambridge University Press, 1974.
[31] G.H. Tattersall, P.F.G. Banfill, The rheology of fresh concrete, Pitman Advanced Pub. Program, 1983. https://trid.trb.org/view/199391 (accessed August 29, 2019).
[32] Z. Li, Rheological model and rheometer of fresh concrete, J. Struct. Constr. Eng. (Transactions AIJ). 80 (2015) 527–537.
[33] Z. LI, Theoretical investigation on rheological properties of fresh concrete, J. Struct. Constr. Eng. (Transactions AIJ). 78 (2013) 895–904.
[34] Z. LI, K. KAJIWARA, M. IIDAKA, Investigation on particle contact angle of fresh concrete using X-ray CT imaging, J. Soc. Mater. Sci. Japan. 62 (2013) 585–591.
[35] Z. Li, Y. Tanigawa, Investigation on granular characteristics of fresh concrete based on visualized experiment using alternative materials, J. Struct. Constr. Eng. (Transactions AIJ). 77 (2012) 1175–1184.
[36] Z. Li, J. Li, Experimental investigation on shear deformation of fresh concrete, J. Struct. Constr. Eng. (Transactions AIJ). 75 (2010) 1173–1180.
[37] H. Zhu, N.S. Martys, C. Ferraris, D. De Kee, A numerical study of the flow of Bingham-like fluids in two-dimensional vane and cylinder rheometers using a Smoothed Particle Hydrodynamics (SPH) based method, J. Nonnewton. Fluid Mech. 165 (2010) 362–375.
[38] F. Galbusera, F. Niemeyer, Mathematical and Finite Element Modeling, in: Biomech. Spine, Elsevier, 2018: pp. 239–255.
[39] J. Murata, K. Suzuki, Study on grout flow in pipe with sliding at wall., Doboku Gakkai Ronbunshu. 1987 (1987) 129–136.
[40] J.J. Monaghan, A. Kos, Solitary waves on a cretan beach, J. Waterw. Port, Coastal, Ocean Eng. 125 (1999) 145–155.

Chapter 4 Numerical Method for Predicting Flow and Segregation Behaviors of Fresh Concrete

4.1 Introduction

4.2 Numerical Simulation Method

4.3 Numerical Analysis Model of Fresh Concrete

4.4 Experimental Program and Numerical Simulations

4.5 Results and Discussion

4.6 Conclusions

Chapter 4
Numerical Method for Predicting Flow and Segregation Behaviors of Fresh Concrete

4.1 Introduction

Concrete has been widely used as a main material to construct building, road, bridge and tunnel, etc. With the advance of sustainable concrete structures, the performance demands for concrete have been rising. Benefiting from the development and usage of chemical and mineral admixtures, especially high-range water reducing agent, the performance of concrete has been improved. As a result, many kinds of high-performance concretes have been developed, such as self-compacting concrete (SCC) [1]. The rheological performance of fresh concrete shows diversity and complexity. For ensuring the quality of concrete construction, fresh concrete should have appropriate workability. Tanigawa [2] proposed the concept and method of numerical flow simulation-based workability evaluation of concrete in 1988. Workability is the ability of fresh concrete to be easily transported and cast into formwork without excessive segregation. Workability can be subdivided into flowability, filling ability, passing ability, pumpability, segregation resistance, etc. Among these, the main concerns are flowability and segregation resistance. The flowability determines the ease of construction, and the segregation resistance affects the quality of hardened concrete, which includes static and dynamic segregation resistance [3]. Static segregation refers to that fresh concrete constituents separate from each other in rest state. Dynamic segregation refers to that fresh concrete segregates during flowing in pumping pipe or formwork or during vibrating. Once the segregation takes place, the aggregate distribution in concrete becomes uneven. The segregation will affect casting efficiency in construction stage, even induce pumping blockage. After hardened, the mechanical property and durability of segregated concrete will get worse [4]. Thus, it is an issue to predict the segregation behavior of fresh concrete during construction.

In order to measure the segregation degree of concrete and evaluate the segregation resistance of fresh concrete, many measurement methods have been proposed [3,5–8]. Using these test methods, the segregation resistance of fresh concretes has been successfully evaluated [5,9–12]. Nevertheless, the current researches on the segregation of fresh concrete are almost experimental approach. Because of the limitation of the measurement methods, it is impossible to observe and analyze the segregation

movement of aggregate particles during the flow of fresh concrete. The change in the flowability of fresh concrete once the segregation occurs cannot be evaluated experimentally. Moreover, the experimental need a lot of materials, and the experimental results of segregation have poor repeatability. Although the test methods would qualitatively evaluate the segregation resistance, there is still lack of simple, precise and widely accepted experimental method.

However, numerical flow simulation-based workability evaluation method is an inexpensive and efficient approach. Numerical simulation is also expected to be used to evaluate the segregation resistance besides flowability. In various numerical approaches, it is considered that the meshless particle methods, such as moving particle semi-implicit (MPS) and smooth particle hydrodynamics (SPH), are suitable for large deformation problem with free surface [13]. These meshless particle methods [14–17] have been used to simulate and predict the flow of many fresh concretes, and a complete implicit improved MPS (I-MPS) method [14] was confirmed to be more appropriate for fresh concrete. However, fresh concrete in these simulations is generally regarded as a homogenous fluid, and is represented by round or spheric particles with the same density and dimensions. Therefore, present numerical approaches are unable to describe the heterogeneous feature and to simulate the segregation behavior of fresh concrete. Indeed, meshless particle methods are able to treat with the interactions among fluid particles, thus have the potential to simulate heterogeneous characteristic of concrete and provide information about the static and dynamic segregation of fresh concrete.

In this paper, we tried to develop a numerical flow approach of fresh concrete based on the I-MPS method, which can predict the segregation behavior together with the flow behavior of fresh concrete simultaneously. A Double-Phase & Multi-Particle (DPMP) model was proposed to express fresh concrete in the numerical simulation. In the DPMP model, fresh concrete is composed of matrix mortar and coarse aggregate (CA). These two phases have different densities and rheological parameters. Each CA particle is represented by several round or spheric elementary particles which have the same size with the matrix mortar particles. The interactions between mortar-mortar particles, CA-CA particles, and mortar-CA particles were discussed and addressed, respectively. This numerical flow approach was verified by simulating the L-box flow of high fluidity concrete. Both the static segregation and dynamic segregation behaviors were investigated quantitatively. Moreover, the numerical results can clarify the changes in the localized rheological parameters of fresh concrete after segregation.

4.2 Numerical Simulation Method

4.2.1 Governing Equations

In the numerical simulation of fresh concrete motion, the governing equations mainly include continuity equation and motion equation. The continuity equation considers the conservation of mass of the fluid, and the motion equation considers the conservation of momentum during the fluid movement. The governing equations are detailed explained in Section 3.2.1 and shown in Eq. (3.1).

4.2.2 Algorithm of I-MPS Method

A complete implicit improved MPS (I-MPS) method [14] proposed in Chapter 3 is used in this chapter to do numerical simulation. In I-MPS, a fluid of any shape is considered to be composed of a limited number of particles, as shown in **Fig. 4.1**. Physical quantities (such as density, position, velocity and pressure) are defined toward particles. Among all the forces acting on the particle, gravity is considered as an external force, whereas pressure and viscosity are treated as the interaction between neighboring particles. The interaction force on the target particle is obtained by weighted average of the interaction with other particles in the influence domain (as shown in **Fig. 4.2**). Particle interaction models are introduced as derivatives of physical quantities in the influence domain with a radius of r_e, as shown in **Fig. 4.3**. The closer the particles are, the stronger the interaction between them and the greater the corresponding weight. The flow chat of I-MPS algorithm is shown in **Fig. 4.4**. Detailed introduction about I-MPS algorithm and employed calculation equations can be find in Section 3.2.

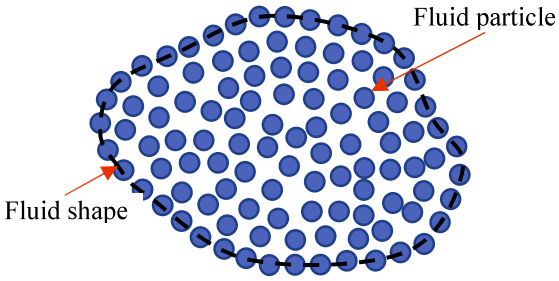

Fig. 4.1 Imaged fluid composition in MPS

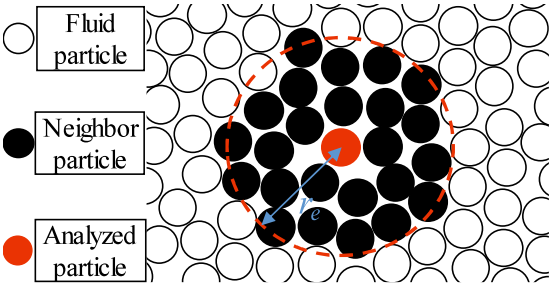

Fig. 4.2 Influence domain of analyzed particle

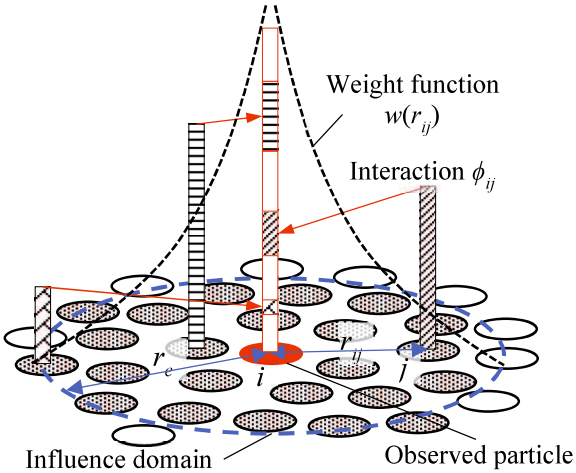

Fig. 4.3 Interaction between particle *i* and neighbor particles

4.2.3 Rheological Model Used of Fresh Concrete

Fresh concrete is generally regarded as a Bingham fluid. The regularized Bingham model [18] is generally used to describe the flow

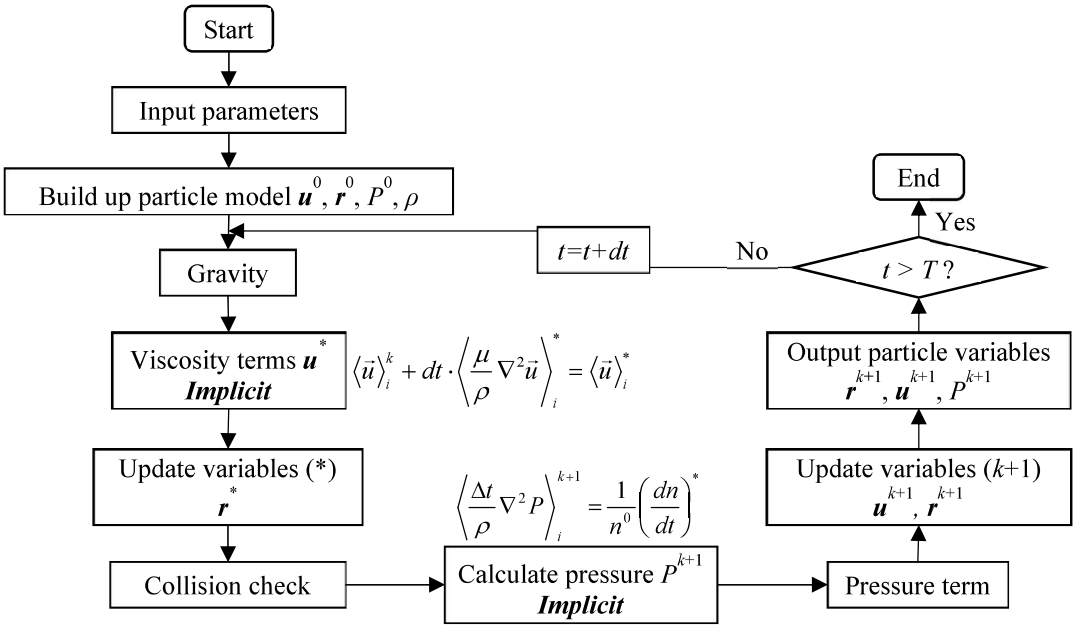

Fig. 4.4 Flow chart of I-MPS algorithm

behaviors of fresh concrete. The detailed introduction is described in Section 3.3.1, Eq. (3.7), and **Fig. 3.1**.

4.2.4 Boundary conditions

The no-slip boundary condition was adopted, i.e., the particle velocity along the flow boundary was zero or assigned to be its moving velocity. The Dirichlet boundary condition [19] was adopted to solve the pressure Poisson equation. The pressure on the free surface was set to be zero.

4.2.5 Validation of I-MPS method

■ **Theoretical Solution of Taylor-Couette Flow**

In order to verify again the reliability of the I-MPS method for the flow analysis of fresh concrete, and to discuss the reasonable particle size for the flow simulation, the Taylor-Couette flow was first simulated in this study. The Taylor-Couette flow model is shown in **Fig. 4.5**. The fluid is located between two cylinders. The inner cylinder has a radius of R_1, and rotates at an angular speed of ω_1. The outer cylinder has a radius of R_2, and rotates at an angular speed of ω_2. Assuming there is no slip between the fluid and the walls of cylinders, the fluid is sheared between the two cylinders, and occurs a steady flow. The fluid only flows in the circumferential direction. Thus, the continuity equation and motion equation of the fluid can be simplified as:

$$\begin{cases} \dfrac{\partial u_R}{\partial \theta} = 0, & \dfrac{\mu}{\rho} \dfrac{\partial}{\partial R} \left[\dfrac{1}{R} \dfrac{\partial}{\partial R} \left(R u_R \right) \right] = 0 \\ \dfrac{u_R^2}{R} = \dfrac{1}{\rho} \dfrac{\partial P}{\partial R}, & g - \dfrac{1}{\rho} \dfrac{\partial P}{\partial z} = 0 \end{cases} \tag{4.1}$$

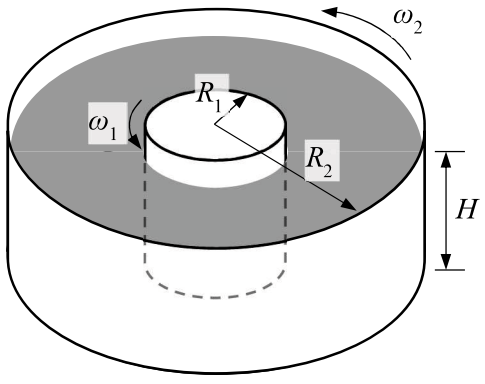

Fig. 4.5 Taylor-Couette flow model

where, u_R is circumferential flow velocity at the radius of R.

For fresh concrete, since the yield stress is usually not zero, its dynamic viscosity changes with the shear rate, as seen from Eq. (3.15). Thus, in order to simplify the calculation of Taylor-Couette flow, the yield stress of fresh concrete was set to zero here, the dynamic viscosity would be constant. Based on Eq. (4.1), the circumferential flow velocity u_R of fresh concrete at the radius of R can be obtained, as shown in the follow:

$$u_R = \frac{\omega_2 R_2^2 - \omega_1 R_1^2}{R_2^2 - R_1^2} R + \frac{(\omega_1 - \omega_2) R_1^2 R_2^2}{R_2^2 - R_1^2} \frac{1}{R} \tag{4.2}$$

The diameter and property parameters for Taylor-Couette flow test are listed in **Table 4.1**. Substituting the parameters in **Table 4.1** into Eq. (4.2), the circumferential flow velocity profile along the radius is calculated, the theoretical result of Taylor-Couette flow is shown in **Fig. 4.6**.

■ **I-MPS Simulation**

The Taylor-Couette flow simulations were done by using different particle sizes (*dis*), which were 10mm and 5mm, respectively, for determining suitable size of fluid particle used in the simulation of I-MPS. The no-slip boundary condition was adopted and zero yield stress was used. The simulated flow velocities are shown and compared to the theoretical results in **Fig. 4.6**. When the particle diameter was 10mm, the simulated results were almost consistent with the theoretical results, but there was small error in the area near the boundary. When the particle diameter was 5mm, the simulated velocity profile in the entire flow profile was consistent with the theoretical result. Therefore, the I-MPS method is able to simulate the flow of fresh concrete provided that the appropriate particle size is used. The particle diameter in the following simulation was set as 5 mm.

Table 4.1 Parameters for Taylor-Couette flow

Radius R_1 (m)	0.05	Height H (m)	0.10
Angular velocity ω_1 (rad/s)	1.00	Density ρ (kg/m^3)	2300.00
Radius R_2 (m)	0.15	Yield stress τ_b (Pa)	0.00
Angular velocity ω_2 (rad/s)	0.00	Plastic viscosity μ_b (Pa·s)	100.00

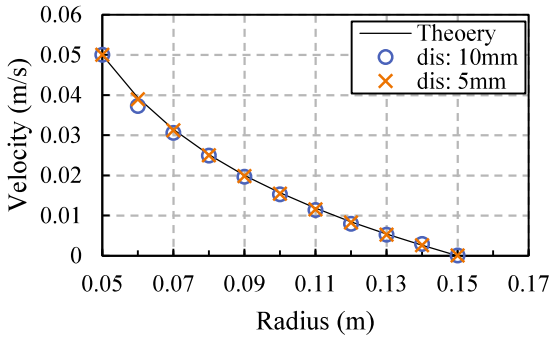

Fig. 4.6 Rotation velocity profiles in Taylor-Couette flow

4.3 Numerical Analysis Model of Fresh Concrete

4.3.1 Constituent model of fresh concrete

Fresh concrete can be regarded as particle assembly with water, binder, and aggregate particles ranging from a few microns to tens centimeters in size. However, fresh concrete is usually modeled as single-phase homogeneous granular material in many numerical simulation of particle methods [15,17,20]. To track the segregation behavior of coarse aggregate, and to analyze the effect of coarse aggregate's segregation on the flow behavior of fresh concrete, it is necessary to treat the coarse aggregate as a separate component of fresh concrete. That is, fresh concrete should be considered as a discontinuous double-phase system composed of matrix mortar and coarse aggregate particles. As shown in **Fig. 4.7**, volume V of fresh concrete is a sum of matrix mortar volume V_M and coarse aggregate volume V_{CA}. Based on the excess paste theory [21,22], the matrix mortar is divided into: the filling mortar (*Mf*) and the mortar tightly adhering to coarse aggregate (*Ma*). The filling mortar fills in the voids and gaps between coarse aggregates, while the tightly adhering mortar covers the surface of coarse aggregate particles. The corresponding volumes are represented by V_{Mf} and V_{Ma}, respectively.

In this study, fresh concrete was represented by matrix mortar particles and CA particles. The double-phase & multi-particle (DPMP) model was used as the constituent model to describe fresh concrete for numerical flow simulation, as shown in **Fig. 4.8**. Coarse aggregate particles have different sizes and random shapes, but matrix mortar phase is represented by spherical particles with same diameter. Coarse aggregate particle is formed by several elementary particles, of which the number is dependent on the geometry and dimension of formed CA particle, as shown in **Fig. 4.9**. The elementary particle is spherical and has the same size to the mortar particle but its specific gravity is different from the mortar particle. **Fig. 4.10** shows examples of formed coarse aggregate particles with different sizes and shapes. The coarse aggregate particles used in the numerical calculation have random shapes, but in the simulation output, the coarse aggregate particles are imaged as spherical particles (circular in the two-dimension case).

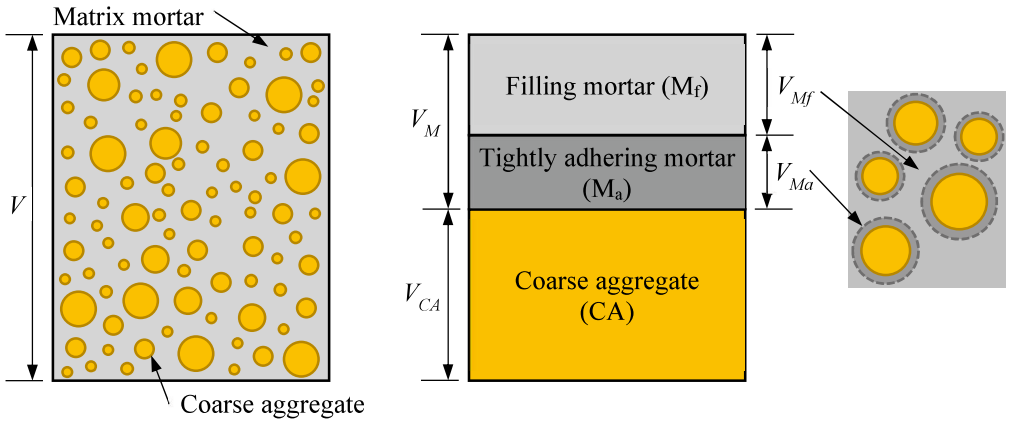

Fig. 4.7 Constituent model of fresh concrete

4.3.2 Interaction models between various particles in fresh concrete

To calculate the movement of the particles, it is necessary to figure out the interactions between the particles. In this study the fresh concrete was considered as a double-phases fluid rather than a homogeneous fluid, composed of matrix mortar particles and coarse aggregate particles. Thus, the following three kinds of interaction between particles should be clarified in advance.

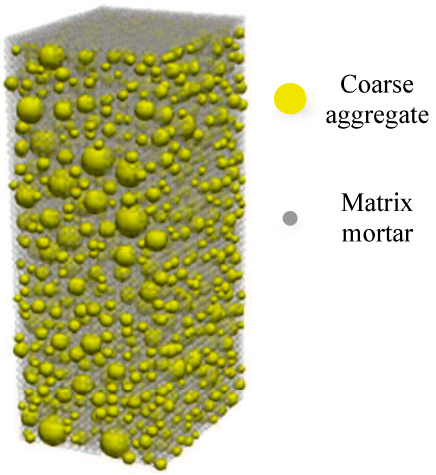

Fig. 4.8 Constituent model of fresh concrete

■ **Between mortar particles**

The Bingham constants of the matrix mortar can be measured directly by a rheometer, then, the dynamic viscosity of mortar particle is calculated by Eq. (3.17). For the accuracy of numerical simulation, the harmonic mean interparticle viscosity is recommended by Shakibaeinia et al. [23]. The viscosities interaction between mortar particles can be calculated by the following multi-viscosity model:

$$\left\langle \frac{\mu}{\rho}\nabla^2\vec{u} \right\rangle_{ij} = \frac{5-d}{n^0}\cdot\frac{2\mu_i\mu_j}{\mu_i+\mu_j}\cdot\frac{1}{\rho_M}\cdot\frac{\vec{u}_{ij}r_e}{r_{ij}^3} \tag{4.3}$$

where, ρ_M is density of matrix mortar.

The Laplacian in the pressure Poisson equation for calculating the inter-pressure of mortar particles is modified as:

$$\left\langle \frac{1}{\rho}\nabla^2 P \right\rangle_{ij}^{k+1} = \frac{5-d}{n^0}\cdot\frac{1}{\rho_M}\cdot\left(P_j^{k+1}-P_j^{k+1}\right)\cdot\frac{r_e}{\left|\vec{r}_j^{\,*}-\vec{r}_i^{\,*}\right|^3} \tag{4.4}$$

■ **Between CA particles**

CA particles are regarded as rigid materials, and the interaction between them should be friction. However, in order to uniformly express the interaction between particles, the Bingham model was used to express the interaction between CA particles in this study. In addition, the CA particles are

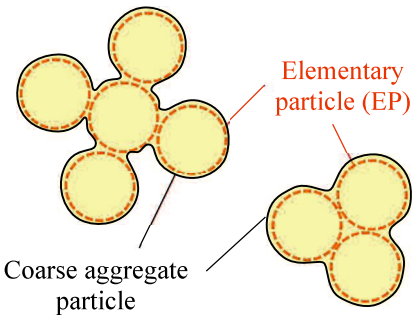

Fig. 4.9 Formation of aggregate particle

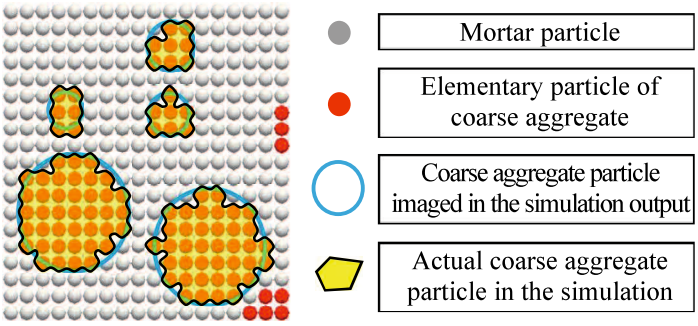

Fig. 4.10 Random sizes and shapes of coarse aggregate particles (2D)

wrapped in a thin mortar layer as described in **Fig. 4.7**, so that it is somehow reasonable that the shear resistance of CA particles follows the Bingham model.

Due to the assumption that the CA particle is formed by several elementary particles, the interaction between two CA particles can be expressed by the interactions between the elementary particles. The interaction between two elementary particles is calculated by the same method to the interaction between mortar particles, as shown in Eqs. (4.5) and (4.6).

$$\left\langle \frac{\mu}{\rho}\nabla^2\vec{u}\right\rangle_{ij} = \frac{5-d}{n^0}\cdot\frac{2\mu_i\mu_j}{\mu_i+\mu_j}\cdot\frac{1}{\rho_{CA}}\cdot\frac{\vec{u}_{ij}r_e}{r_{ij}^3} \tag{4.5}$$

$$\left\langle \frac{1}{\rho}\nabla^2 P\right\rangle_{ij}^{k+1} = \frac{5-d}{n^0}\cdot\frac{1}{\rho_{CA}}\cdot\left(P_j^{k+1}-P_j^{k+1}\right)\cdot\frac{r_e}{\left|\vec{r}_j^{\,*}-\vec{r}_i^{\,*}\right|^3} \tag{4.6}$$

where, ρ_{CA} is density of coarse aggregate.

■ **Between mortar particle and CA particle**

The interaction between mortar particle and coarse aggregate particle is more complicated than the above two cases, because two kinds of particles have different rheological properties and densities. Duan et al. [24] suggested to use arithmetic mean density to improve the stability of the numerical results. The viscous interaction can be calculated by Eq. (4.7).

$$\left\langle \frac{\mu}{\rho}\nabla^2\vec{u}\right\rangle_{ij} = \frac{5-d}{n^0}\cdot\frac{2\mu_i\mu_j}{\mu_i+\mu_j}\cdot\frac{2}{\rho_i+\rho_j}\cdot\frac{\vec{u}_{ij}r_e}{r_{ij}^3} \tag{4.7}$$

The Laplacian in the pressure Poisson equation is modified by the following multi-density model:

$$\left\langle \frac{1}{\rho}\nabla^2 P\right\rangle_{ij}^{k+1} = \frac{5-d}{n^0}\cdot\frac{2}{\rho_i+\rho_j}\cdot\left(P_j^{k+1}-P_j^{k+1}\right)\cdot\frac{r_e}{\left|\vec{r}_j^{\,*}-\vec{r}_i^{\,*}\right|^3} \tag{4.8}$$

Three types of interaction models of particles are summarized in **Fig. 4.12**. The pressure gradient shown in Eq. (3.13) is divided into two terms for fresh concrete composed of two kinds of particle in density as following [24]:

$$\begin{aligned}\left\langle \frac{1}{\rho}\nabla P\right\rangle_i = {} & \frac{d}{n^0}\sum_{j\neq i}\left[\frac{2\left(P_j-P_i\right)}{\left(\rho_i+\rho_j\right)\left|\vec{r}_j^{\,*}-\vec{r}_i^{\,*}\right|^2}\left(\vec{r}_j^{\,*}-\vec{r}_i^{\,*}\right)w\left(r_{ij}^*\right)\right] \\ & + \frac{d}{n^0}\sum_{j\neq i}\left[\frac{\left(P_i-P'_{i,\min}\right)}{\left|\vec{r}_j^{\,*}-\vec{r}_i^{\,*}\right|^2}\left(\vec{r}_j^{\,*}-\vec{r}_i^{\,*}\right)w\left(r_{ij}^*\right)\right]\end{aligned} \tag{4.9}$$

where, $P'_{i,min}$ is the minimum pressure among the same type of neighboring particles of particle *i*.

The harmonic mean dynamic viscosity $\overline{\mu}_i$ of particle *i* can be calculated by:

$$\overline{\mu}_i = \frac{N_i}{\sum_{j\neq i}^{N_i} 1/\mu_j} \tag{4.10}$$

where, N_i is number of neighboring particles in the influence domain of particle *i*.

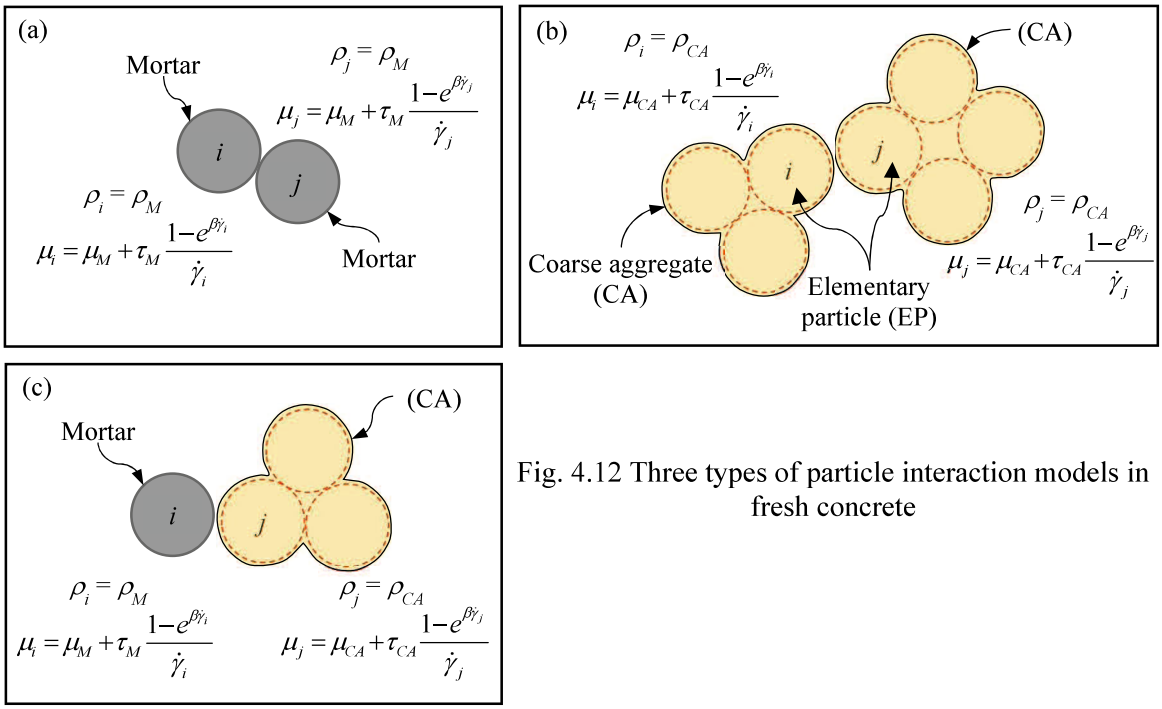

Fig. 4.12 Three types of particle interaction models in fresh concrete

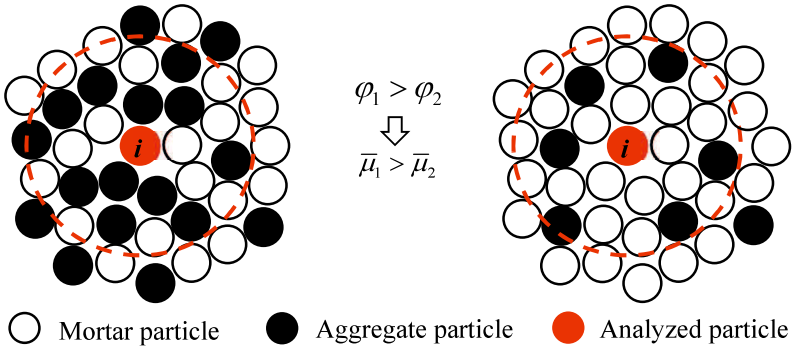

Fig. 4.11 Change of mean dynamic viscosity with aggregate volume fraction (left: φ_1, right: φ_2)

As shown in **Fig. 4.11**, the larger the volume fraction (φ) of CA, the larger the probability of CA particles existing in an influence domain of particle *i*, and the higher the mean dynamic viscosity ($\bar{\mu}$) of particle *i*. Thus, Eq. (4.10) can reflect the effect of CA's volume fraction on the dynamic viscosity of fresh concrete, i.e., fresh concrete with larger volume fraction of CA has higher dynamic viscosity. Moreover, if fresh concrete segregates, the CA distribution becomes uneven, part of concrete has a larger CA volume fraction, it presents a higher dynamic viscosity. Therefore, the DPMP model has the potential to reflect the influence of CA segregation.

4.3.3 Rheological Parameters for Expressing Inter-Particle Resistance

When considering the interaction between particles follows the Bingham model, the Bingham constants describing three types of particle interaction, shown in **Fig. 4.12**, should be determined first. The Bingham constants (μ_M , τ_M) of matrix mortar can be measured directly by a rheometer, as mentioned above. However, there is currently no method to determine the Bingham constants (μ_{CA} , τ_{CA}) of CA particle system. As shown in **Fig. 4.13** (b), the volume fraction of CA in the CA particle

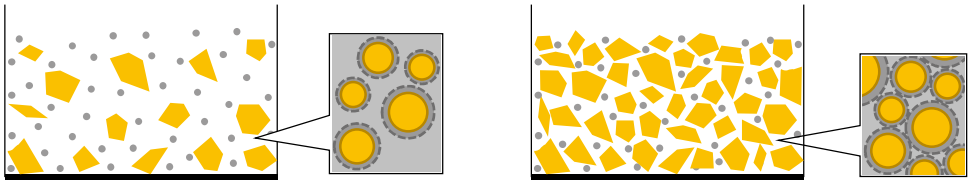

(a) Normal fresh concrete (b) CA particle system

Fig. 4.13 Schematic diagram of normal fresh concrete and CA particle system

system is larger than that in normal fresh concrete, the CA particles are in close contact by tightly adhering mortar, and the filling mortar is just used to fill the voids between CA particles.

Ferraris and deLarrard [25,26] found that either the plastic viscosity or yield stress of fresh concrete is a function of the volume fraction of solid material and the maximum packing volume fraction of the individual components. Based on the Einstein's model [27], Roscoe [28] and Krieger-Dougherty [29] further proposed the models to predict the plastic viscosity of suspension by the volume fraction of dispersed spherical particles and their maximum packing volume fraction. Struble and Sun [30] modified the model and suggested an equation to predict the plastic viscosity of fresh concrete, as shown in the following:

$$\mu = \mu_M \cdot \left(1 - \frac{\varphi}{\varphi_m}\right)^{-\mu_* \cdot \varphi_m} \tag{4.11}$$

where, μ_M is viscosity of matrix mortar, φ is volume fraction of coarse aggregate, φ_m is maximum packing volume fraction of coarse aggregate, μ_* is intrinsic viscosity of system.

Moreover, Chateau et al, [31] provided a prediction equation of the yield stress of fluid, as follows:

$$\tau = \tau_M \cdot \sqrt{(1-\varphi)\cdot\left(1 - \frac{\varphi}{\varphi_m}\right)^{-\tau_* \varphi_m}} \tag{4.12}$$

where, τ_M is yield stress of matrix mortar, τ_* is intrinsic yield stress of system.

Both μ_* and τ_* are 2.5 for the suspension consisting of spherical particles with the same size [30,31]. However, CA particles have irregular shapes and random sizes, as shown in **Fig. 4.14**. Therefore, for estimating the Bingham constants (μ_{CA} , τ_{CA}) of the CA particle system, it is necessary to first determine the intrinsic constants μ_* and τ_*. Eqs. (4.11) and (4.12) have already been used to successfully estimate the plastic viscosity and yield stress of fresh concrete [32–35]. Hence, by using the measured Bingham constants of matrix mortar and fresh concrete, the μ_* and τ_* and can be estimated on the basis of Eqs. (4.11) and (4.12).

Fig. 4.14 Coarse aggregates with different sizes and shapes

Here, the volume fraction of CA in the CA particle system is donated as φ', and the φ_m of the CA particle system is the maximum packing volume fraction of CA. The calculated Bingham constants by Eqs. (4.11) and (4.12) were used as the rheological parameters of CA particle system in

the numerical simulation. The following will discuss the volume fraction φ' of CA in the CA particle system.

Originally, the packing volume fraction φ_0 of CA is a ratio of CA volume (V_{CA}) to the sum of CA volume and void volume (V_{Air}) among CA particles, i.e., $V_{CA}/(V_{CA}+V_{Air})$. However, in fresh concrete, CA particle is surrounded by the tightly adhering mortar, as mentioned in **Fig. 4.15**, so that the distance between adjacent CA particles is increased. Therefore, the corresponding volume fraction φ' of CA in the CA particle system is less than φ_0. Based on the schematic diagram in **Fig. 4.15**, the φ' can be calculated as $V_{CA}/(V_{CA}+V_{Mf}+V_{Ma})$. Assuming all the CA particles are spherical, it is proposed in Ref. [36] that when the packing volume fraction of CA is between 0.52 and 0.74, the thickness of the mortar adhering on CA particle is proportional to the radius (R_{CA}) of the CA particle. In the CA particle system, the packing volume fraction φ_0 of CA equals to the maximum packing volume fraction φ_m, which normally falls in the range of 0.52 ~ 0.74. If denoting the ratio of the thickness (ε) of tightly adhering mortar layer to R_{CA} as α, the relationship between α and φ_m (maximum packing volume fraction of CA) can be described as [36]:

$$\alpha = e^{(2.9-10.3\varphi_m)} + 0.077, \varphi_m \in (0.52, 0.74) \tag{4.13}$$

The φ_m of CA used in this study was 0.592, based on Eq. (18), α was calculated as 0.118. The size distribution of the used CA was 5mm ~ 20mm, i.e., the radius of the CA particle was in the range of 2.5mm ~ 10mm. The thickness ε of tightly adhering mortar layer was thin and ranged from 0.295mm to 1.180mm.

The volume of adhesive mortar layer can be calculated as:

$$V_{Ma} = \frac{4\pi}{3}\sum (R_{CA}+\varepsilon)^3 - \frac{4\pi}{3}\sum R_{CA}^3 = (1+\alpha)^3 V_{CA} - V_{CA} \tag{4.14}$$

where, R_{CA} is radius of coarse aggregate particle, ε is thickness of adhesive mortar layer.

For the CA particle wrapped by the tightly adhering mortar, its total radius is $(1+\alpha)$ times its original size of CA, thus its total volume becomes $(1+\alpha)^3$ times CA's volume. Correspondingly, the void volume among CA particles will increase at the same times, that is, the volume V_{Mf} of the filling mortar is equal to $(1+\alpha)^3 \cdot V_{Air}$. Thus, the volume fraction φ' of CA in the CA particle system can be calculated as follows:

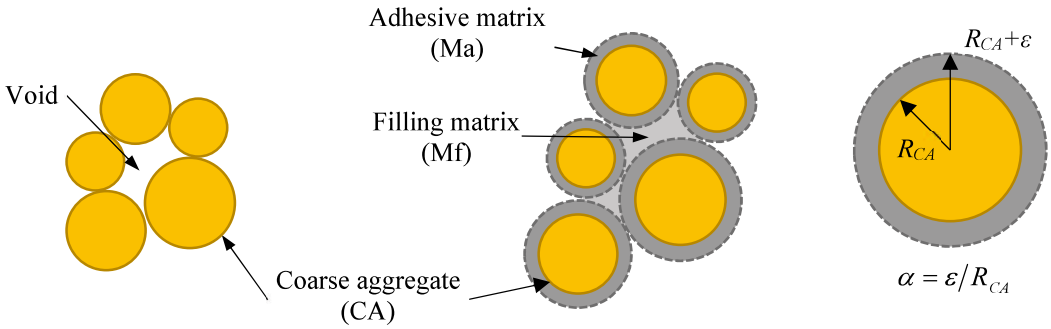

Fig. 4.15 Increasement of CA particle size due to adhesive mortar

$$\varphi' = \frac{V_{CA}}{V_{CA}+V_{Md}+V_{Me}} = \frac{V_{CA}}{V_{CA}+(1+\alpha)^3 V_{Air}+(1+\alpha)^3 V_{CA}-V_{CA}} = \frac{1}{(1+\alpha)^3}\frac{V_{CA}}{V_{CA}+V_{Air}} = \frac{\varphi_m}{(1+\alpha)^3} \tag{4.15}$$

Once the values of μ_*, τ_*, φ', and φ_m are known, Eqs. (4.11) and (4.12) are used to calculate μ_{CA} and τ_{CA}, considering the CA particle system as a suspension. The determining methods of all rheological parameters in numerical simulation are shown in **Fig. 4.16.**

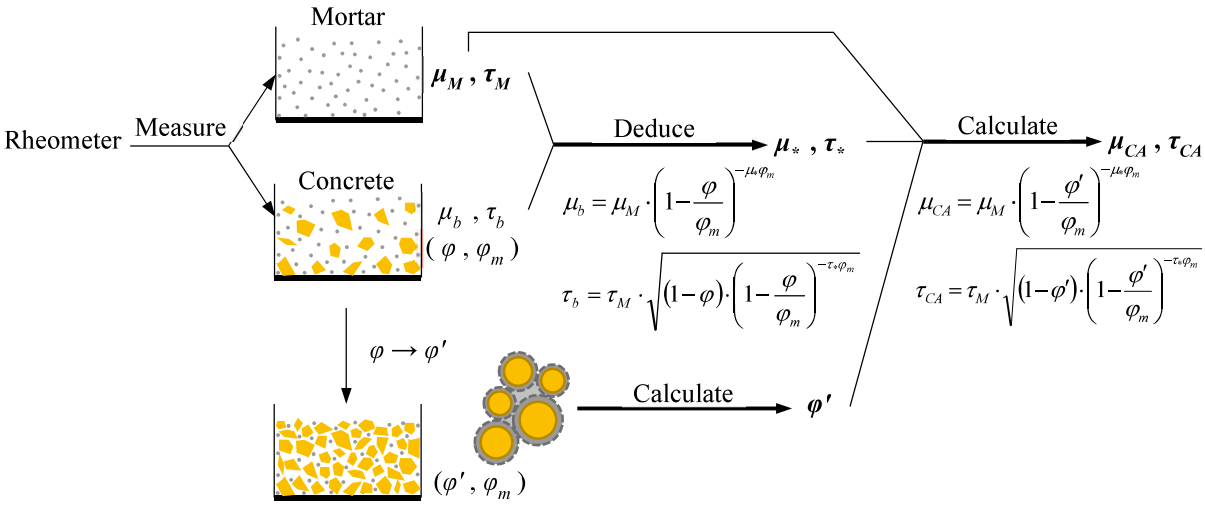

Fig. 4.16 Determination of rheological parameters used in numerical simulation

4.3.4 Movement calculation of coarse aggregate particle

The movement of coarse aggregates (CA) is calculated by two steps (see **Fig. 4.17**), using the Passively Moving Solid (PMS) model [37]. In the first step, the movements of elementary particles are calculated, which are caused by their self-gravity and the interactions between the elementary particles and between elementary particles and mortar particles. In the second step, the calculated velocities and positions of element particles are revised on basis of the conservation of angular momentum to ensure that the shape of the CA particle is unchanged. The angular momentum of the CA particle in time-step k+1 is calculated according to the velocities of the elementary particles in the former time step k, as shown in Eq. (4.16).

$$\vec{L} = m \cdot \sum_i \left(\vec{r}_i^{\,k} - \vec{r}_g^{\,k}\right) \times \vec{u}_i'^{\,k+1} \tag{4.16}$$

where, $\vec{L}$ is angular momentum, m is mass of CA particle, $\vec{u}'$ is velocity vector after revising the position of elementary particles, k is time step, $\vec{r}_g^{\,k}$ is center position of CA particle at time step k.

Based on the conservation of angular momentum, the angular velocity of each CA particle in the step k+1 is obtained.

$$\vec{I}_g^{\,k} \cdot \vec{\omega}^{\,k+1} = \vec{L} \tag{4.17}$$

$$\vec{\omega}^{k+1} = m\left(I_g^k\right)^{-1} \cdot \sum_i \left(\vec{r}_i^{\,k} - \vec{r}_g^{\,k}\right) \times \vec{u}_i'^{k+1} \tag{4.18}$$

where, $\vec{I}_g^k$ is inertia tensor.

Then, the position and velocity of elementary particle can be revised by:

$$\vec{r}_i^{\,k+1} = \vec{r}_i^{\,k} + \left(\vec{r}_g^{\,k+1} - \vec{r}_g^{\,k}\right) + \vec{\omega}^{k+1} \times \left(\vec{r}_i^{\,k} - \vec{r}_g^{\,k}\right)\Delta t \tag{4.19}$$

$$\vec{u}_i^{\,k+1} = \vec{u}_i^{\,k} + \left(\vec{u}_g^{\,k+1} - \vec{u}_g^{\,k}\right) + \vec{\omega}^{k+1} \times \left(\vec{r}_i^{\,k} - \vec{r}_g^{\,k}\right) \tag{4.20}$$

where, Δt is time interval.

On the right side of Eqs. (4.19) and (4.20), the second term represents the translation of whole rigid body, and the third term represents the motion of the elementary particles due to the rotation of rigid body.

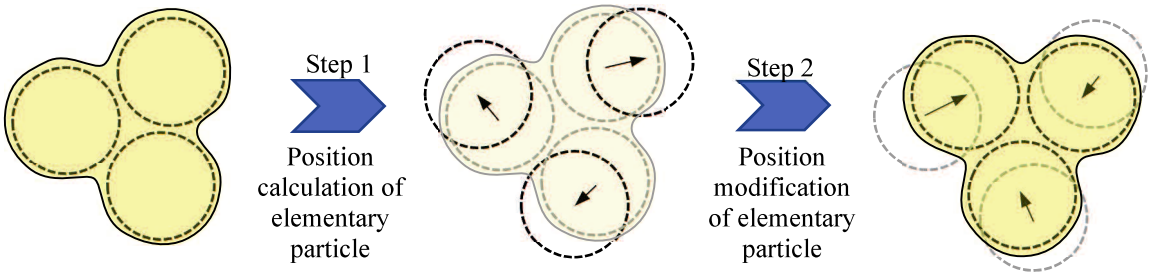

Fig. 4.17 Position calculation and modification of CA particle

4.4 Experimental Program and Numerical Simulations

4.4.1 Concrete Mixtures and Rheological Properties

Two series of high fluidity concrete were numerically analyzed in this study, which had different segregation resistance. The mix proportions are given in **Table 4.2**. Ordinary Portland cement with the Blaine fineness of 3500 cm^2/g and the density of 3150 kg/m^3 was used. JIS type II fly ash with the Blaine fineness of 4392 cm^2/g and the density of 2300 kg/m^3 was used. The fine aggregate sea sand had the particle size of 0 - 5 mm and the surface dry density of 2590 kg/m^3, and its water absorption capacity was 1.36% and fineness modulus was 2.9. CA was crashed stone with the size of 5 - 20 mm and its surface dry density was 2730 kg/m^3. Water absorption capacity of CA was 0.47% and its fineness modulus was 6.72. The maximum packing volume fraction φ_m of CA was 59.2%. Using Eqs. (4.13) and (4.15), the volume fraction (φ') of CA in the CA particle system was calculated as 42.4%.

The slump flow tests of No.1 and No.2 were performed, as shown in **Fig. 4.18**, the test results are shown in **Table 4.2**. It was found that no segregation occurred in No.1, but the aggregate of No.2 segregated. The Bingham constants of the matrix mortars and the fresh concretes were measured by the rheometer, called RSNS, as shown in **Fig. 4.19**, which is classified as parallel plate rheometer. The upper blade cannot rotate, but its subjected torque can be detected. During the measurement the torque

Table 4.2 Mix proportions of concrete mixture

Series	w/b	Unit mass (kg/m^3)						Vol (%)	Bulk density (kg/m^3)	*Sl* (cm)	*Sf* (mm)	t_{500} (s)
		Water	Cement	Fly ash	Sand	Crashed stone	HRWRA					
No.1	0.30	170	283	283	767	830	8.5	31.0	2385	27.0	690	8.5
No.2	0.45	170	189	189	845	911	5.7	34.6	2393	24.5	640	6.0

[Notes:] w/b is water-to-binder ratio by mass, HRWRA is high-range water-reducing agent, Vol is volume fraction of coarse aggregate in concrete, *Sl* is slump value, *Sf* is slump flow value, and t_{500} is flow time of 500mm.

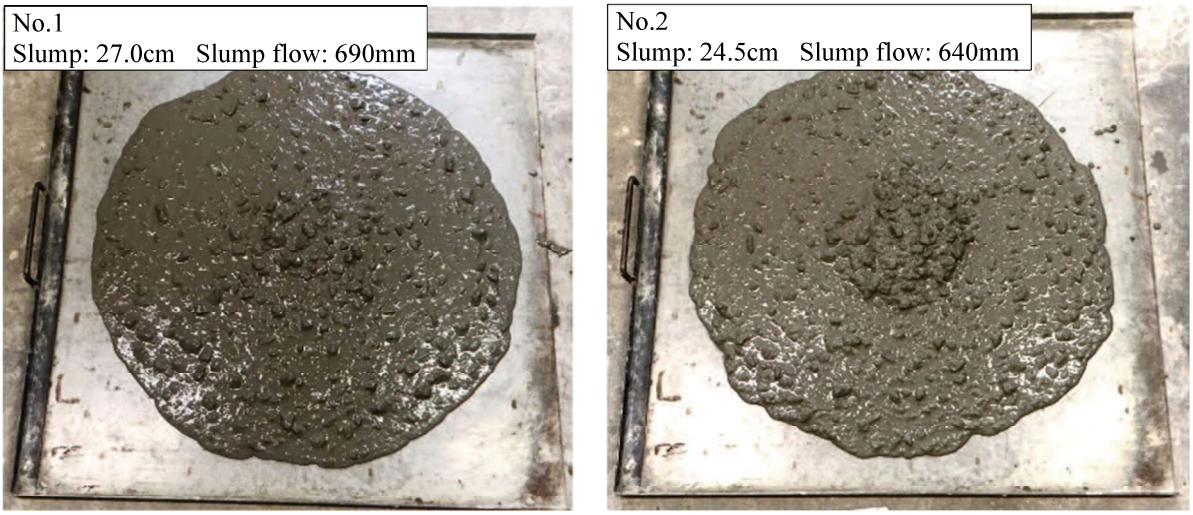

Fig. 4.18 The slump test of two concretes

should be over zero. The lower blade is driven by a motor. Using the rotation speed and torque of the lower blade, the shear strain rate and shear stress of the sample are calculated, further the plastic viscosity and yield stress are obtained [38]. Based on the measured plastic viscosities and yield stresses of matrix mortars and fresh concretes, the values of intrinsic viscosity μ_* and intrinsic yield stress τ_* of two concretes were deduced to be 4.2 and 3.2, respectively, by using Eqs. (4.11) and (4.12). Finally, Eqs. (4.11) and (4.12) were used to calculate the Bingham constants of the CA particle system in the two series of concretes based on the Bingham constants of the matrix mortars. All the Bingham constants used in numerical simulation are shown in **Table 4.3**.

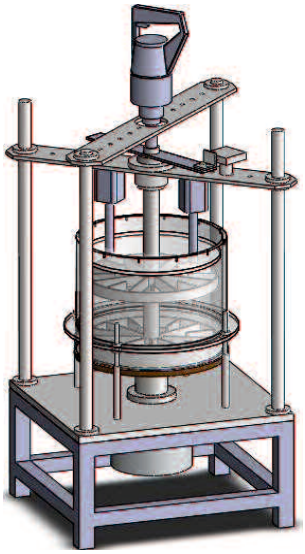

Fig. 4.19 RSNS rheometer

Table 4.3 Rheological parameters of materials

Series / Parameters	No.1			No.2		
	Mortar	Concrete	Coarse aggregate (calculated)	Mortar	Concrete	Coarse aggregate (calculated)
Plastic viscosity (Pa·s)	79.7	508.6	1826.2	43.9	376.9	1005.9
Yield stress (Pa)	12.6	21.3	31.5	8.7	16.2	21.8

4.4.2 L-box flow test and segregation measurement

The L-box flow tests of two concretes were conducted and the segregation degrees of CA at different positions after flowing were evaluated. The test procedure was as follows:

(1) Right after mixing, fresh concrete sample was casted into the left vertical room of the L-box shown in **Fig. 4.20**.

(2) The gate was lifted up quickly within 1 second.

(3) After the concrete sample stopped flowing, the flow distance and flow time were recorded. Then, the concrete was divided into 7 parts in the horizontal direction at an interval of 100mm, as shown in **Fig. 4.20**. The volume of concrete in each part was measured.

(4) The CA in each part was sieved out with a 5 mm opening sieve and washed off the adhering mortar, then the volume of CA in each part in the surface dry state was measured. The volume fraction of CA in each part was further calculated.

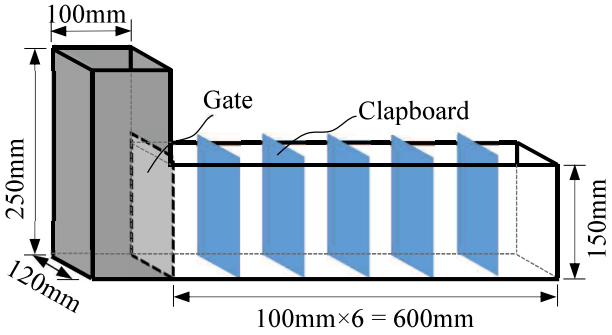

Fig. 4.20 Geometry of L-box

(5) The segregation degree (*SD*) of fresh concrete in each part was calculated by Eq. (4.21). The more the *SD* deviates from 1.0, the more severe the segregation.

$$SD_i = \varphi_i / \overline{\varphi} \tag{4.21}$$

where, SD_i is segregation degree of CA in part *i*, φ_i is volume fraction of CA in part *i*, $\overline{\varphi}$ is volume fraction of CA of whole concrete.

4.4.3 Configuration of Numerical Simulations

The L-box flow simulations were conducted for the two series of concrete using the I-MPS method and the DPMP model. As discussed in Section 4.2.5, for ensuring the simulation accuracy, the diameter of mortar particle and elementary particle was set to 5mm. The number of coarse aggregate particles in Series No.1 and No.2 was 1754 (number of elementary particles: 6774) and 1982 (number of elementary particles: 7561), respectively, which randomly distributed in the matrix mortar. The numbers of matrix mortar particles are shown in **Table 4.4**. The volume fractions of CA particles in the range of 5-10mm, 10-15mm and 15-20mm were set to be 28%, 36%, and 36%, respectively, for making the fineness modulus (F.M.) of simulated coarse aggregate to be consistent with the experimental value (F.M.=6.72). The detail configuration information of particles was shown in **Table 4.4**.

Table 4.4 Configuration information of particles

Series of concrete	Double-phase & multi-particle model					
	Mortar particle			Coarse aggregate particle		
	Density (kg/m^3)	Shape, diameter	Number	Density (kg/m^3)	Shape, size	Number
No.1	2215	Sphere, 5mm	15076	2730	Random 5-10mm, 32% 10-15mm, 36% 15-20mm, 32%	1754
No.2	2230		14289			1982

4.5 Results and Discussion

4.5.1 L-box Flow Behaviors

After lifting the gate of L-box, the concrete sample quickly flowed out from the vertical room into the horizontal room. In the experiments, the flow time (t_{stop}) of No.1 was 80.0 seconds, and the flow distance was 695mm, but the flow of No.2 stopped after 60.0 seconds, and the flow distance was 630mm. The final shapes of the L-box flow are shown in **Fig. 4.21** (a). In numerical simulations, both two series of L-box flow were simulated twice, by using a single-phase fluid model and the DPMP model, respectively. The final flow shapes obtained by the simulations are shown in **Fig. 4.21** (b) and (c). When using the single-phase fluid, the flow of No.1 and No.2 stopped at 75.7 seconds and 51.7 seconds, the flow distances were 578mm and 553mm, respectively. However, when using the DPMP model, the flow of No.1 and No.2 stopped at 77.9 seconds and 59.4 seconds, and the flow distances were 668mm and 688mm, respectively. Compared with the single-phase fluid model, the simulations using the DPMP model proposed in this study gave the flow stop times and flow distances that were closer to the experimental results. The errors between simulation results of the DPMP model and the experimental results were calculated by Eq. (4.22). Both the errors of flow stop time and flow distance were less than 10%.

$$Error = \frac{\left|\text{simulation result} - \text{experimental result}\right|}{\text{experimental result}} \times 100\% \tag{4.22}$$

The flow behaviors of fresh concretes were simulated using the DPMP model, obtained velocity distributions are shown in **Fig. 4.22**. The velocity direction of the particle is indicated by arrow, and

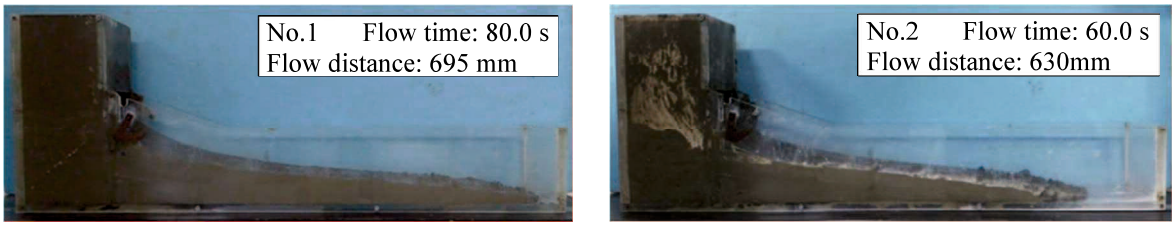

(a) Experiment result

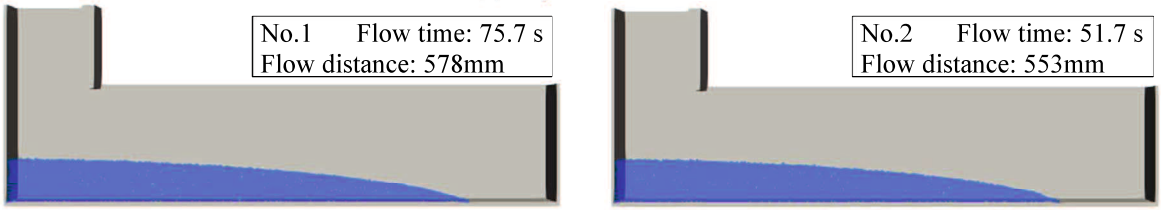

(b) Simulation result (SPMP model)

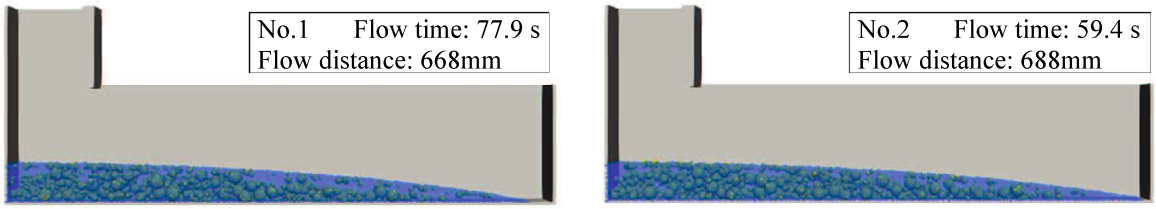

(c) Simulation result (DPMP model)

Fig. 4.21 Final flow shape of the fresh concrete in the L-box flow test

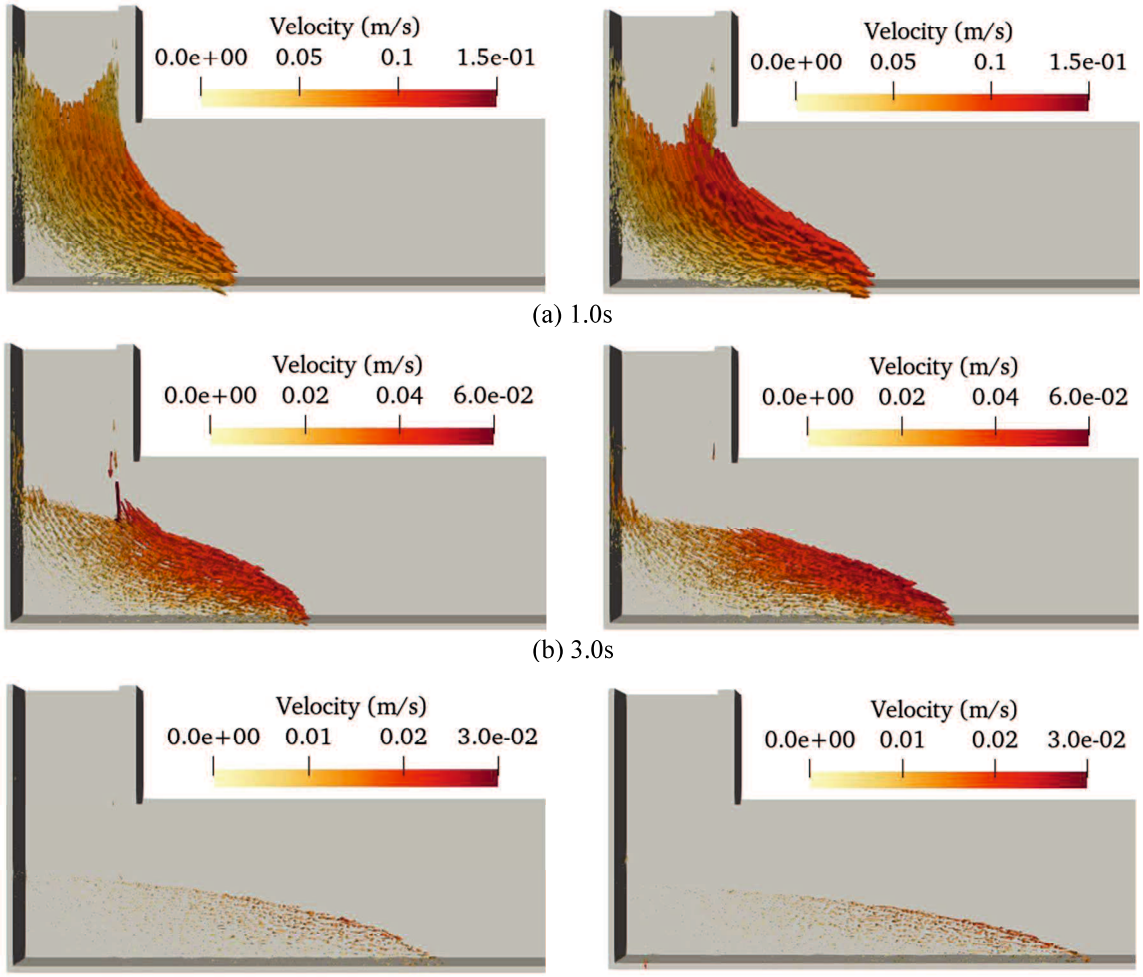

Fig. 4.22 Velocity profile of fresh concrete simulated by using DPMP model
(Left: No.1, Right: No.2)

the length and color of the arrow represent the magnitude of the particle velocity. Since the flow of fresh concrete near the walls or bottom of L-box was affected by the boundary resistance, the flow velocities of the particles were low. The concrete sample at the left bottom corner was subjected to two boundary resistances from the side and the bottom of L-box at the same time, thus the concrete sample was hard to flow. However, the concretes near the free top surface and in the front of the flow flowed very quickly. After the concrete sample rushed out of the vertical room to enter into the horizontal room, the flow direction changed, and the flow velocity rapidly decreased, and the lower part of concrete eventually stopped, but the upper concrete in the flow front continued to flow forward slowly for a certain time. Since No.2 had lower plastic viscosity, it flowed faster than No.1.

4.5.2 Segregation Simulation of Fresh Concrete

■ **Static Segregation**

To simulate and analyze the static segregation of coarse aggregate, the concrete sample in the vertical room was allowed to stand for 10 seconds before the gate was lifted up. Although the static segregation degree within 10 seconds is not great, the qualitative analysis of static segregation is

possible by the simulation of 10 seconds. The concrete in the vertical room of L-box was equally divided into three parts (bottom, middle, and top), and the *SD* of CA in each part was recorded over time, as shown in **Fig. 4.23**. Since the CA particles settled down in the fresh concrete, the *SD* of the top part was less than 1.0, and gradually decreased, while the *SD* in the bottom concrete was larger than 1.0, and approached to a certain value, because of the existence of the maximum packing volume.

CA is simultaneously subjected to its own gravity, buoyancy, and viscous force from matrix mortar, as shown in **Fig. 4.24**. As a Bingham fluid, matrix mortar has a yield stress. When the yield stress of the matrix mortar is less than the difference between gravity and buoyance of the CA particle, the CA particle starts to settle down. If the viscosity of the matrix mortar is small, the CA particles settle down at a great speed, the segregation is serious. **Fig. 4.25** shows the changes of segregation degree (ΔSD) of different parts in concrete No.1 and No.2 in standing period. Since the matrix mortar in No. 2 had a lower yield stress, the ΔSD of No.2 was larger than that of No.1. It should be noted that since the regularized Bingham constitutive equation in Eq. (3.17) was used in this study, the calculated shear stress acting on coarse aggregate was underestimated (see **Fig. 3.1**) and was not able to resist the action of gravity together with the buoyancy, the CA settled down slightly. Hence, slight segregation was also observed in the concrete No.1. Since the difference in density between coarse aggregate and

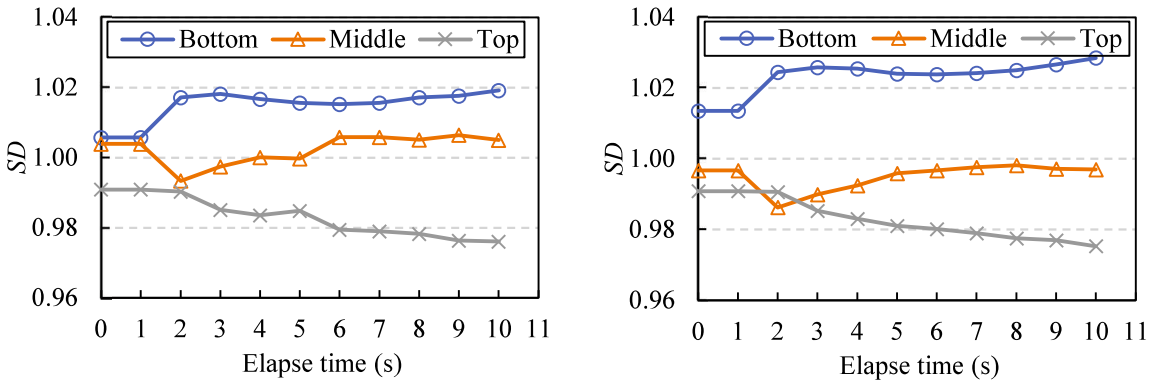

Fig. 4.23 The static *SD* of coarse aggregate in each portion (left: No.1, right: No.2)

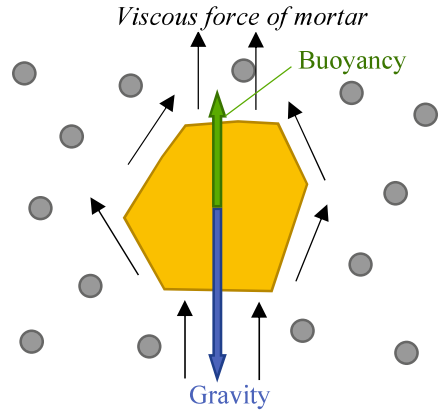

Fig. 4.24 Schematic diagram of forces acting on coarse aggregate particle

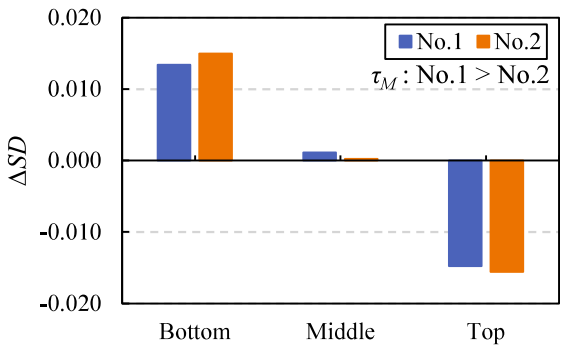

Fig. 4.25 Change of *SD* before and after static segregation

mortar in No.1 and No.2 is almost the same, and the observation time is not long enough, the CA segregation degrees of the two concretes are close.

The viscous resistance from the mortar is an area force, and its magnitude is proportional to the sectional projection area of the coarse aggregate, but the gravity and buoyance of the coarse aggregate are body force, which are proportional to the volume of the coarse aggregate. Regarding the CA particles are spheres, the ratio $F_{vis}/\Delta G$ of viscous resistance force (F_{vis}) to the difference (ΔG) between gravity and buoyancy is:

$$\frac{F_{vis}}{\Delta G}=\frac{2\pi R^2\tau_M}{\frac{4}{3}\pi R^3\rho_{CA}-\frac{4}{3}\pi R^3\rho_M}=\frac{3\tau_M}{2(\rho_{CA}-\rho_M)R} \tag{4.23}$$

where, ΔG is difference between gravity and buoyancy, ρ_{CA} is density of coarse aggregate, ρ_{Mor} is density of matrix mortar. R_{CA} is radius of CA particle.

According to Eq. (4-23), $F_{vis}/\Delta G$ has a negative correlation with the radius R_{CA} of CA particle. When the radius R_{CA} is large and the ratio $F_{vis}/\Delta G$ is less than 1.0, the CA particle segregates. However, when the radius R_{CA} is small and the ratio $F_{vis}/\Delta G$ is greater than 1, the aggregate does not settle down in matrix mortar. Therefore, aggregate particles with a larger radius are more likely to segregate. Here, the difference of moving velocities between CA particle and surrounding mortar is defined as the segregation velocity of the CA particle, and vertical upward and horizontal right are set to be positive directions. **Fig. 4.26** shows the segregation velocity of CA particles with different size ranges in the vertical direction. The static segregation velocities of CA particles are fast at the beginning, and then approach to certain values, the smaller the CA particle, the smaller the static segregation velocity.

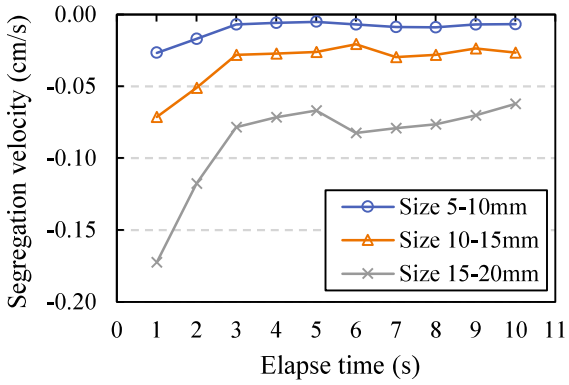

Fig. 4.26 Segregation velocities of CA particles with different size ranges (static segregation, No.2)

■ **Dynamic Segregation**

During the flow, the dynamic segregation of CA may occur not only in the vertical direction, but also in the horizontal direction. Right after the gate of L-box was opened, the fresh concretes flowed out rapidly, and the height of concrete in the vertical room decreased quickly. Because of greater gravity and standstill inertia of CA, its downward movement speed was less than that of the surrounding matrix mortar at the beginning. As the concrete flowed out of the vertical room, the flow speed of the concrete gradually decreased. However, the CA particles continued to move horizontally at a relatively large speed due to their greater motion inertia. Finally, with the stop of the concrete flow and the gradual increase of the CA volume fraction in the bottom concrete, the dynamic segregation velocity in the vertical direction gradually decreased. The vertical segregation velocities

of CA particles in both concretes No.1 and No.2 are shown in **Fig. 4.27**. Within 10 seconds, the segregation velocity of No.2 was larger than that of No.1. **Fig. 4.28** shows the dynamic segregation velocities of CA particles with different dimensions in the vertical direction. During flowing, the larger the CA particle, the greater the vertical segregation velocity of the CA particle. In addition, the yield stress and plastic viscosity of the matrix mortar of No. 2 are lower than those of No. 1, thus the mortar of No.2 had a lower ability to prevent segregation motion of CA particles in the initial flow stage. Therefore, the dynamic segregation velocity of No. 2 in the vertical direction was higher than that of No. 1, and the vertical segregation velocity of CA with the size of 15 - 20mm was the largest.

In the horizontal direction, the flow velocity was the fastest immediately after the gate was opened, i.e., the deformation rate of the fluid was the largest. The CA particles stayed still due to their gravity and standstill inertia, but the matrix mortar had a higher flow velocity at the beginning of the concrete flow. The difference in flow velocity between matrix mortar and CA was large, which lead to a large segregation velocity at the beginning. The flow velocity of matrix mortar gradually decreased and the flow velocity of CA increased due to motion inertia, their flow velocity difference decreased, thus the segregation velocity decreased accordingly. **Fig. 4.29** shows the horizontal segregation velocity of CA particles in No.1 and No.2. Because No. 2 had a smaller plastic viscosity, its CA segregation velocity was higher. **Fig. 4.30** shows the change of segregation velocity of CA particles in the horizontal direction with the dimensions of CA particles. The results show that the larger the CA particle, the greater the dynamic segregation velocity.

After the concrete stopped to flow, the segregation degree of CA in each horizontal part was calculated according to Eq. (4.21). The experimental and numerical results are shown in

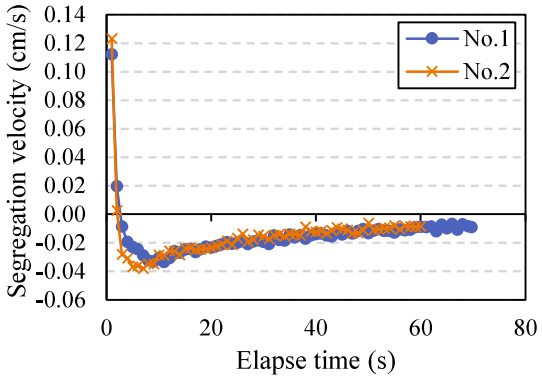

Fig. 4.27 Vertical segregation velocities of aggregates in different concretes (dynamic segregation)

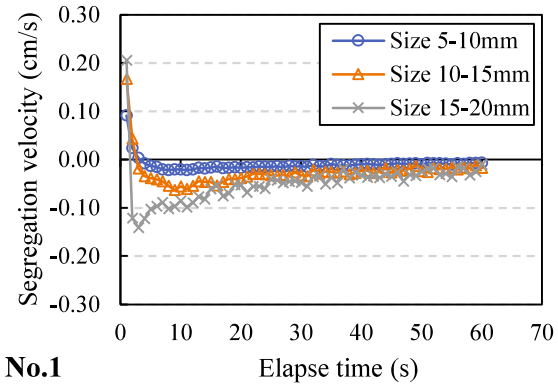

No.1

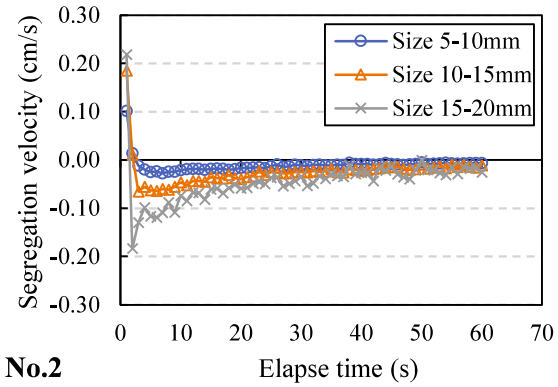

No.2

Fig. 4.28 Vertical segregation velocities of aggregates with different sizes (dynamic segregation)

Fig. 4.31. When fresh concrete flowed through the gate of L-box, the flow velocity direction changed dramatically in the horizontal distance of 10 ~ 40 cm, the coarse aggregate segregated due to the effect of standstill inertia. This explains why the segregation degree was larger in the horizontal range of 10 ~ 40cm near the gate of L-box. **Fig. 4.32** shows the position change of three parts of concrete No.1 in the vertical room during the flow in L-box. It was found that the concrete in the flow front mainly came from the top part of concrete in the vertical room. And from **Fig. 4.23** it was found that the CA in the top part of concrete in the vertical room was the least. This can explain why the *SD* in the 50 ~ 70 cm range was small, as shown in **Fig. 4.31**. Therefore, the flow behaviors of concrete affect CA segregation. The difference between the numerical and the experimental results in this range was mainly due to the assumption that there was no slip between the concrete and the bottom of L-box in the simulation. Therefore, it is necessary to study the slip behavior of concrete on the boundary, which will be reported in details in our other paper.

In addition, there are many other reasons for the inconsistency between the numerical and the experimental results, including initial distribution of CA particles in the vertical room of L-box, and the difference in the shapes and dimensions of CA particles between numerical simulations and actual situation. Moreover, it is known that even for the same fresh concrete, different rheometers would give different measuring results of rheological parameters (yield stress and plastic viscosity) [39]. Therefore, it is difficult to match completely the numerical results with the experimental results. Nevertheless, this study aims to develop a numerical approach which has the ability to predict the segregation behavior of fresh concrete. Although part of the simulation results was not fully consistent with the experimental results, the proposed numerical

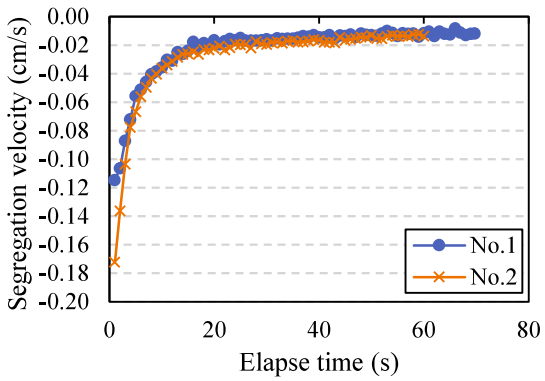

Fig. 4.29 Horizontal segregation velocities of aggregates in different concrete (dynamic segregation)

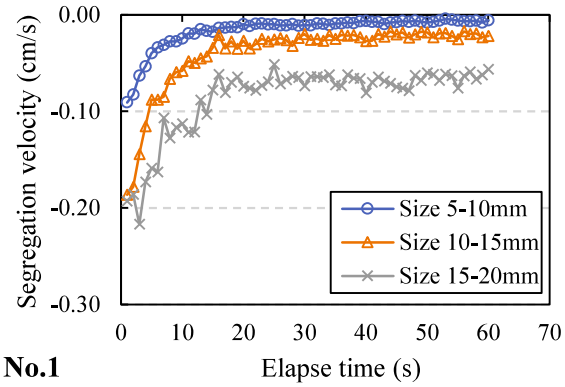

No.1

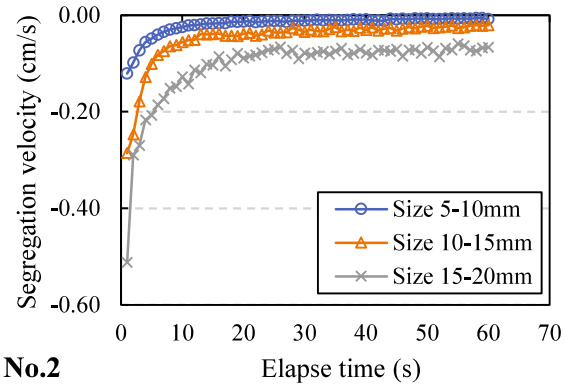

No.2

Fig. 4.30 Horizontal segregation velocities of aggregates with different sizes (dynamic segregation)

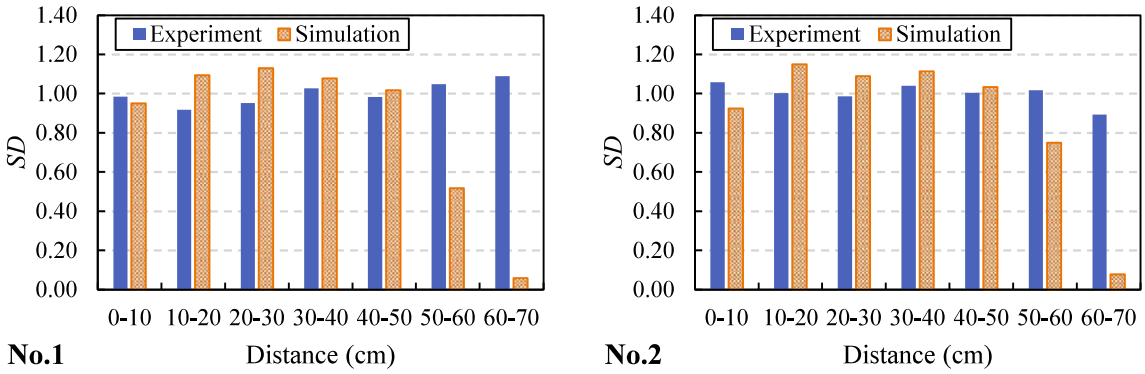

Fig. 4.31 Segregation degree of coarse aggregate in different horizontal zones

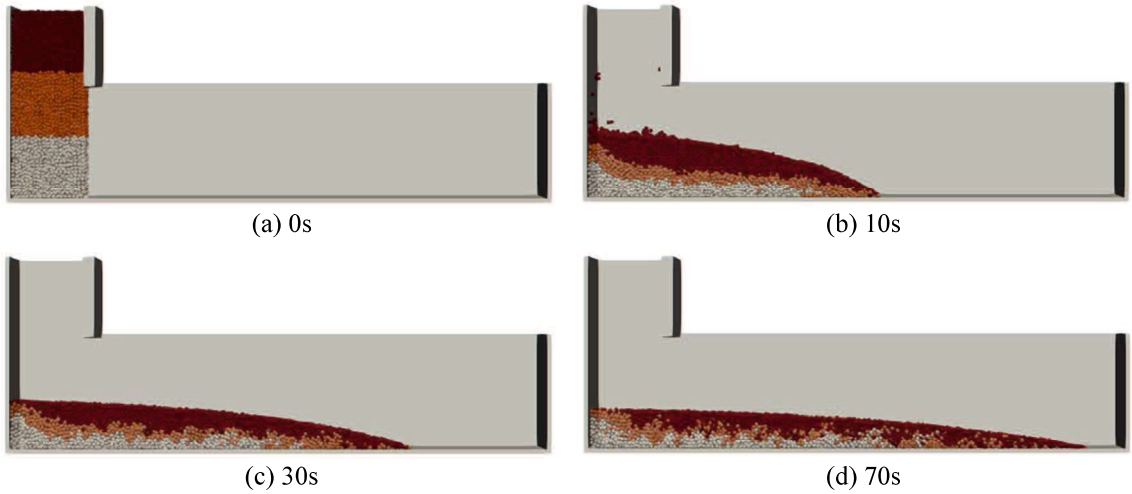

Fig. 4.32 Position change of three parts of fresh concrete in the vertical room during the L-flow (No.1)

approach still has potential to simulate both the static and dynamic segregation behaviors of fresh concrete, and show the uneven distribution of CA particles in fresh concrete.

4.5.3 Dynamic viscosity distribution

Based on Eq. (4.10), the dynamic viscosity distribution at different flow times were calculated. **Fig. 4.33** shows the calculating results for different flow times (1.0s, 3.0s, and 10.0s) after the static segregation in the vertical room of L-box before opening the gate. With the static segregation, i.e., as part of CA particles settle down, the viscosity of the concrete at the lower position gradually increases.

The uneven distribution of dynamic viscosity, induced by the dynamic segregation occurring during the flow can also be clarified, as shown in **Fig. 4.34**. As explained in Section 4.5.1, due to the two boundary resistances the concretes have a high dynamic viscosity at the left-bottom corner. Along the flow direction, dynamic viscosity decreases, and in the rear of the flow, the dynamic viscosity of the concrete gradually increases with flow time, but the concrete in the front of flow has low dynamic viscosity because of less CA and more mortar. Also, it can be found that No.1 has a lower unevenness of dynamic viscosity than No.2. This is because that No.1 has greater Bingham constants than No.2.

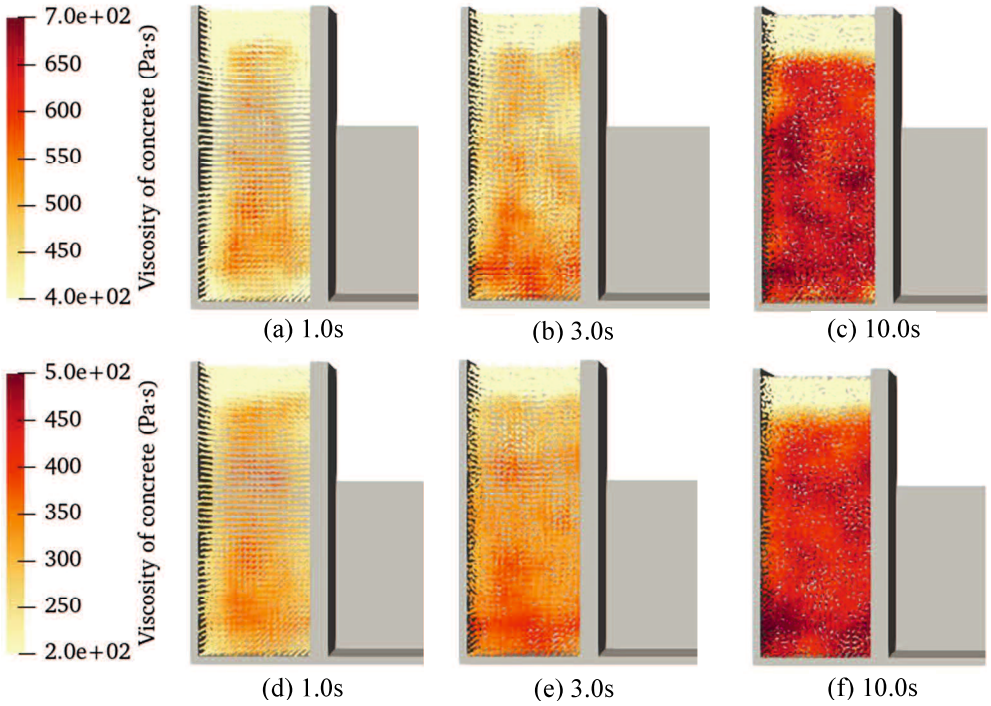

(a) 1.0s (b) 3.0s (c) 10.0s

(d) 1.0s (e) 3.0s (f) 10.0s

Fig. 4.33 Viscosity distribution of fresh concrete in the vertical room after static segregation (upper: No.1, lower: No.2)

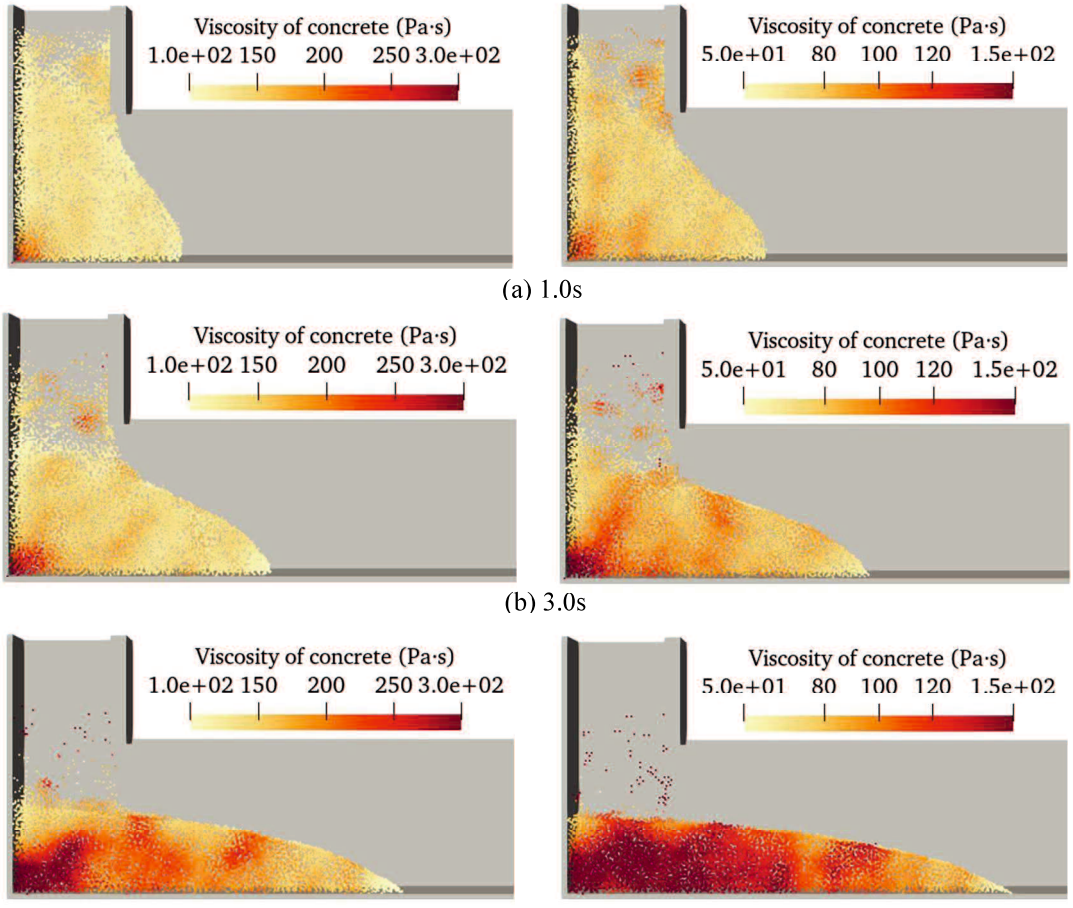

(a) 1.0s

(b) 3.0s

(c) 10.0s

Fig. 4.34 Viscosity distribution of fresh concrete after dynamic segregation (Left: No.1, Right: No.2)

4.6 Conclusions

In this Chapter, a double-phase & multi-particle (DPMP) model was developed and used in the flow simulation of fresh concrete. Based on this constitute model of fresh concrete and the I-MPS method, a numerical flow approach was proposed to simulate the flow behavior and the segregation behavior of fresh concrete. This numerical flow approach was verified by the L-flow simulation of two high fluidity concretes. The following conclusions can be drawn:

(1) The proposed numerical flow approach of fresh concrete can well simulate the flow behavior of fresh concrete, which is regarded as a double-phase fluid composed of matrix mortar and coarse aggregate (CA) with a particle size distribution and random particle shapes. The proposed numerical flow approach has higher accuracy than normal simulation treating fresh concrete as a homogeneous fluid.

(2) For the use of the DPMP model, the interactions between mortar-mortar particles, CA-CA particles, mortar-CA particles were quantitatively discussed, respectively. The densities of matrix mortar and coarse aggregate were also differentiated according to their actual values. The proposed numerical flow approach can predict the movement of coarse aggregate and simulate the segregation behavior of CA particles from matrix mortar. Moreover, the numerical flow approach can also clarify the change in the viscosity of fresh concrete after the segregation of coarse aggregate.

(3) The CA segregation can be divided as static segregation and dynamic segregation. Static segregation was defined as the segregation occurring in the vertical direction, caused only by the density difference between CA and matrix mortar. However, the dynamic segregation occurs during the flow of concrete, not only due to the density difference, but also due to the flow velocity difference between CA and matrix mortar. Dynamic segregation occurs in both vertical and horizontal directions.

(4) The smaller the yield stress of the matrix mortar, the easier it is for the coarse aggregate to segregate. The lower the plastic viscosity of the mortar, the faster the segregation velocity of CA. The larger the coarse aggregate, the easier its segregation, and the faster the segregation velocity.

Reference

[1] H. Okamura, M. Ouchi, Self-Compacting Concrete, J. Adv. Concr. Technol. 1 (2003) 5–15.

[2] Z. Li, State of workability design technology for fresh concrete in Japan, Cem. Concr. Res. 37 (2007) 1308–1320.

[3] L. Shen, L. Struble, D. Lange, Testing static segregation of SCC, in: SCC2005, Proc. 2nd North Am. Conf. Des. Use SCC, 2005: pp. 1–3.

[4] D.K. Panesar, B. Shindman, The effect of segregation on transport and durability properties of self consolidating concrete, Cem. Concr. Res. 42 (2012) 252–264.

[5] J. Pan, X. Gao, H. Ye, Influence of Rheological Behavior of Mortar Matrix on Fresh Concrete Segregation and Bleeding, Iran. J. Sci. Technol. - Trans. Civ. Eng. (2020) 1–15.

[6] L. Shen, H. Bahrami Jovein, Z. Sun, Q. Wang, W. Li, Testing dynamic segregation of self-consolidating concrete, Constr. Build. Mater. 75 (2015) 465–471.

[7] P. Turgut, K. Turk, H. Bakirci, Segregation control of SCC with a modified L-box apparatus, Mag. Concr. Res. 64 (2012) 707–716.

[8] J. Han, K. Wang, X. Wang, P.J.M. Monteiro, 2D image analysis method for evaluating coarse aggregate characteristic and distribution in concrete, Constr. Build. Mater. 127 (2016) 30–42.

[9] M.I. Safawi, I. Iwaki, T. Miura, The segregation tendency in the vibration of high fluidity concrete, Cem. Concr. Res. 34 (2004) 219–226.

[10] X. Gao, J. Zhang, Y. Su, Influence of vibration-induced segregation on mechanical property and chloride ion permeability of concrete with variable rheological performance, Constr. Build. Mater. 194 (2019) 32–41.

[11] J. Spangenberg, N. Roussel, J.H. Hattel, H. Stang, J. Skocek, M.R. Geiker, Flow induced particle migration in fresh concrete: Theoretical frame, numerical simulations and experimental results on model fluids, Cem. Concr. Res. 42 (2012) 633–641.

[12] S. Hurukawa, Y. Kato, M. Suzuki, S. Takahashi, Effect of mortar viscosity and coarse aggregate amount on segregation of high-fluidity concrete, Proc. Japan Concr. Inst. 42 (2020) 989-994 (in Japaness).

[13] G.R. Liu, M.B. Liu, Smoothed Particle Hydrodynamics, World Scientfic, 2003.

[14] Z. Xu, Z. Li, F. Jiang, The applicability of SPH and MPS methods to numerical flow simulation of fresh cementitious materials, Constr. Build. Mater. 274 (2021) 121736.

[15] G. Cao, Z. Li, Z. Xu, A SPH simulation method for opening flow of fresh concrete considering boundary restraint, Constr. Build. Mater. 198 (2019) 379–389.

[16] W.S. Alyhya, S. Kulasegaram, B.L. Karihaloo, Simulation of the flow of self-compacting concrete in the V-funnel by SPH, Cem. Concr. Res. 100 (2017) 47–59.

[17] S. Urano, H. Nemoto, K. Sakihara, Application of flow simulation for evaluation of filling-ability of self-compacting concrete, J. Japan Soc. Civ. Eng. Ser. E2 (Mater. Concr. Struct.). 68 (2012) 38-48 (in Japaness).

[18] H. Zhu, N.S. Martys, C. Ferraris, D. De Kee, A numerical study of the flow of Bingham-like fluids in two-dimensional vane and cylinder rheometers using a Smoothed Particle Hydrodynamics (SPH) based method, J. Nonnewton. Fluid Mech. 165 (2010) 362–375.

[19] F. Galbusera, F. Niemeyer, Chapter 14 - Mathematical and Finite Element Modeling, in: F. Galbusera, H.-J. Wilke (Eds.), Biomech. Spine, Academic Press, 2018: pp. 239–255.

[20] S. Kulasegaram, B.L. Karihaloo, A. Ghanbari, Modelling the flow of self-compacting concrete, Int. J. Numer. Anal. Methods Geomech. 35 (2011) 713–723.

[21] C.T. Kennedy, The Design of Concrete Mixes, ACI J. Proc. 36 (1940) 373–400.
[22] T.C. Powers, The Properties of Fresh Concrete, Wiley, 1968.
[23] A. Shakibaeinia, Y.C. Jin, MPS mesh-free particle method for multiphase flows, Comput. Methods Appl. Mech. Eng. 229–232 (2012) 13–26.
[24] G. Duan, B. Chen, S. Koshizuka, H. Xiang, Stable multiphase moving particle semi-implicit method for incompressible interfacial flow, Comput. Methods Appl. Mech. Eng. 318 (2017) 636–666.
[25] C.F. Ferraris, F. De Larrard, N. Martys, Fresh Concrete Rheology - Recent Developments, Mater. Sci. Concr. VI. 6 (2001) 215–241.
[26] C.F. Ferraris', F. de Larrard, Testing and modelling of fresh concrete rheology, Gaithersburg, MD, 1998.
[27] A. Einstein, A new determination of molecular dimensions, Ann. Phys. 19 (1906) 289–306.
[28] R. Roscoe, The viscosity of suspensions of rigid spheres, Br. J. Appl. Phys. 3 (1952) 267–269.
[29] I.M. Krieger, T.J. Dougherty, A Mechanism for Non-Newtonian Flow in Suspensions of Rigid Spheres, Trans. Soc. Rheol. 3 (1959) 137–152.
[30] L.J. Struble, G.-K. Sun, Cement Viscosity As A Function Of Concentration, MRS Proc. 289 (1992) 173.
[31] X. Chateau, G. Ovarlez, K.L. Trung, Homogenization approach to the behavior of suspensions of noncolloidal particles in yield stress fluids, J. Rheol. (N. Y. N. Y). 52 (2008) 489–506.
[32] A. Ghanbari, B.L. Karihaloo, Prediction of the plastic viscosity of self-compacting steel fibre reinforced concrete, Cem. Concr. Res. 39 (2009) 1209–1216.
[33] J. Yammine, M. Chaouche, M. Guerinet, M. Moranville, N. Roussel, From ordinary rhelogy concrete to self compacting concrete: A transition between frictional and hydrodynamic interactions, Cem. Concr. Res. 38 (2008) 890–896.
[34] F. Mahaut, S. Mokéddem, X. Chateau, N. Roussel, G. Ovarlez, Effect of coarse particle volume fraction on the yield stress and thixotropy of cementitious materials, Cem. Concr. Res. 38 (2008) 1276–1285.
[35] A. Salinas, D. Feys, Estimation of lubrication layer thickness and composition through reverse engineering of interface rheometry tests, Materials (Basel). 13 (2020) 1799.
[36] N.S. Klein, S. Cavalaro, A. Aguado, I. Segura, B. Toralles, The wetting water in cement-based materials: Modeling and experimental validation, Constr. Build. Mater. 121 (2016) 34–43.
[37] S. Koshizuka, A. Nobe, Y. Oka, Numerical analysis of breaking waves using the moving particle semi-implicit method, Int. J. Numer. Methods Fluids. 26 (1998) 751–769.
[38] Z. Li, Rheological model and rheometer of fresh concrete, J. Struct. Constr. Eng. (Transactions AIJ). 80 (2015) 527-537 (in Japaness).
[39] C.F. Ferraris, L.E. Brower, Comparison of concrete rheometers, Concr. Int. 25 (2003) 41–47.

Chapter 5 Numerical Approach to Pipe Flow of Fresh Concrete

5.1 Introduction

5.2 Numerical Model of Pipe Flow

5.3 Numerical Simulation

5.4 Numerical Results and Discussion

5.5 Summary

Chapter 5
Numerical Approach to Pipe Flow of Fresh Concrete

5.1 Introduction

Concrete pumping has become one of the most widely used approaches to place concrete. This method can greatly improve the construction efficiency, consequently reduce the cost of construction, and allow concrete casting in the difficulty to access locations. Its usage continues to grow due to an increase in demand for large-scale construction projects such as high-rise buildings, long-span bridges, and others. However, some problems may occur during pumping, such as insufficient pumping pressure, pipe blockage, segregation, slump loss and air loss [1,2], etc. Thus, when considering pumpable concrete, pumpability should refer to a concrete that can flow through a pipeline with help of a pressure pump without unpredictable changes in its properties.

In many construction sites and guidelines, the use of pumping is determined according to qualitative assessment of concrete pumpability based on the slump test or the slump flow test. However, for concrete pumping, the shear rate is typically around 10 s^{-1} to 100 s^{-1}, whereas, for the slump test, it is only 1 s^{-1} or less [3]. At such low shear rate, the results of slump test do not encapsulate the effects such as dynamic segregation and slip layer (also referred to as a boundary layer or lubrication layer), which may play a dominant role during pumping. Hence, the slump test may not be relevant for predicting the ability of concrete to flow in a pipe. Moreover, with the development of concrete's admixtures, the rheological properties of fresh concrete, such as self-compacting concrete (SCC) and high-performance concrete (HPC), are very different from conventional concrete [4] so that the knowledge and the guidelines of concrete pumping based on conventional concrete may be no longer applicable to new types of concrete [5]. Consequently, the optimization and development of prediction methods for concrete pumping have been becoming a crucial issue for the concrete industry.

If one can accurately predict required pressure for pumping of a concrete mixture based on its properties, and accurately evaluate other aspects of pumpability such as static and dynamic stability, concrete mixtures can be adjusted in the laboratory for optimizing the pumpability. Fresh concrete is generally regarded as a Bingham fluid with a yield stress. For this reason, the Buckingham-Reiner equation [6] is used to predict pressure required for concrete to flow through a pipeline. However, it

is found that the Buckingham-Reiner equation leads to overestimation of pumping pressures at certain flow rates [5]. This is primarily due to the fact that a slip layer forms along the pipe wall, and therefore, the material does not remain homogenous during pumping. To address the inhomogeneous nature of concrete in the pipeline, several pressure prediction models were recently developed, such as Kaplan's model [7], Choi's model [8], Kwon's model [2], and Mechtcherine's model [9], etc. These models incorporate not only the rheological properties of bulk concrete, but also the rheological properties of slip layer.

Besides the pumping pressure required for concrete flow, other concern about fresh concrete under pumping flow is the possibility of segregation, i.e. the separation of the paste from the aggregate phase, which usually leads to hose blockage. As mentioned above, the slip layer plays a dominant role during pumping. The slip layer is formed by that large aggregate particles tend to migrate towards the low shear zone. It is considered that coarse aggregates undergo the shear-induced migration towards the inner, while cement paste and a fraction of finer material move towards the pipe wall [8,10,11]. Thus, the slip layer is composed of cement paste and a limited fraction of fine aggregate, aggregates are not evenly distributed in diameter direction. Also, in front of the concrete, the concentration of coarse aggregate is high, even a plug of coarse aggregates is formed [1,12]. Thus, the segregation prediction of pumped concrete is also an important issue.

Although pumping experiment of concrete is able to evaluate the pump pressure, it is almost impossible to clear segregation behaviors of solid particles during the pumping process due to the invisibility of internal flow. The commercial CFD software is usually employed to simulate the pipe flow to predict the velocity distribution and pressure loss, considering fresh concrete is a single-phase fluid, but it is unable to provide information about the dynamic segregation of concrete in pipe for predicting blockage [3,11,13]. Recently, the meshless particle method, such as Smoothed Particle Hydrodynamics (SPH) method [14], has been increasingly used in the flow simulation of fluid, which represents the fluid with particles. This implies that the meshless particle method has the potential to numerically discuss aggregate segregation [15]. The SPH method has been proved to be applied to simulate the flow of fresh concrete [16–19]. Choi et al. suggested that SPH approach can be used to predict the flow of pumped concrete [3]. During pumping process, accurate calculation of the pressure distribution is important for predicting the pumping behaviors. However, since the SPH usually used the ideal equation of state to calculate the pressure, under high-pressure conditions, such as pumping, fluid particles may be compressed, and since the magnitude of time step is limited in the SPH, the calculation accuracy and efficiency are greatly reduced. For analyzing incompressible fluid problems, Koshizuka [20] developed a new meshless method called Moving Particle Semi-implicit (MPS). The MPS has been successfully used in the simulation of multiphase flows under high pressure [21], and the flow simulations of fresh mortar [22]. In the original MPS, an explicit algorithm is used for the viscous item. However, for a fluid with high viscosity, such as fresh concrete, the calculation time step

needs to be set very small to stabilize the calculation results [23], accordingly the calculation efficiency is reduced. Therefore, the MPS algorithm needs to be improved for the flow simulation of fresh concrete. Moreover, there is no meshless particle method that can predict pressure loss together with segregation behavior of pumped concrete now. It is urgent to establish a proper numerical model for concrete pumping based on the flow characteristics of fresh concrete in pipe.

As a fundamental study on the prediction of pumpability of fresh concrete, in this study, I proposed a new numerical simulation method for the pipe flow of concrete. The tribological behavior model [5,24,25] was adopted to describe the shear resistance of slip layer. I improved the MPS method to have complete implicit algorithms to simulate the vertical pipe flow and segregation of fresh concrete. In the simulation, two types of constituent models, named single-phase & mono-particle (SPMP) model and double-phase & multi-particle (DPMP) model, were used to describe fresh concrete. The former expresses fresh concrete with spherical fluid particles having same size and density. But in the latter, fresh concrete is regarded as two-phase material of matrix mortar and coarse aggregate, and the coarse aggregate particles are composed of elementary particles so as to have different sizes and random shapes. After the discussion on the reasonable particle size and the effect of the thickness of slip layer on the vertical pipe flow simulation, pressure-discharge relationships and velocity profiles were investigate numerically for three series of concrete with different slump values. In addition, the dynamic aggregate segregation was also discussed by using the DPMP model.

5.2 Numerical Model of Pipe Flow

5.2.1 Numerical Analysis Method

In this chapter, an improved MPS method proposed in Chapter 4 is used to do the numerical simulation of pipe flow. This improved MPS has introduced a complete implicit algorithm into general MPS method to improve the calculating accuracy and to shorten the calculating time of fresh concrete's flow simulation. Moreover, differentiating from the general MPS method that uses a single type of spherical fluid particles with the same size, in the improved MPS method elementary particles were employed to form coarse aggregate particles to have a size distribution and random shape, for making the MPS to be applicable to the simulation of dynamic segregation of fresh concrete.

5.2.2 Rheological Model of Bulk Concrete

The regularized Bingham model [26] is used to describe the flow behaviors of bulk concrete. The detailed introduction is described in Section 3.3.1, Eq. (3.7), and **Fig. 3.1**.

5.2.3 Slip Layer Treatment

It is generally considered that fresh concrete behaves as a fluid with yield stress, which is the minimum stress for initiating irreversible deformation and flow. Also, fresh concrete is a complex fluid because it contains aggregates with a wide range of sizes. Dynamic segregation is an additional factor that can influence concrete flow in a pipe. Though a concrete can display no segregation while at rest, it can undergo segregation during shearing. Segregation during pumping can involve the phenomena that aggregates move slightly towards the pipe center where the shear rate is lower. As a consequence, cement paste and a fraction of finer material move towards the pipe wall, forming the slip layer [10]. Kaplan suggested that at low velocities, the concrete moves as a block in the pipe, with only a small thickness of slip layer near the pipe wall (often identified as plug flow). As the velocity increases, the pressure imposed on bulk concrete is sufficient to initiate shear flow in the bulk concrete (the applied shear stress is greater than the yield stress), accordingly generating a viscous flow in the concrete [1]. Thus, concrete flow in a pipe typically occurs in three layers or regions, as shown in **Fig.**

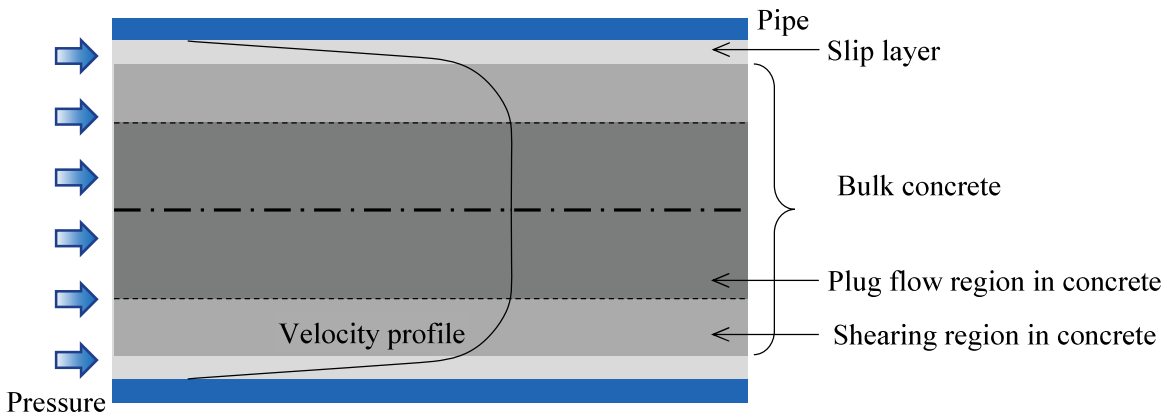

Fig. 5.1 Concrete flow in pipe

5.1: (i) slip layer or lubrication layer, (ii) shearing layer, (iii) plug flow layer. Total of the shearing layer and the plug flow layer is referred to as bulk concrete.

Depending on the scale of observation, either a slip layer or a slip velocity may be observed [27]. At large scales of observation (macroscopic level), an apparent slip velocity may be measured whereas, at smaller scales of observation, a fine material, slip layer appears, in which the velocity evolves from zero at the wall to the apparent slip velocity at the boundary of the slip layer (see **Fig. 5.2**).

Aleekseev [28] and Weber [29] first proposed the existence of slip layer, and it was confirmed and investigated widely by both experiments and numerical simulations [8,14,32]. The slip layer contains more liquid and fine particles and has a lower value of the maximum aggregate size, accordingly with lower yield stress and lower viscosity than the bulk concrete, is highly sheared [24]. The size of the slip layer has been widely debated and there is no consensus in the literature as to its thickness. Ngo et al. [31] found that the thickness of slip layer is proportional to the volume of the cement paste, the water-to-cement ratio, and the dosage of superplasticizer. The slip layer thickness also decreases with a higher amount of fine sand. The length and diameter of pipeline are also considered to change the thickness of the slip layer. Ngo et al. [31] observed that the slip-layer is between 1 mm to 9 mm thick, by visualizing the material flow in the rheometer. However, Choi et al. [8] found that the thickness of the slip layer is around 2 mm for the concretes, not depending on flow rate, but varying with sand and gravel particle's initial volume fractions and pipe diameter. Le et al. [24] found that the thickness of the slip layer is not constant in space and time, varying from 0 to 3 mm by the PIV velocity measuring technique. Jo et al. [30] proposed that the slip layer ranges from about 1 mm to 5 mm based on the numerical analysis of shear-induced particle migration, depending particle concentrations of cement, sand, gravel, as well as pipe size. For special types of concrete, e.g. ultra-high performance concrete (UHPC), the formation of a slip layer is not induced by shear-induced particle migration [10].

For conventional concrete, several kinds of tribometer have been developed to measure the rheological properties (viscous constant and yield stress) of slip layer [11,31–33]. Although design parameters of each tribometer are different, the underlying principle of these devices is identical: a

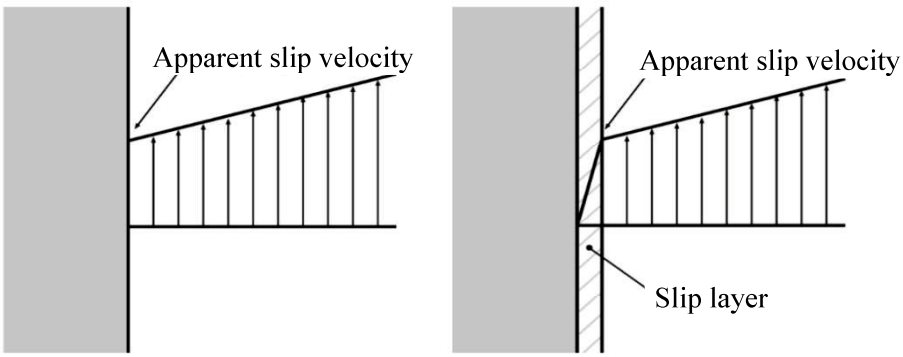

Fig. 5.2 Apparent slip velocity and slip layer: velocity in the fluid at the fluid –solid interface. Macroscopic scale (left) microscopic scale (right)

smooth cylinder is spun in a container containing fresh concrete mixture, allowing formation of the slip layer. Since no information on the thickness of slip layer is available [10], it is impossible to obtain its plastic viscosity using the rotational velocity-torque to shear rate-stress transformation. Viscous constant (Pa.s/m) is viscosity (Pa.s)-to-thickness (m) ratio of the slip layer. When measuring the rheological properties of the slip layer, it is desirable that only slip layer is sheared in tribometer. However, other two flow conditions may be observed in tribometer for fresh concretes with different fluidity: i) Both slip layer and bulk concrete are completely sheared; ii) slip layer is sheared while concrete is partially sheared. In these two cases, a correction must be made to the measured rotational velocity value for removing the effect of sheared concrete. That is to say, accurate measurement of rheological properties of slip layer is still an issue for different concretes.

Since the slip layer and the bulk concrete have different rheological properties and different particle sizes, in the numerical analysis of pumped concrete, the computational zone should be divided into two layers. It is conceivable that prediction of concrete flow in a pipe will need the characterization of each of the layers. The rheological properties of slip layer must be measured by the tribometer or other methods, and an assumption about the thickness of the slip layer is required, which is not easy to clearly define [3]. Also, though in this study I proposed the method, as explained in Section 4.4.2, to make that the particles with different sizes and random shapes can be used in the MPS simulation, numerically expressing the tiny particles in the slip layer will result in a long calculating time because numerous particles are required in the simulation.

Since in this study I do not aim to clarify the formation mechanism of slip layer, for avoiding an assumption of slip layer's thickness and reducing the number of numerical particles, apparent slip velocity is used to represent the flow of slip layer from macroscopic viewpoint in this numerical simulation. That is to say, the slip layer's thickness is ignored, and the slip layer is not included as a part of fresh concrete. However, the effect of ignoring slip layer's thickness on the flow simulation was discussed in this study. Also, the shear resistance caused by the deformation of slip layer is called slip resistance here.

Le et al. [24], Suzuki et al. [25], and Feys et al. [5] focus on the macro effect of the slip layer, and use a tribological behavior model to calculate the slip resistance. The flow velocity of outer surface of slip layer to be zero [8], and the slip layer is regarded as part of the pipe wall. In the tribological behavior model, the shear stress is a linear function of the slip velocity and has a slip yield stress, as follow:

$$\tau_L = \eta_L \cdot V_L + \tau_{L0}. \tag{5.1}$$

where, τ_L is slip resistance stress, η_L is viscous constant of slip layer (Pa·s/m), τ_{L0} is slip yield stress of slip layer (Pa), V_L is apparent slip velocity of slip layer (m/s).

It should be noted that the slip yield stress is essentially different from the yield stress of the two Bingham constants of fresh concrete. It is the minimum stress for initiating slip flow of slip layer, while the yield stress of fresh concrete is the minimum shear stress for initiating shear flow.

As the thickness (δ) of slip layer is several millimeters, a small size, compared to the radius of the pipe [8]. If ignoring this thickness, the average shear stress in the slip layer can be approximated as $\tau_L = RP/2L$. Therefore, the V_L in Eq. (5.1) can be calculated by Eq. (5.2). Since the pressure on the free surface is zero, the pressure gradient can be expressed by P/L.

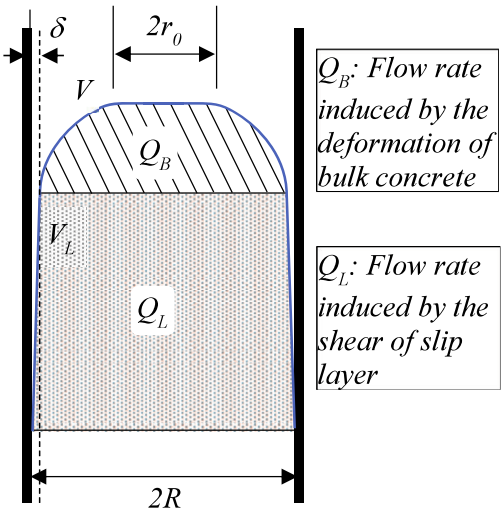

Fig. 5.3 Velocity profile of pipe flow considering slip layer

$$V_L = \frac{RP/2L - \tau_{L0}}{\eta_L} \tag{5.2}$$

where, R is inner radius of pipe, L is concrete length, P is pressure.

The velocity profile in concrete's pipe flow is shown in **Fig. 5.3**. The total volumetric flow rate Q is formed by the flow rate Q_B induced by the shear deformation of bulk concrete, and the flow rate Q_L induced by the flow of slip layer. When considering the bulk concrete to be Bingham fluid, the Q_B can be calculated according to the Buckingham-Reiner equation [6], as shown in the following:

$$Q_B = \frac{\pi(R-\delta)^4}{8\mu_b} \cdot \frac{P}{L}\left[1 - \frac{4}{3}\left(\frac{r_0}{R-\delta}\right) + \frac{1}{3}\left(\frac{r_0}{R-\delta}\right)^4\right], \tag{5.3}$$

where, r_0 is radius of plug flow, which equals to $2\tau_b \cdot L/P$.

The Q_L can be obtained by:

$$Q_L = \pi R^2 \cdot V_L = \pi R^2 \frac{RP/2L - \tau_{L0}}{\eta_L}. \tag{5.4}$$

where, τ_b is yield stress of bulk concrete, μ_b is plastic viscosity of bulk concrete.

Combining Eq. (5.3) and Eq. (5.4), the relationship between the flow rate and pressure is obtained, as follows:

$$Q = \frac{\pi(R-\delta)^4}{8\mu_b} \cdot \frac{P}{L}\left[1 - \frac{4}{3}\left(\frac{r_0}{R-\delta}\right) + \frac{1}{3}\left(\frac{r_0}{R-\delta}\right)^4\right] + \frac{\pi R^2}{\eta_L}\left(\frac{R}{2} \cdot \frac{P}{L} - \tau_{L0}\right). \tag{5.5}$$

However, when the thickness of slip layer is ignored, Eq. (5.5) can be simplified as:

$$Q \approx \frac{\pi R^4}{8\mu_b} \cdot \frac{P}{L}\left[1 - \frac{4}{3}\left(\frac{r_0}{R}\right) + \frac{1}{3}\left(\frac{r_0}{R}\right)^4\right] + \frac{\pi R^2}{\eta_L}\left(\frac{R}{2} \cdot \frac{P}{L} - \tau_{L0}\right). \tag{5.6}$$

Usually shear flow rate of bulk concrete accounts a small percentage of total flow rate, and the thickness of slip layer is very small, this approximation will not cause a great error.

5.2.4 Constituent Models of Fresh Concrete

Two types of constituent models were used to describe fresh concrete (see **Fig. 5.4**). In the single-phase & mono-particle (SPMP) model, as shown in **Fig. 5.4** (a), fresh concrete is regarded as a single-phase fluid represented by spherical fluid particles with same size and specific gravity. But in the double-phase & multi-particle (DPMP) model, as shown in **Fig. 5.4** (b), fresh concrete is regarded as two-phase material of matrix mortar and coarse aggregate having different densities. Matrix mortar phase is represented by spherical particles with same diameter. Coarse aggregate particles have different sizes and random shapes, although the coarse aggregates imagined in **Fig. 5.4** (b) are represented by spheres. The formation and treatment of coarse aggregates in DPMP model are explained in details in Section 4.4.2.

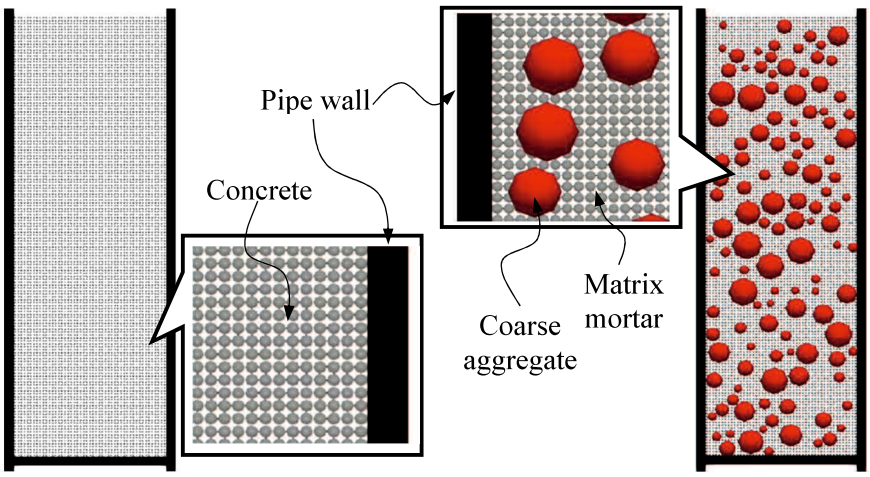

(a) Single-phase & mono-particle model (b) Double-phase & multi-particle model

Fig. 5.4 Constituent models of fresh concrete

5.3 Numerical Simulation

5.3.1 Concrete Mixtures

In our MPS simulation, three series of concrete were used, of which mix proportions are presented in **Table 5.1**. Ordinary Portland cement with the Blaine fineness of 3410 cm^2/g and the density of 3150 kg/m^3 was used in these concretes. The fine aggregate had the particle size of 0-5 mm and the surface dry density of 2620 kg/m^3, and its water absorption capacity was 2.45% and fineness modulus was 2.83. Coarse aggregate was gravel with the size 5 - 20 mm and its surface dry density was 2630 kg/m^3. Water absorption capacity of gravels was 1.15% and its fineness modulus was 6.72. A polycarboxylate ether compound-based superplasticizer was added. Used viscosity modifying agent is mainly composed of cellulose-based compound. It is found in Ref. [25] that the slump values of the concretes were 13 cm, 18 cm, and 22 cm, respectively, and the bulk densities of the concretes were 2354 kg/m^3, 2345 kg/m^3, and 2338 kg/m^3, respectively.

Table 5.1 Mix proportions of concrete mixture

Series	Cement (kg/m^3)	Sand (kg/m^3)	Gravel (kg/m^3)	Water (kg/m^3)	SP (%)	VMA (%)	Bulk density (kg/m^3)	Slump (cm)
No.1	323	912	946	171	0.808	0.646	2354	13
No.2	338	890	936	179	0.845	0.676	2345	18
No.3	360	872	913	191	0.900	0.720	2338	22

Notes: SP is superplasticizer, VMA is viscosity modifying agent.

5.3.2 Rheological Properties

The Bingham constants of the fresh concretes are shown in **Table 5.2** [25]. These constants were measured by a BML rheometer in Ref. [25]. The radius of the inner cylinder of the BML rheometer was 150 mm, the height was 200 mm, and the radius of the outer cylinder was 200mm. The multipoint method was used to determine the Bingham constants. During the measurement, a large number of polystyrene foam particles with a diameter of 1 mm were placed on the upper surface of the concrete sample. The flow velocity of these particles was recorded with a video tracker, which represents the moving speed of concrete sample. The Bingham constants were automatically determined based on the relative movement and the flow range of the concrete sample by a computer.

In Ref. [25], a series of pipe flow experiments were conducted for different flow rates to calculate the parameters η_L and τ_{L0} of the slip resistance model shown in Eq. (5.1). The pumping device used in the experiments is shown in **Fig. 5.5**. A seamless stainless-steel mobile pipe had an inner radius of 5 cm and a length of 2 m. The mobile pipe was connected to a docking hose of pump. The joint was an acrylic sleeve with

Table 5.2 Bingham constants of fresh concretes

Series	No.1	No.2	No.3
μ_b (Pa·s)	397	305	297
τ_b (Pa)	190	181	149

Notes: μ_b is plastic viscosity, τ_b is yield stress.

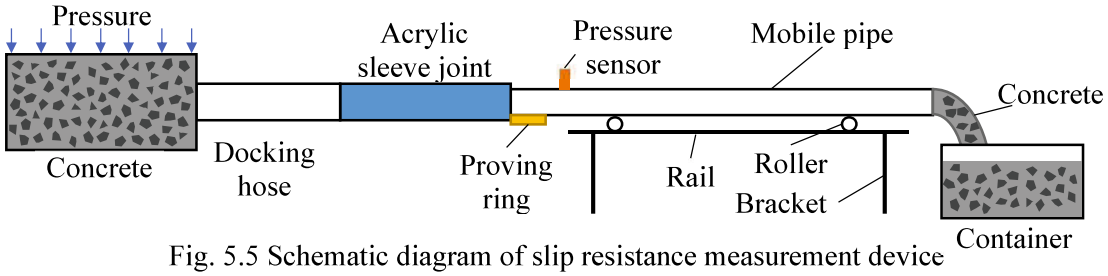

Fig. 5.5 Schematic diagram of slip resistance measurement device

an inner diameter of 1mm larger than the diameter of outer mobile pipe, so that the mobile pipe can move horizontally under the concrete's slip resistance when fresh concrete was pumped. The slip resistance of concrete pumping was detected by a proving ring. The pressure in the pipe was measured by a diaphragm type pressure gauge, which was located 15cm far from the inlet of the mobile pipe. Several flow rates corresponding to pressures in the pipe were measured. Based on the values of flow rate and pressure provided by Ref. [25], the η_L and the τ_{L0} of slip layer with different thickness were calculated by using Eq. (16). The calculated results are shown in **Table 5.3**. It can be seen that no matter if the thickness of slip layer was considered and no matter what thickness was used, the calculated result of η_L and τ_{L0} had no great difference. This is because the Q_B contributed by the bulk concrete is very small, compared to that of Q_L, which is caused by the slip layer. For a given flow rate Q, the Q_B changes slightly with the thickness of the slip layer, but the Q_L is not greatly influenced. Therefore, the rheological constants η_L and the τ_{L0} vary slightly with the thickness of the slip layer according to Eq. (5.4), which are calculated on basis of the Q_L. Hence, in the following simulations, the η_L and the τ_{L0} of 0 mm thickness of slip layer were used.

Table 5.3 Rheological constants of slip resistance equation

Series	Rheological constants	Thickness of slip layer (mm)			
		0*	2	4	6
No.1	η_L (Pa·s/m)	893	889	885	882
	τ_{L0} (Pa)	251	251	251	251
No.2	η_L (Pa·s/m)	844	839	834	831
	τ_{L0} (Pa)	239	239	239	239
No.3	η_L (Pa·s/m)	922	914	908	902
	τ_{L0} (Pa)	204	204	204	204

Notes: η_L is viscous constant of slip layer, τ_{L0} is slip yield stress of slip layer, * referred to Ref. [25].

5.3.3 Configuration of Numerical Simulations

When considering the shape and the size distribution of coarse aggregate particles in the MPS simulation, the diameter of the elementary particles should be small, which are used to form the coarse aggregate particles, because the minimum size of coarse aggregate is only 5 mm. This will cause to have to use so many elementary particles that long calculation time is needed unless parallel computation is conducted. For performing the pipe flow simulation in personal computer and cutting down the calculation time, two-dimensional calculation was adopted in this study.

In vertical pipe flow, the pumping pressure is caused by both the weight of concrete and the shear resistance of slip layer. In case of three-dimension (3D) model, the theoretical pressure can be expressed by:

$$P_{3D} = \rho gL + \frac{\tau_L \cdot 2\pi R \cdot L}{\pi R^2} = \rho gL + \frac{2\tau_L \cdot L}{R} . \tag{5.7}$$

However, in case of two-dimension (2D) model, the pipe wall is simplified into two lines from a circumferential surface in 3D, as illustrated in **Fig. 5.6**, thus the pressure should be calculated by:

$$P_{2D} = \rho gL + \lim_{\Delta x \to 0} \frac{\tau_L \cdot 2L \cdot \Delta x}{2R \cdot \Delta x} = \rho gL + \frac{\tau_L \cdot L}{R} . \tag{5.8}$$

It can be found that the pressure loss caused by the slip resistance in 2D is half of that in 3D. Simultaneous Eqs. (5.1), (5.5), and (5.8), the *P*-*Q* relationship in two-dimensional vertical pipe flow can be obtained as:

$$Q = \frac{\pi(R-\delta)^4}{4\mu_b} \cdot \frac{(P_{2D} - \rho gL)}{L} \left[1 - \frac{4}{3}\left(\frac{r_0}{R-\delta}\right) + \frac{1}{3}\left(\frac{r_0}{R-\delta}\right)^4 \right] + \frac{\pi R^2}{\eta_L} \left[R \cdot \frac{(P_{2D} - \rho gL)}{L} - \tau_{L0} \right], \tag{5.9}$$

When the thickness of slip layer is ignored, Eq. (29) can be simplified as:

$$Q \approx \frac{\pi R^4}{4\mu_b} \cdot \frac{(P_{2D} - \rho gL)}{L} \left[1 - \frac{4}{3}\left(\frac{r_0}{R}\right) + \frac{1}{3}\left(\frac{r_0}{R}\right)^4 \right] + \frac{\pi R^2}{\eta_L} \left[R \cdot \frac{(P_{2D} - \rho gL)}{L} - \tau_{L0} \right], \tag{5.10}$$

The V_L can be calculation by:

$$V_L = \frac{R(P_{2D} - \rho gL)/L - \tau_{L0}}{\eta_L} . \tag{5.11}$$

In the flow simulation using any of particle methods, the more the particles, the slower the calculation. Using larger particles can reduce the number of particles, but may harm the precision of the simulation. Thus, this chapter firstly investigated the reasonable size of particle and whether ignoring the thickness of slip layer greatly affects the simulation result or not. These investigations were conducted through 2D vertical pipe flow simulation of series No.1, using the single-phase & mono-particle model. The length of concrete was 300 mm, and the inner diameter of vertical pipe was 100 mm. In the simulation, the flow rate of concrete was first set up, the inlet flow velocity was then calculated by dividing the flow rate by the pipe cross-sectional area. Besides the resistance of slip layer described by Eq. (5.1), the Dirichlet boundary condition was adopted. The pressure on the free surface was set to be zero, and the boundary particles should satisfy the same pressure calculation equation (see Eq. (5.9)), as the fluid particles. The piston moved in a still pipe at the inlet flow velocity. The time step was set as 0.0005s, and the simulation time was 5s.

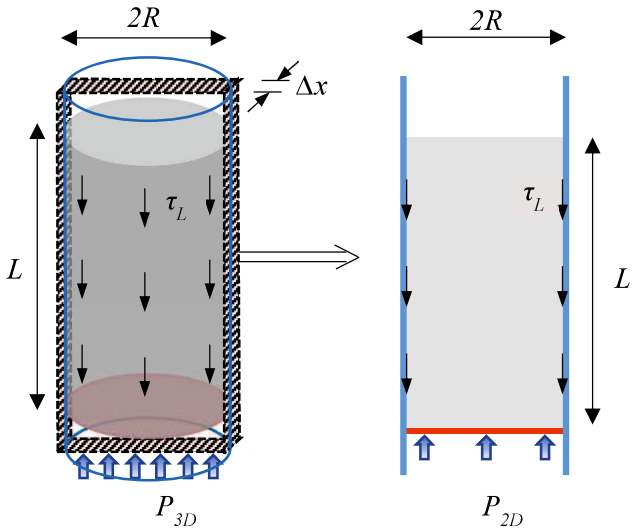

Fig. 5.6 Pressure analysis in 3D and 2D models

When the volumetric flow rate Q is 1500 cm^3/s, the 2D pumping pressure P_{2D} and the apparent slip velocity V_L is 9.40 kPa and 18.6 cm/s according to Eqs. (5.10) and (5.11), respectively.

The resolution convergence study was conducted by using different inter-particle distances, which were 20 mm, 10 mm, 5 mm, 3 mm, and 2 mm, respectively, and the thickness of slip layer was ignored. A comparison between the theoretical pressure (9.40 kPa) and the calculated pressures of the flow simulations is shown in **Fig. 5.7**. It is shown that the smaller the fluid particle, the closer the calculated pressure is to the theoretical value, but the simulation results are almost independent of the particle diameter when it is less than 5mm. Hence, in the following simulations, the diameters were set as 2mm for the fluid particles in the single-phase & mono-particle model, and for the elementary particles in the double-phase & multi-particle model.

Since a macroscopic approach was used to treat the slip layer, the thickness of slip layer is ignored in the simulation, i.e. the radius of bulk concrete is equal to the inner radius of the pipe. However, for clarifying the effect of ignoring the thickness of slip layer, this chapter assumed three thicknesses and calculated the rheological constants η_L and τ_{L0} of slip layer by Eq. (5.5), as shown in **Table 5.3**. The radius of bulk concrete is a difference between the inner radius of the pipe and the thickness of slip layer. **Fig. 5.8** shows the effect of bulk concrete's radius on the calculated pressures of Concrete No.1's vertical pipe flow. Though considering the thickness of slip layer to reduce the bulk concrete's radius yielded different calculated pressures, they were not greatly different from the theoretical value, even the thickness was set to be 0 mm. It is also found with the increase of the thickness, the calculated pressure slightly increased. This is because the increase of the thickness results in a decrease of bulk concrete volume, accordingly a high pressure is required for the same flow rate. In the simulation, ignoring the thickness of slip layer has no great effect on the simulation result. As explained in section 4.2.4, the flow rate Q_B of bulk concrete accounts a small percentage of the total flow rate Q, the small change of bulk concrete in size does not result in a great change of pressure.

After the discussion above, vertical pipe flow simulations were conducted for the three concretes using the improved MPS method. Like as the investigations on the reasonable particle diameter and the effect of slip layer's thickness, the concretes length was 300 mm, and the inner diameter of vertical

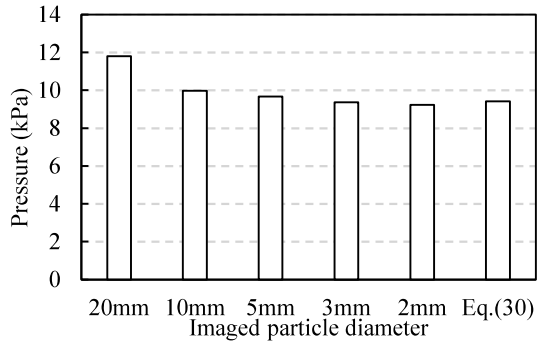

Fig. 5.7 Pumping pressure under 1500 cm^3/s of flow rate, calculated by using different diameters of fluid particle

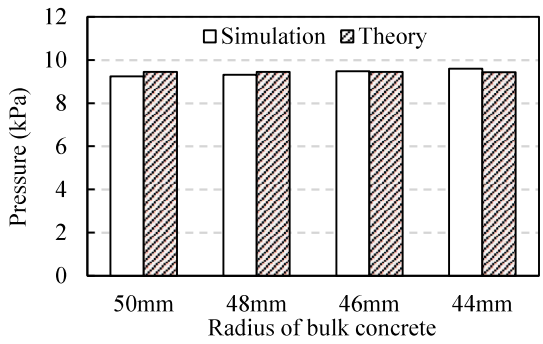

Fig. 5.8 Pumping pressure under 1500 cm^3/s of flow rate, considering different thicknesses of slip layer

pipe was 100 mm. When using the single-phase & mono-particle (SPMP) model, three series of fresh concrete were represented respectively by 7350 round fluid particles with 2 mm diameter, and all the fluid particles had the same density to the concrete. However, in the double-phase & multi-particle (DPMP) model, the difference of density between matrix mortar and coarse aggregate was considered for analyzing the dynamic segregation of coarse aggregate. In the Concrete No.1~No.3, there were 4666, 4733, and 4797 mortar particles with 2 mm diameter, respectively, and the number of coarse aggregate particles was 119, 118, and 113, respectively, which randomly distributed in the matrix mortar, and were formed by the elementary particles of 2 mm diameter. The same coarse aggregate was actually used in the three series of concrete. The volume fractions of coarse aggregate particles in the range of 5-10 mm, 10-15 mm and 15-20 mm were set to be 30%, 40%, and 30%, respectively, for making the fineness modulus of simulated coarse aggregate to be consistent with the experimental value (= 6.72). The detail configuration information of particles was shown in **Table 5.4**. The SPMP model and the DPMP model used the same parameters of slip layer, and the same Bingham constants of bulk concrete for a given concrete.

Table 5.4 Configuration information of particles

Series of concrete	Single-phase & mono-particle model			Double-phase & multi-particle model					
	Fluid particle			Mortar particle			Coarse aggregate particle		
	Density (kg/m^3)	Shape, diameter	Number	Density (kg/m^3)	Shape, diameter	Number	Density (kg/m^3)	Shape, size	Number
No.1	2354	Round, 2mm	7350	2190	Round, 2mm	4666	2630	Random	119
No.2	2345			2187		4733		5-10mm, 30% 10-15mm, 40%	118
No.3	2338			2182		4797		15-20mm, 30%	113

5.4 Numerical Results and Discussion

Using the improved MPS and the two constituent models of concrete, the upward flows of the three concretes in the vertical pipe were simulated for different volumetric flow rates (Q). The thickness of the slip layer was not considered, i.e. the diameter of bulk concrete was equal to the inner diameter of pipe. The rheological parameters shown in **Table 5.2** and **Table 5.3** were used for characterizing the shear flow and the slip flow of concrete, respectively. For a certain flow rate Q, the corresponding moving speed of the piston was firstly calculated by $Q/\pi R^2$. Then, upward pipe flow was simulated to get 2D pumping pressure and velocity profiles by letting the lowest particles that contact the piston move at the same speed to the piston. For a comparison with the numerical results, theoretical two-dimensional P-Q relationships were also obtained by using Eq. (30).

As an example of numerical results, **Fig. 5.9** and **Fig. 5.10** show the pressure distribution and the velocity profiles in the Concrete No.1 that was pumped at a flow rate of 1500 cm^3/s. It should be noted that this velocity profiles refer to bulk concrete (= whole concrete here due to no thickness of slip layer), do not include the slip velocity of slip layer. Present program outputs round shape images for the coarse aggregate particles, but in actual simulation, the coarse aggregate particles were formed by the elementary particles, thus have random shapes. From **Fig. 5.9**, it can be found that the pressure distributions obtained by the SPMP model and the DPMP model are almost the same, and the pressure gradually decreases from the bottom to the upper of concrete. From **Fig. 5.10**, It can be seen that a plug flow zone is formed in the center of the pipe. The flow velocity of concrete near the pipe wall is slower than that around the center axis because of the wall effect. This phenomenon is more obvious in the DPMP model, because the coarse aggregates near the pipe wall obstruct the shear flow of the matrix mortar. The flow velocity of the front concrete is almost the same as the end concrete. The

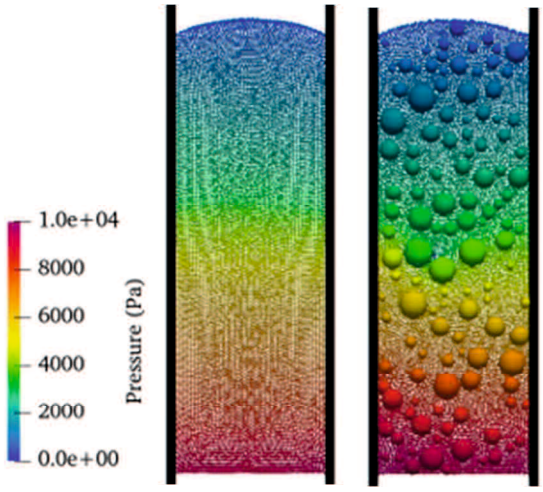

Fig. 5.9 Pressure distribution in Concrete No.1 at a flow rate Q=1500cm^3/s (t=5s)
Left: SPMP model; Right: DPMP model

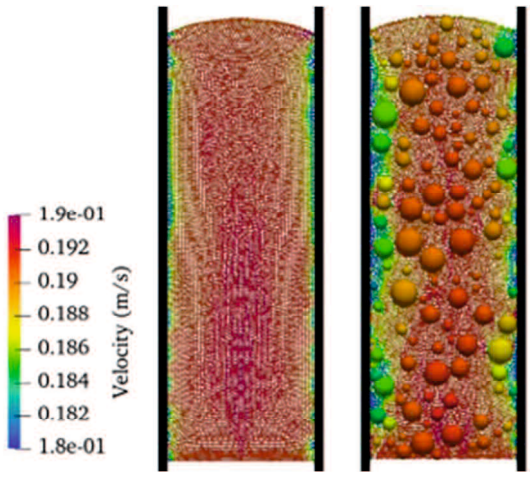

Fig. 5.10 Velocity profile in Concrete No.1 at a flow rate Q=1500cm^3/s (t=5s)
Left: SPMP model; Right: DPMP model

simulated pressure (P)-flow rate (Q) relationships, velocity profiles in different zones, as well as dynamic segregation of coarse aggregate will be discussed in the following.

5.4.1 Pumping Pressure-Flow Rate Relationship

The pressure (P)-flow rate (Q) relationships of three series of fresh concrete are shown in **Fig. 5.11**. For any of the concretes, no matter which constituent model was used, the numerically P-Q relationship are well coincident with the theoretically one. Therefore, it is possible to use the MPS method to predict pumping pressure of concrete. When only the pressure is desired to calculate, the SPMP model is convenient, since it is not necessary to form coarse aggregate particles with elementary particles and modify the positions of the elementary particles at each step.

Though the numerical pressures were close to the theoretical values, it is found that the numerical pressures of the SPMP model were smaller than those of the DPMP model, and the theoretical values in most cases. Also, when the flow rates were large, the numerical pressures were slightly larger than the theoretical values, especially for the Concrete No.1 with smaller sump value. At present, the reasons are unknown. A detailed investigation is needed, considering the effects of segregation of coarse aggregate, particle size and shape, scope of application of Bingham model, etc.

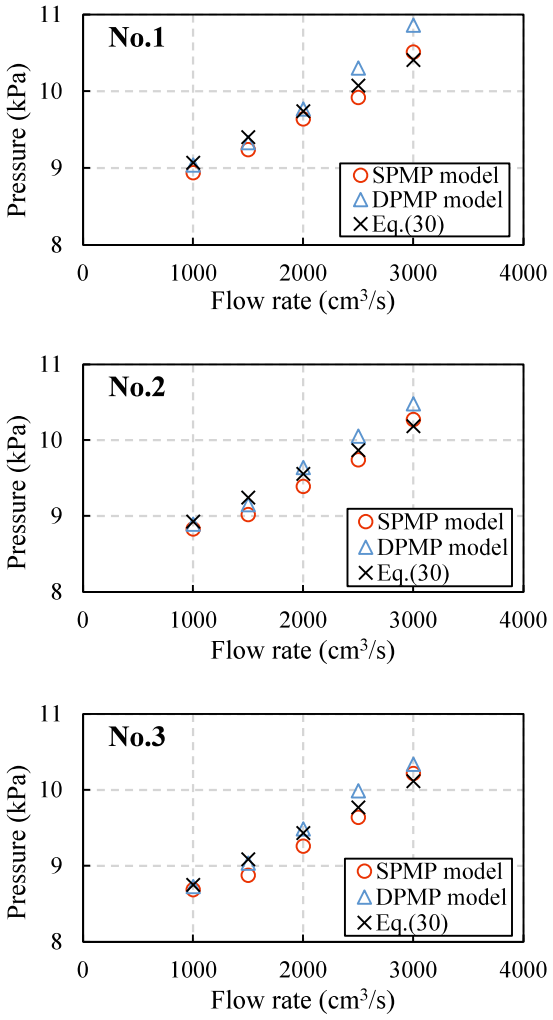

Fig. 5.11 Numerical and theoretical pressures under different flow rates for Concretes No.1~No.3

Fig. 5.12 shows a detailed comparison between the numerically calculated pressures and the theoretically calculated pressures under the flow rate Q = 1500cm^3/s. All the numerical pressures are consistent with the theoretical results by the errors of less than 3%. The error may be caused by the influence of ignoring the thickness of slip layer. The errors when using the

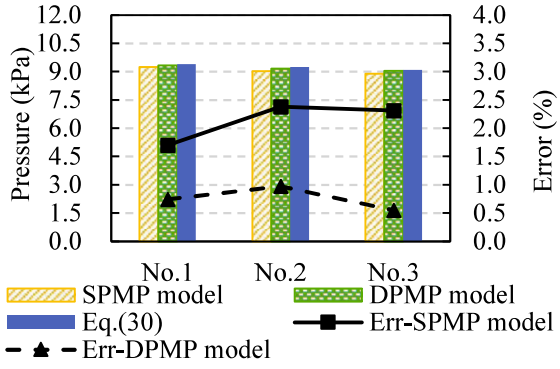

Fig. 5.12 Comparison of numerical and theoretical pressures

DPMP model are slightly lower than those of using the SPMP model. Considering the size distribution and the shape of coarse aggregate would be benefit to the prediction precision of pumping pressure.

5.4.2 Velocity Profile

During the simulation, the flow velocities from the pipe wall to the center axis were recorded for heights of 24 cm, 15 cm, and 6 cm from the piston at the bottom of concrete. The recorded velocity profiles at the three heights represent the flow characteristics of the concrete in the upper, middle and lower positions. Taking the Concrete No.1 as an example, **Fig. 5.13** (a) and (b) show the velocity profiles calculated by using the SPMP model, and the DPMP model, respectively. Detailed variations of flow velocity from the pipe wall are shown in **Fig. 5.13** (c) and (d). The characteristics of velocity profiles agree with the theoretical model of pipe flow shown in **Fig. 5.3**. It can be found that the velocity profiles of the concrete at different heights are almost the same. The shear rate (tangent slope of the velocity curve) of the concrete close to the pipe wall is very large. The farther the concrete is from the pipe wall, the lower the shear rate. For the SPMP model, the concrete in the central zone of about 1.0 cm radius, the flow velocity is almost uniform, showing a plug flow. However, for the DPMP model, the concrete in the central zone of about 2.0 cm radius shows a plug flow. That is to say, if the size, shape and density of coarse aggregate are considered in the constituent model of concrete as its reality as possible, central zone of non-shear deformation will be enlarged due to a larger interaction between particles. Numerically calculated apparent slip velocities at the interface of pipe wall and

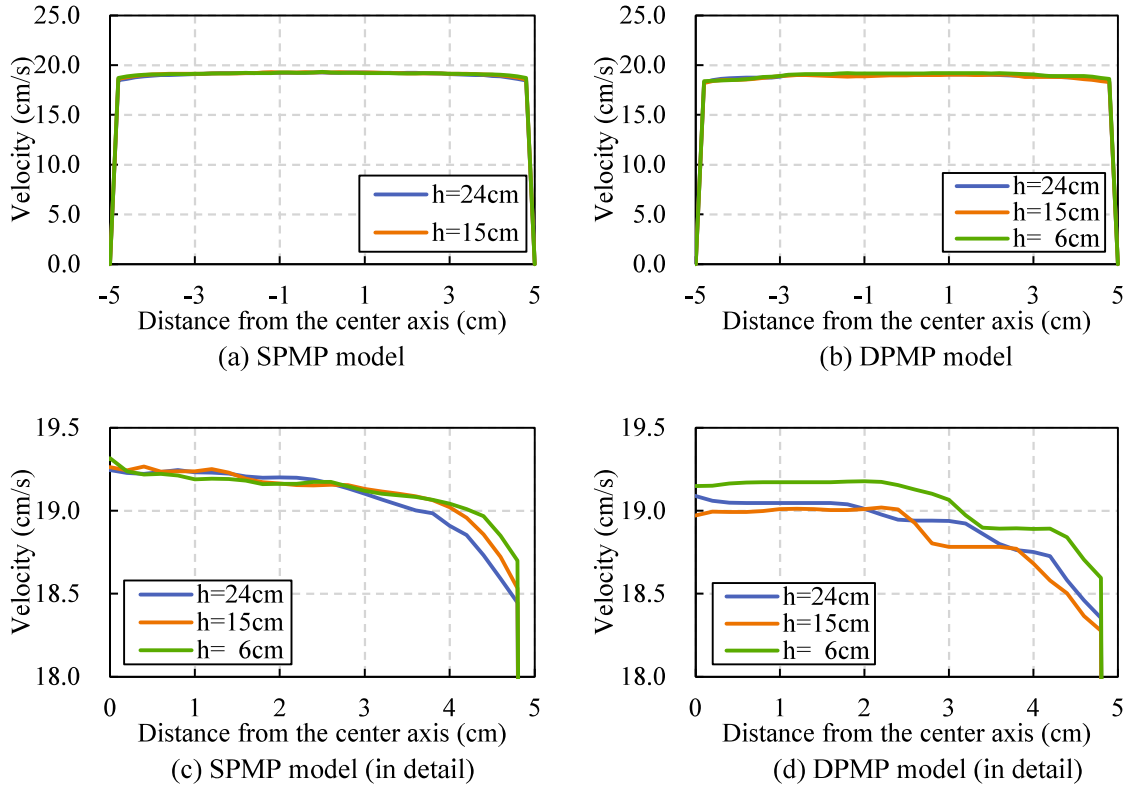

Fig. 5.13 Velocity profile in the pipe at different height *h* (Concrete No.1)

concrete are 18.6 cm/s, and 18.4 cm/s, respectively, for the SPMP model and the DPMP model, which are well consistent with the theoretically calculated results (18.6 cm/s). Hence, both the proposed constituent models can be used to simulate the pipe flow of fresh concrete. However, as explained latter, only the DPMP model would provide the dynamic segregation information of coarse aggregate.

5.4.3 Uneven Migration of Coarse Aggregates

The positions of several coarse aggregate particles in bulk concrete were noticed at different time points, as shown in **Fig. 5.14**. The blue color particles gradually came close, which were the coarse aggregates in the end of the vertical pipe flow, and the coarse aggregate particle in contact with the pipe wall moved downward due to the boundary resistance. The green color particles, locating in the central of the concrete, remained almost unchanged relative positions because of the plug flow. The orange color particles in the upper of the concrete changed in their relative positions due to the velocity difference between the inner and outer layers of the concrete.

Although the particles in different positions of the bulk concrete have different velocities, as shown in **Fig. 5.10**, the shear deformation of bulk concrete is not as large as that of the slip layer. Moreover, the time of flow simulation was only 5s, the deformation of the bulk concrete was not very intensive. Therefore, the migration of coarse aggregates in **Fig. 5.14** was not obvious. To discuss the migration of coarse aggregates in detail, as shown in **Fig. 5.15**, the concrete was divided into two portions in the radius direction (inner and outer portions), and in the flow direction (upper and lower portions), respectively, for investigating the variation of the distribution of coarse aggregate particles with the vertical pipe flow. The volume fraction (φ) of the coarse aggregate particles in each portion was counted, and the variations of the φ with the elapsed time are shown in **Fig. 5.16**. **Fig. 5.16** (a) shows the variations of the φ along the radius direction. It was observed that the coarse aggregate particles migrated toward the inside of bulk concrete. With the increase of flow time, the φ of the inner portion increased, but the φ of the outer portion decreased. This result well agrees with the well-known knowledge that large particles move toward the inner of concrete where the shear rate is lower [8,11]. Concrete No.1 had the lowest slump,

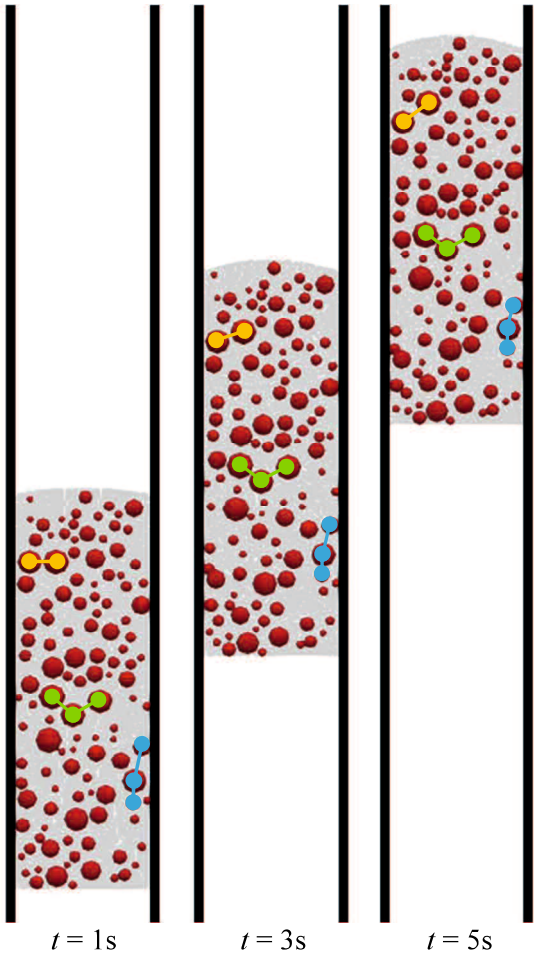

Fig. 5.14 Migration of coarse aggregates during pipe flow

compared to other series of concrete, and the variation rate of the φ along the radial direction is the smallest. This means that the formation of the slip layer is slow for the fresh concrete with low fluidity. It was also noticed that this migration movement along the radius direction did not continue after 2 seconds. This is because as the volume fraction of aggregate particles increases, the obstacle to inward migration increases, and finally dynamic equilibrium is reached. Hence, This MPS simulation is possible to simulate the segregation behavior of fresh concrete in pipe flow.

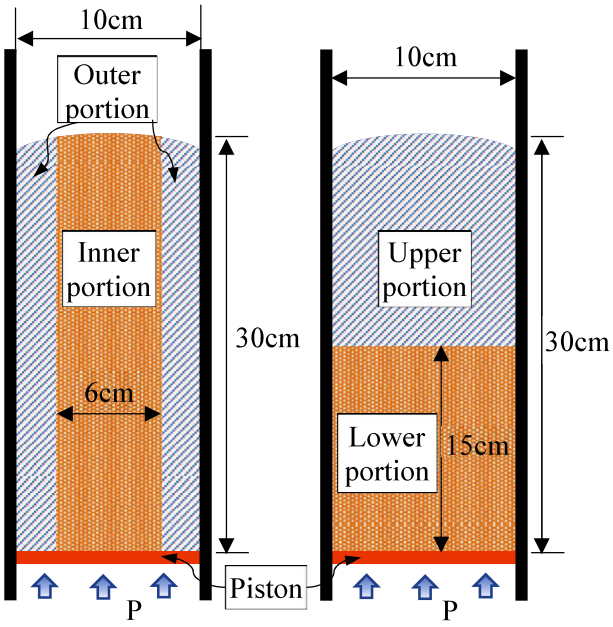

Fig. 5.15 Zoning of concrete for segregation analysis

The variations of the φ along the flow direction are shown in **Fig. 5.16** (b). It is considered that coarse aggregates, under the action of viscosity and inertia, resist the impact of gravity and move ahead of the surrounding mortar [12], so that the φ in the front concrete is larger than that of the lower portion. Also, if concrete has lower viscosity, its coarse aggregates is easier to segregate. This well-known fact can be found from **Fig. 5.16** (b). Concrete No.2 and No.3 had lower viscosity (305 Pa·s, and 297 Pa·s, respectively) than Concrete No.1, the variations of the φ of these two concretes were larger along the flow direction than Concrete No.1.

Hence, using the improved MPS and the DPMP model can not only predict the pressure and velocity profile of pipe flow, but also would be able to simulate the segregation behaviors of coarse aggregate. Detail numerical investigation on the formation of sip layer caused by shear-induced segregation and the influencing factors of dynamic segregation of pumped concrete will be reported in other papers.

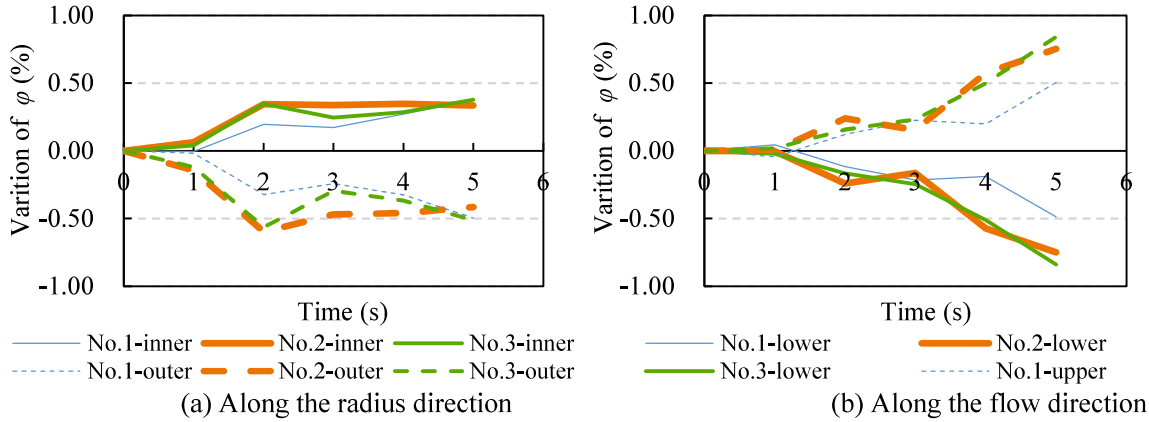

(a) Along the radius direction (b) Along the flow direction

Fig. 5.16 Variations of volume fraction φ of coarse aggregate with pipe flow time

5.5 Summary

The slip layer has a great influence on the pumpability of fresh concrete. However, the rheological properties and thickness of the slip layer are not easy to be clearly defined. In the numerical simulation, for avoiding an assumption of slip layer's thickness and the use of large numbers of tiny particles, apparent slip velocity is used to represent the shear flow of the slip layer from a macroscopic viewpoint, and the tribological behavior model was adopted to describe the slip resistance of the slip layer.

In this chapter, an improved MPS method was used to do the numerical simulation of pipe flow. Differentiating from the general MPS method that uses a single type of spherical fluid particles with the same size, in the improved MPS method elementary particles were employed to form coarse aggregate particles to have a size distribution and random shape, for making the MPS to be applicable to the simulation of dynamic segregation of fresh concrete.

Two types of constituent models were used to describe fresh concrete, named single-phase & mono-particle (SPMP) model and double-phase & multi-particle (DPMP) model. In the SPMP model, fresh concrete is regarded as a homogeneous fluid represented by same spherical particles. But in the DPMP model, fresh concrete is regarded as two-phase material of matrix mortar and coarse aggregate having different densities. Matrix mortar phase is represented by same spherical particles, but coarse aggregate particles have different sizes and random shapes.

The improved MPS method, combined any of the above constituent models, was proved to be able to predict the pressure of pipe flow of fresh concrete. And when using the DPMP model, the dynamic segregation of aggregate particles can be also simulated. Thus, this numerical method has the potential to simulate the formation of slip layer and to discuss the influencing factors of concrete segregation during pumping flow.

Reference

[1] M. Jolin, D. Burns, B. Bissonnette, F. Gagnon, L.-S. Bolduc, B. Bissonnette, Understanding the pumpability of concrete, in: Shotcrete Undergr. Support XI, 2009.

[2] H. Kwon, C.K. Park, J.H. Jeong, S.D. Jo, S.H. Lee, Prediction of concrete pumping : part II — analytical prediction and experimental verification, ACI Mater. J. 110 (2013) 657–668.

[3] M. Choi, C.F. Ferraris, N.S. Martys, D. Lootens, V.K. Bui, H.R.T. Hamilton, Metrology deeds for predicting concrete pumpability, Adv. Mater. Sci. Eng. 2015 (2015) 1–10.

[4] D. Feys, G. De Schutter, R. Verhoeven, K.H. Khayat, Similarities and differences of pumping conventional and self-compacting concrete, RILEM Bookseries. (2010).

[5] D. Feys, G. De Schutter, R. Verhoeven, Parameters influencing pressure during pumping of self-compacting concrete, Mater. Struct. Constr. 46 (2013) 533–555.

[6] E. Buckingham, On plastic flow through capillary tubes, Proc. Am. Soc. Test. Mater. (1921) 1154–1156.

[7] T. Kaplan, D., De Larard, F., & Sedran, Design of concrete pumping circuit, ACI Mater. J. 102 (2005) 110–117.

[8] M. Choi, N. Roussel, Y. Kim, J. Kim, Lubrication layer properties during concrete pumping, Cem. Concr. Res. 45 (2013) 69–78.

[9] V. Mechtcherine, V.N. Nerella, K. Kasten, Testing pumpability of concrete using Sliding Pipe Rheometer, Constr. Build. Mater. 53 (2014) 312–323.

[10] G. De Schutter, D. Feys, Pumping of fresh concrete: insights and challenges, RILEM Tech. Lett. 1 (2016) 76.

[11] E. Secrieru, J. Khodor, C. Schröfl, V. Mechtcherine, Formation of lubricating layer and flow type during pumping of cement-based materials, Constr. Build. Mater. 178 (2018) 507–517.

[12] M. Choi, C.F. Ferraris, N.S. Martys, V.K. Bui, H.R.T. Hamilton, D. Lootens, Research needs to advance concrete pumping technology, Gaithersburg, MD, 2015.

[13] M.S. Choi, Y.J. Kim, S.H. Kwon, Prediction on pipe flow of pumped concrete based on shear-induced particle migration, Cem. Concr. Res. 52 (2013) 216–224.

[14] G.R. Liu, M.B. Liu, Smoothed Particle Hydrodynamics, World Scientfic, 2003.

[15] Z. Li, Z. Xu, R. Yoshioka, Flow simulation of fresh concrete using SPH method with consideration of geometry of particles, in: Sixth Int. Conf. Constr. Mater., Fukuoka, Japan, 2020: p. (in press).

[16] G. Cao, Z. Li, Z. Xu, A SPH simulation method for opening flow of fresh concrete considering boundary restraint, Constr. Build. Mater. 198 (2019) 379–389.

[17] W.S. Alyhya, S. Kulasegaram, B.L. Karihaloo, Simulation of the flow of self-compacting concrete in the V-funnel by SPH, Cem. Concr. Res. 100 (2017) 47–59.

[18] G. Cao, Z. Li, Numerical flow simulation of fresh concrete with viscous granular material model and smoothed particle hydrodynamics, Cem. Concr. Res. 100 (2017) 263–274.

[19] M.S. Abo Dhaheer, S. Kulasegaram, B.L. Karihaloo, Simulation of self-compacting concrete flow in the J-ring test using smoothed particle hydrodynamics (SPH), Cem. Concr. Res. 89 (2016) 27–34.

[20] S. Koshizuka, Y. Oka, Moving-Particle Semi-implicit method for fragmentation of incompressible fluid, Nucl. Sci. Eng. 123 (1996) 421–434.

[21] Y. Shimizu, H. Gotoh, A. Khayyer, An MPS-based particle method for simulation of multiphase flows characterized by high density ratios by incorporation of space potential particle concept, Comput. Math. with Appl. 76 (2018) 1108–1129.
[22] Z. Xu, Z. Li, G. Cao, F. Jiang, Comparison of SPH and MPS methods for numerical flow simulations of fresh mortar, Proc. Japan Concr. Inst. 41 (2019) 1127–1132.
[23] J.J. Monaghan, J. J., On the problem of penetration in particle methods, J. Comput. Phys. 82 (1989) 1–15.
[24] H.D. Le, E.H. Kadri, S. Aggoun, J. Vierendeels, P. Troch, G. De Schutter, Effect of lubrication layer on velocity profile of concrete in a pumping pipe, Mater. Struct. 48 (2015) 3991–4003.
[25] K. Suzuki, S. Koshikawa, Y. Itoh, Studies on pipe flow of concrete, Concr. Res. Technol. 15 (2004) 47–57.
[26] H. Zhu, N.S. Martys, C. Ferraris, D. De Kee, A numerical study of the flow of Bingham-like fluids in two-dimensional vane and cylinder rheometers using a Smoothed Particle Hydrodynamics (SPH) based method, J. Nonnewton. Fluid Mech. 165 (2010) 362–375.
[27] F. De Larrard, N. Roussel, Flow simulation of fresh concrete under a slipform machine, Road Mater. Pavement Des. 12 (2011) 547–566.
[28] S.N. Alekseev, On the calculation of resistance in pipe of concrete pumps, Mekhanizatia Storit. 9 (1952) 8–13.
[29] R. Weber, The transport of concrete by pipeline, London,UK Cem. Concr. Assoc. (1968).
[30] S.D. Jo, C.K. Park, J.H. Jeong, S.H. Lee, S.H. Kwon, A computational approach to estimating a lubricating layer in concrete pumping, Comput. Mater. Contin. (2012).
[31] T.T. Ngo, E.H. Kadri, R. Bennacer, F. Cussigh, Use of tribometer to estimate interface friction and concrete boundary layer composition during the fluid concrete pumping, Constr. Build. Mater. 24 (2010) 1253–1261.
[32] V.N. Nerella, V. Mechtcherine, Virtual sliding pipe rheometer for estimating pumpability of concrete, Constr. Build. Mater. 170 (2018) 366–377.
[33] D. Feys, A. Perez-Schell, R. Khatib, Development of a tribometer to characterize lubrication layer properties of self-consolidating concrete, Cem. Concr. Compos. 54 (2014) 40–52.

Chapter 6 Conclusions and Future Works

6.1 Conclusions

6.2 Future Works

Chapter 6
Conclusions and Future Works

6.1 Conclusions

This thesis based on the particle method and developed a numerical pipe flow model to study the flow behaviors of fresh concrete in pipeline. The research findings are concluded as follows:

In Chapter 2, previous researches relevant to the pipe flow model of fresh concrete are reviewed. The prediction on flow behaviors of fresh concrete pipe flow is valuable. And the segregation of aggregates has a great influence on the pumping behavior and need to be further studied. Although the measurement and prediction of the rheological properties of fresh concrete are accessible, the study of numerical segregation simulation and pipe flow simulation are almost vacant. SPH and MPS methods have the potential to simulate the segregation of fresh concrete and are suitable for pipe flow simulation. However, some necessary works, such as segregation model and pipe flow model are lacked.

In Chapter 3, the calculation efficiency and the applicability of WCSPH and I-MPS methods for the flow simulation of fresh cementitious materials (FCM) are discussed. The MPS method has a higher efficiency than the SPH method. the SPH method would be suitable for their flow simulation when the FCMs have low fluidity or they are subjected to low pressure. Whereas the MPS method is of a wide application. Especially for the FCMs with high fluidity or subjected to a high pressure. For properly simulating the flow behaviors of FCMs, it is necessary to take the boundary slippage resistance into account. The results suggest that I-MPS method is relatively more appropriate for pumping simulation.

In Chapter 4, the I-MPS method was further improved to have the ability to calculate two-phases flow problems, considering the differences in particle size, density, and interaction of different sorts of particle. A new constituent model, called Double-phase & multi-particle (DPMP) model, was proposed and incorporated into the I-MPS to establish a numerical flow & segregation model for fresh concrete. It was verified that the flow & segregation model can simulate the segregation behavior of coarse aggregate in fresh concrete together with fresh concrete's flow behavior. Both the static and dynamic segregation behaviors of fresh concrete were investigated numerically, and the author found that the smaller the yield stress of the matrix mortar, the easier it is for the coarse aggregate to segregate. Low plastic viscosity of matrix mortar, large size of coarse aggregate, and large difference of flow

speed between coarse aggregate and matrix mortar will result in an increase in the segregation velocity of coarse aggregate.

In Chapter 5, a numerical pipe flow method was proposed based on the flow & segregation model described in Chapter 4 to simulate the flow &segregation behaviors of fresh concrete in pipe. First, a macroscopic approach was used to describe the slip layer in pipe flow. This macroscopic approach can not only avoid the assumption of the composition and thickness of slip layer, but also simplify the numerical model and thus raise the calculation efficiency of numerical simulation. Then, based on this macroscopic approach of slip layer, the pressure-pipe flow rate relationship was clarified by theoretical investigation. Finally, a new numerical method of concrete's pipe flow was developed based on the flow & segregation model, the slip layer model, and the I-MPS method, and was used to predict the pumping pressure of concrete, and to simulate the flow & segregation behaviors of fresh concrete in the pipeline, including particle velocity distribution, pressure distribution, deformation distribution, and coarse aggregate distribution, etc. By comparing the numerical and theoretical results, the numerical pipe flow method developed in this study was verified.

6.2 Future Works

The primary object of the present research is to develop a numerical approach to the pipe flow of fresh concrete based on meshless particle method. This numerical approach can not only predict the pressure and velocity profile of fresh concrete in pipeline, but also simulate the segregation behaviors of coarse aggregate in concrete. This research provides a new numerical approach to pipe flow. However, the numerical research on fresh concrete pipe flow has just begun. There are a lot of problems and challenges to be solved. Future work is listed as follows.

6.2.1 Influencing Factors of Segregation During Pipe Flow

Although many studies have discussed the influencing factors of segregation during casting and vibrating, there are few reports on the influencing factors of segregation during pipe flow. Due to the different incentives for concrete flow during casting and pumping, the former is gravity-induced active flow, while the latter is forced flow driven by external forces. Therefore, the segregation behavior of concrete in these two cases should be different. Considering the great influence of segregation in pipes on the pumpability of concrete, it is necessary to study the influencing factors of pipe flow segregation.

6.2.2 Flow Behaviors in Bend and Taper Pipes

The flow of concrete through bend and taper pipes is much more complicated than that in straight pipes. However, the bend and taper are essential parts of the pipeline, and pipe blockage is often found in these places. Hence, studying the flow behaviors of fresh concrete when passing through the bend and taper is part of the work to figure out the entire flow behaviors in pipe flow, although it must be a difficult task.

6.2.3 Formation Mechanism of Concrete Blockage in Pipeline

It is inevitable that concrete will segregate during pumping. Although segregation will promote pumping flow on the one hand, such as the formation of a slip layer, segregation on the other hand is more likely to cause pipe blockage and hinder pumping process. After grasping the formation mechanism of blockage, corresponding measure can be taken out to avoid blocking.

Paper List

Referred Papers in Journal etc.

1. Z. Xu, Z. Li, F. Jiang, The Applicability of SPH and MPS Methods to Numerical Flow Simulation of Fresh Cementitious Materials, *Construction and Building Materials*, Vol. 274, pp. 121736, 2021.
(Related Articles: Chapter 3)

2. Z. Xu, Z. Li, F. Jiang, Numerical Approach to Pipe Flow of Fresh Concrete, *Cement and Concrete Research*, Revised and Under Reviewer.
(Related Articles: Chapter 5)

Referred Papers in International Conference Proceedings

3. Z. Xu, Z. Li, G. Cao, F Jiang, Comparison of SPH and MPS Methods for Numerical Flow Simulation of Fresh Mortar, *Proceedings of the Japan Concrete Institute*, Vol. 41, No. 1, pp. 1127-1132, 2019.
(Related Articles: Chapter 3)

4. Z. Li, Z. Xu, F. Jiang, R Yoshioka, Flow Simulation of Fresh Concrete Using SPH Method with Consideration of Geometry of Particles, Sixth International Conference on Construction Materials, Japan, in CD, 2020.
(Related Articles: Chapter 4)

Technical Papers

5. Z. Xu, Z. Li, G. Cao, F. Jiang, Comparison of SPH and MPS Methods for Numerical Flow Simulations of Fresh Cementitious Materials, *Proceedings of Annual Research Meeting Chugoku Chapter, Architectural Institute of Japan (AIJ)*, Vol. 42, pp. 79-82, 2019.
(Related Articles: Chapter 3)

6. 吉岡励, 李柱国, 蒋飛, 徐支松, フレッシュコンクリートの流動と分離の数値解析法に関する研究, 日本建築学会中国支部研究報告集, Vol. 43, pp. 53-56, 2020.
(Related Articles: Chapter 4)